Schweizerische Eidgenossenschaft
Confédération suisse
Confederazione Svizzera
Confederaziun svizra

Federal Department of the Environment, Transport, Energy and Communications DETEC

Swiss Federal Office of Energy SFOE
Energy Research and Cleantech Division

Final report dated 18.12.2024

TriSolHP project

Direct coupling of a PVT field with a heat pump system using natural refrigerant for space heating and DHW production in existing multifamily buildings

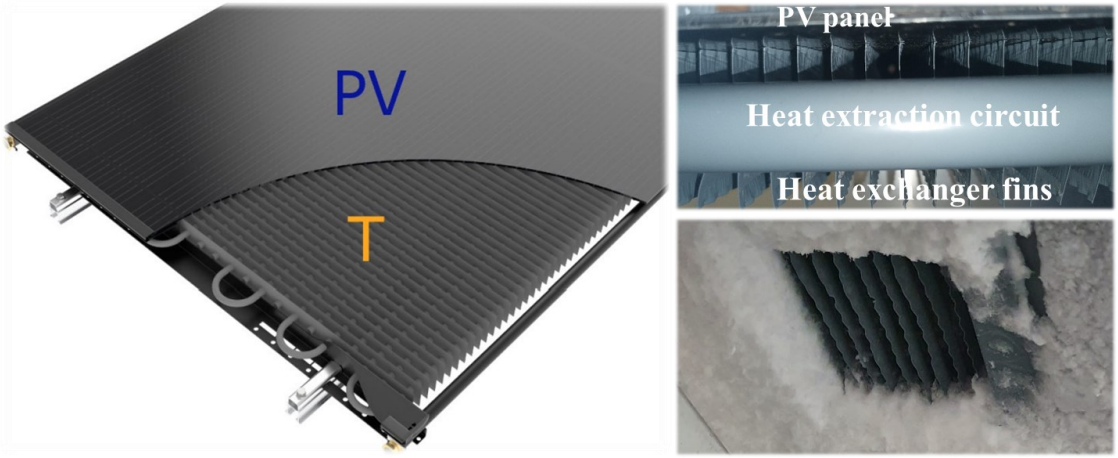

Source: Consolar Solare Energiesysteme GmbH (left) and pictures from test performed during the TriSolHP project (right)

Date: 18.12.2024

Location: Yverdon-les-Bains

Publisher:
Swiss Federal Office of Energy SFOE
Energy Research and Cleantech
CH-3003 Bern
www.bfe.admin.ch

Grant provider:
Office fédéral de l'énergie OFEN
Section Recherche énergétique et cleantech
CH-3003 Berne
www.ofen.admin.ch

Co-financing:
Service Industriel de Genève (SIG)
Chemin du Château-Bloch 2, 1219 Vernier
https://ww2.sig-ge.ch/

SolTop Energie SA
Rue des Sablons 8, 3960 Sierre
https://www.energie-solaire.com/

Subsidy recipients:
Haute Ecole d'Ingénierie et de Gestion du canton de Vaud (HEIG-VD)
Route de Cheseaux 1, Case postale, CH-1401 Yverdon-les-Bains
https://heig-vd.ch/

Université de Genève (UNIGE)
Boulevard Carl-Vogt 66, 1205 Genève
https://www.unige.ch/

Authors:
Alexis Duret, alexis.duret@heig-vd.ch
Enrico Da Riva, enrico.da-riva@heig-vd.ch
Stefano Pauletta, stefano.pauletta@heig-vd.ch
Pierre Hollmuller, pierre.hollmuller@unige.ch
Omar Montero Dominguez, omar.monterodominguez@unige.ch
Ruben Novoa-Herzog, ruben.novoa@unige.ch
Pauline Brischoux, pauline.brischoux@unige.ch

SFOE project coordinators:
Andreas Eckmanns, andreas.eckmanns@bfe.admin.ch
Stephan Mathez, stephan.a.mathez@solarcampus.ch

SFOE contract number: SI/502283-01

The authors bear the entire responsibility for the content of this report and for the conclusions drawn therefrom.

Zusammenfassung

Das TriSolHP-Projekt entwickelt ein neues Heizsystem für Mehrfamilienhäuser, das ein PVT (photovoltaisch-thermisches) Kollektorfeld mit Wärmepumpen (HP) unter Verwendung natürlicher Kältemittel kombiniert. Das System ist darauf ausgelegt, effizienter und umweltfreundlicher zu sein als herkömmliche Luftwärmepumpen (LW-WP). Das im Projekt verwendete PVT wurde optimiert, um als Wärmequelle für die WP verwendet werden zu können.

Die erste Phase des Projekts konzentrierte sich auf die Messung der Leistung des PVT-WP-Kollektors in einer Klimakammer. Die Ergebnisse zeigten, dass der Kollektor Umgebungswärme effizient aufnehmen kann, selbst wenn er mit Eis bedeckt ist (siehe **Abschnitt 2**).

Dann wurden numerische Modelle einer klassischen (subkritischen, mit R290-Kältemittel) und einer transkritischen (mit R744-Kältemittel) WP entwickelt (siehe **Abschnitt 3**). Die Modelle wurden mit experimentellen Daten validiert und zur Bewertung der Leistung des TriSolHP-Systems verwendet.

In **Abschnitt 4** werden zwei hydraulische Kreisläufe für das TriSolHP-System zusammen mit den Regulierungsprinzipien und Dimensionierungsregeln beschrieben. Der erste Kreislauf verwendet eine R290-WP sowohl für die Raumheizung (RH) als auch für die Produktion von Warmwasser (WW). Der zweite Kreislauf verwendet eine R744-WP für die WW-Produktion und eine R290-WP für die RH.

Die Leistungen des TriSolHP-Systems für verschiedene Gebäudetypologien (definiert in **Abschnitt 5**) wurden in **Abschnitt 6** simuliert. Die Ergebnisse zeigten, dass das System die Anforderungen an RH und WW von Mehrfamilienhäusern mit einem SPF, einschliesslich PV-Eigenverbrauch durch die WP, effektiv erfüllen kann, mit Werten zwischen 2,74 und 4,97. Das System übertrifft auch LW-WP-Systeme in Bezug auf Energieeffizienz und Emissionseinsparungen.

Die finanzielle Machbarkeit des TriSolHP-Systems wurde in **Abschnitt 7** bewertet. Die Ergebnisse zeigten, dass das System Wärmegestehungskosten (LCOH) zwischen 19 und 25 Rp./kWh hat. Dies ist geringfügig höher als der LCOH von LW-WP-Systemen, aber der Unterschied könnte durch steigende Stromkosten in der Zukunft ausgeglichen werden.

Das Diffusionspotenzial und das Dekarbonisierungspotenzial des TriSolHP-Konzepts wurden in **Abschnitt 8** für den Kanton Genf geschätzt. Die Ergebnisse zeigten, dass das System in 53% der Gebäude installiert werden könnte (entsprechend 30% der Energiebezugsfläche). Eine umfangreiche Verbreitung des TriSolHP-Systems könnte zu einer Verminderung der CO2eq-Emissionen um 26 und 51% des Gebäudebestands in Genf beitragen.

Insgesamt hat das TriSolHP-Projekt gezeigt, dass das System eine vielversprechende Alternative zu LW-WP für Mehrfamilienhäuser ist. Das System ist effizienter und umweltfreundlicher als LW-WP-Systeme und kann in einer Vielzahl von Gebäuden installiert werden.

Résumé

Le projet TriSolHP développe un nouveau système de chauffage pour les immeubles multifamiliaux qui associe un champ de collecteurs PVT (photovoltaïques thermiques) à des pompes à chaleur (HP) utilisant des réfrigérants naturels. Le système est conçu pour être plus efficace et respectueux de l'environnement que les pompes à chaleur traditionnelles à air (ASHP). Le PVT utilisé dans le projet a été optimisé pour être utilisé comme source de chaleur pour les pompes à chaleur.

La première phase du projet s'est concentrée sur la mesure des performances du collecteur PVT HP dans une chambre climatique. Les résultats ont montré que le collecteur peut capturer efficacement la chaleur ambiante, même lorsqu'il est recouvert de glace (voir **Section 2**).

Ensuite, des modèles numériques d'une pompe à chaleur classique (sub-critique, avec un réfrigérant R290) et d'une pompe à chaleur transcritique (avec un réfrigérant R744) ont été développés (voir **Section 3**). Les modèles ont été validés par rapport aux données expérimentales et utilisés pour évaluer les performances du système TriSolHP.

Dans la **Section 4**, deux circuits hydrauliques pour le système TriSolHP sont décrits, ainsi que les principes de régulation et les règles de dimensionnement. Le premier circuit utilise une pompe à chaleur R290 pour le chauffage des locaux (CL) et la production d'eau chaude sanitaire (ECS). Le deuxième circuit utilise une pompe à chaleur R744 pour la production d'eau chaude sanitaire et une pompe à chaleur R290 pour le SH.

Les performances du système TriSolHP pour diverses typologies de bâtiments (définies dans la **Section 5**) ont été simulées dans la **Section 6**. Les résultats ont montré que le système peut répondre efficacement à la demande de SH et DHW des immeubles multifamiliaux avec un SPF, y compris l'autoconsommation PV par la PAC, variant de 2,74 à 4,97. Le système surpasse également les systèmes ASHP en termes de performance énergétique et d'économies d'émissions.

La viabilité financière du système TriSolHP a été évaluée dans la **Section 7**. Les résultats ont montré que le système a un coût nivelé de la chaleur (LCOH) compris entre 19 et 25 ctsCHF/kWh. Cela est légèrement supérieur au LCOH des systèmes ASHP, mais la différence pourrait être compensée par l'augmentation des coûts de l'électricité à l'avenir.

Le potentiel de diffusion et le potentiel de décarbonation du concept TriSolHP ont été estimés dans la **Section 8** pour le canton de Genève. Les résultats ont montré que le système pourrait être installé dans 53% des bâtiments (correspondant à 30% de la surface de référence énergétique). Une large diffusion du système TriSolHP pourrait contribuer à une réduction des émissions de CO2eq comprise entre 26 et 51% du stock immobilier de Genève.

Dans l'ensemble, le projet TriSolHP a montré que le système est une alternative prometteuse aux ASHP pour les immeubles multifamiliaux. Le système est plus efficace et respectueux de l'environnement que les systèmes ASHP, et il peut être installé dans une grande variété de bâtiments.

Summary

The TriSolHP project is developing a new heating system for multifamily buildings that combines a PVT (photovoltaic thermal) collector field with heat pumps (HP) using natural refrigerants. The system is designed to be more efficient and environmentally friendly than traditional air-source heat pumps (ASHP). The PVT used in the project has been optimized to be used as a heat source for HP.

The first phase of the project focused on measuring the performance of the PVT HP collector in a climate chamber. The results showed that the collector can efficiently capture ambient heat, even when covered in ice (see **Section 2**).

Then numerical models of a classical (sub-critical, with R290 refrigerant) and a transcritical (with R744 refrigerant) HP have been developed (see **Section 3**). The models were validated against experimental data and used to assess the performance of the TriSolHP system.

In **Section 4**, two hydraulic circuits for the TriSolHP system are described together with the regulation principles and sizing rules. The first circuit uses a R290 HP for both space heating (SH) and domestic hot water (DHW) production. The second circuit uses a R744 HP for DHW production and a R290 HP for SH.

The performances of the TriSolHP system for a variety of building typologies (defined in **Section 5**) have been simulated in **Section 6**. The results showed that the system can effectively meet the SH and DHW demand of multifamily buildings with SPF including PV autoconsumption by the HP ranging from 2.74

up to 4.97. The system also outperforms ASHP systems in terms of energy performance and emissions savings.

The financial viability of the TriSolHP system were assessed in **Section 7**. The results showed that the system has a levelized cost of heat (LCOH) of between 19 and 25 ctsCHF/kWh. This is slightly higher than the LCOH of ASHP systems, but the difference could be offset by rising electricity costs in the future.

The diffusion potential and the decarbonation potential of the TriSolHP concept were estimated in **Section 8** for the Geneva canton. The results showed that the system could installed in 53% of the building (corresponding to 30% of the Energy Reference Area). A large diffusion of the TriSolHP system could contribute to a CO2eq emission reduction of between 26 and 51% of the Geneva building stock.

Overall, the TriSolHP project has shown that the system is a promising alternative to ASHP for multifamily buildings. The system is more efficient and environmentally friendly than ASHP systems, and it can be installed in a wide variety of buildings.

Main findings

- Experimental measurements with a PVT collector designed to be used as heat source for HP (WISC solar collector) have confirmed (1) the interest of this concept to **extract heat from ambient air** in the absence of irradiation, (2) the **moderate impact of ice formation** on the collector ability to capture ambient heat and (3) that the **current Solar Keymark numerical model is not able to reproduce accurately the wind effect** on WISC performances.
- **R744 HP** is **well suited for DHW production** provided that a high temperature difference is guaranteed between inlet and outlet of the gas cooler. R744 HP is not adapted for space heating. **R290 HP** exhibits **similar to higher COP** than classical HPs (i.e. R410A).
- TriSolHP systems have similar or higher $SPF_{grid.sys}$ (taking in to account PV electricity auto consumed by the HP) than ASHP system with a lower CO_{2eq} content per kWh of produced heat. The TriSolHP system heat cost is slightly higher than the ASHP heat cost. The TriSolHP concept is therefore an **attractive technology as alternative to ASHP for multifamily building**.
- An analysis based on the Geneva building stock has shown that 70% of the heated floor area could be heated with the TriSolHP system. In addition, the study estimates that TriSolHP implementation could contribute to a CO_{2eq} emission reduction of 26% to 51% for the Geneva building stock in 2040.

Contents

Abbreviations

ASHP	Air Source Heat Pump
COP	Coefficient of Performance
DHN	District Heating Network
DHW	Domestic Hot Water
EEV	Electronic Expansion Valve
ERA	Energy Reference Area
GHG	Greenhouse gas
HP	Heat Pump
HP	Heat Pump
HTF	Heat Transfer Fluid
HX	Heat Exchanger
IHX	Internal Heat Exchanger
PVT	Hybrid Photovoltaic and Thermal solar panel
R290	Propane refrigerant
R744	CO_2 refrigerant
SC	Sub-Cooling
SH	Space Heating
SH	Super-Heating (may also be Space Heating in other documents of this project)
SPF	Seasonal Performance Factor
WISC	Wind and/or infrared sensitive solar thermal collector

1 Introduction

1.1 Background information and current situation

Switzerland's building sector comprises 1.8 million structures, including 500,000 multi-family dwellings. Since 1990, the sector has achieved a remarkable 34% reduction in greenhouse gas (GHG) emissions. This decline is attributed to two key factors: enhanced average energy efficiency of buildings and the replacement of fuel oil with less carbon-intensive energy sources. Notably, heat pumps have been installed in nearly 20% of buildings as of 2018. However, fossil fuels remain the primary energy source for approximately 60% of the building stock. It's worth noting that Switzerland is among the European countries with the highest reliance on fuel oil for building space heating.

The Confederation wishes to accelerate the decarbonization of Switzerland in order to meet the objectives set by the Energy Strategy 2050 (SE2050). Regarding the buildings sector, the authorities propose to focus more on the reduction of greenhouse gas emissions and less on the reduction of specific final energy consumption. This change in philosophy is due to the fact that the current rate of building retrofits (<1%/year) alone is not sufficiently high to meet the GHG reduction targets of the SE2050. Consequently, the retrofitting effort should be coupled with a strong decarbonization of the building heating system and DHW production.

Heat pumps (HP) are an interesting and efficient technology for reducing greenhouse gas (GHG) emissions for heating and DHW production in existing multifamily buildings [1]. As good quality heat sources (geothermal, groundwater or lake/river water) are only available in specific locations, air-to-water heat pumps are often the only option for a renewable heat production system. In addition, the initial investments for air-to-water heat pumps are often much lower than geothermal HP. For these reasons, air-to-water heat pumps represent about 75% of the heat pumps installed in Switzerland [2]. Various programs to reduce GHG emissions in Switzerland are based on this observation. For example, the SIG (Services Industriels de Genève) recently launched a subsidy program for the installation of air-to-water heat pumps on existing multifamily buildings when replacing a boiler using fossil fuel in order to reduce GHG emissions for this category of buildings.

The potential of diffusion of air-to-water HP remains nevertheless limited in particular because of the noise pollution they cause. This can be particularly problematic in dense urban areas. In addition, the COPs remain low especially for buildings with high temperature heating systems and for buildings where heat consumption for the production of DHW is higher than that related to heating (recent buildings with high energy efficiency). Finally, synthetic refrigerants, which are widely used in heat pumps on the market, have a very high global warming potentials in case of leakage. A new legislation has been put in place to limit their use and eventually to eliminate them [3].

For these reasons, it is important to propose alternatives to the air-to-water HP to decarbonize the heating and the production of DHW in existing collective buildings. HP using solar thermal collectors as a heat source, is an attractive alternative that has been studied a lot during the last ten years. In this configuration, the solar thermal collector can operate at a temperature below ambient temperature maximizing solar heat production and allowing ambient heat absorption.

In recent years, different system architectures, coupling a solar thermal collector field with a water-to-water HP in series have been proposed. For example, the integration of an ice storage, at the level of the heat source, makes it possible to guarantee annual COPs similar to those of geothermal heat pumps. This has been demonstrated on several important collective buildings such as the building of the cooperative "la Cigale" in Geneva which was the subject of a P+D project of the SFOE [4]. This type of system is nevertheless disadvantaged by important initial investments, but also by the requirement of available volume close to the boiler room to install the ice storage. To remedy these limitations, systems coupling directly in series a solar thermal installation to a heat pump without buffer or ice storage have been deployed on new collective buildings such as the SolarCity project in Geneva. The performance of this installation has been monitored in the framework of a PhD thesis at the University of Geneva [5].

The conclusions of this study show that this type of system can be very interesting for recent buildings with high energy efficiency with COPs higher than air-to-water heat pumps. Nevertheless, the COP for the production of DHW by the heat pump remain relatively low. This can potentially be problematic for buildings where the heat demand is mainly for DHW production. Finally, this study has also shown that these systems can be deployed even on existing collective buildings without renovation with annual system COPs of about 3 provided that the ratio of roof area to energy reference area is more than 0.2 to 0.25 m^2/m^2. This limits the diffusion of this concept to four-story buildings.

The systems coupling a solar thermal installation to a HP in series remain an attractive alternative to the air-to-water HP because they eliminate the noise problem while having equivalent or better performances. Nevertheless, those systems require large roof surfaces and have low COPs for the production of DHW, especially in winter restricting its diffusion to low-rise buildings. The concept proposed within the framework of the TriSolHP project can potentially allow to reduce the necessary roof surface while improving the COP in particular for the production of DHW.

1.2 Purpose of the project

The TriSolHP project objective is to develop a modular system for heating and DHW production comprising a PVT collector field coupled in series with a HP system using natural refrigerant (propane/R290 and/or carbon dioxide/R744). The PVT collectors allow to densify the use of the roofs by producing photovoltaic electricity, solar heat and by absorbing heat from the ambient air (tri function). In order to minimize the required PVT collector surface, the TriSolHP project focuses in particular on PVT collectors with very good heat exchange coefficients with the ambient air (see ***Figure 2*** below). The use of two complementary heat pumps allows to maximize the range of usable heat source temperature but also to produce DHW with good COP. Finally, the use of natural refrigerants is compatible with the desire to drastically reduce the use of synthetic refrigerants with significant global warming potentials. ***Figure 1*** below presents the TriSolHP concept schematically.
The R744 heat pump used in this project is a commercially available heat pump. The R290 HP is a pilot HP developed by Professor Da Riva of the HEIG-VD [6]. Within the framework of the TriSolHP project, these two heat pumps will be used to calibrate and validate two numerical models. Those numerical models will then be used to simulate the performance of the complete system.

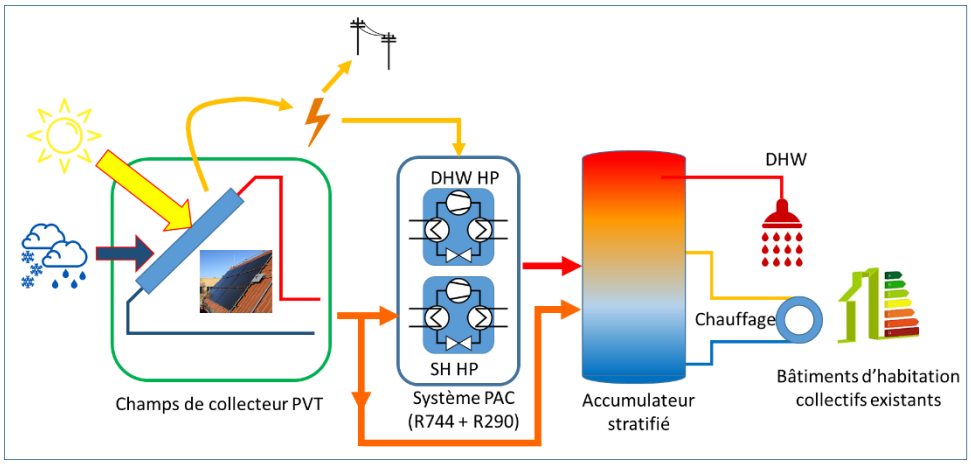

Figure 1 Schematic diagram of the TriSolHP concept (note: the hydraulic integration of this concept is shown very schematically)

As mentioned above, one of the objectives of the TriSolHP project is to maximize the utilization of PVT collectors by operating them below ambient temperatures. In order to effectively operate the PVT collector array under those conditions, it is important to use PVT technology that has been optimized to

absorb heat from the ambient air by convection. The company Consolar in collaboration with Energie Solaire SA (now Soltop Energie SA) has recently introduced on the market a PVT collector that is equipped with fins on the collector back side that increase the heat exchange area by a factor of 10 compared to the PV module area (see ***Figure 2*** below). This concept has clearly been developed to operate in series with a heat pump (PVT collector used as heat source). The amount of heat per unit area that these modules can absorb from the ambient air is therefore much higher than an unglazed flat plate collector (see ***Figure 3*** below).

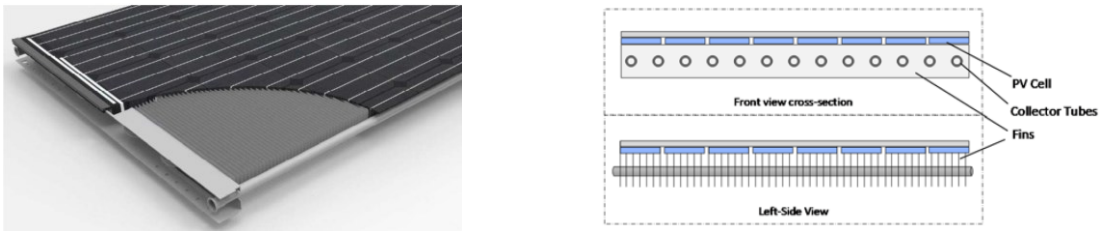

(a) (b)

Figure 2 (a) Exploded view and (b) cross-section of Consolar's Solink collector showing the location of the fins on the back side [7]

A comparison of the specific heat output as a function of the difference between the average collector temperature and the ambient temperature has been made between different technologies of simple solar thermal collectors and PVT (see ***Figure 3*** below). This figure clearly shows that for low irradiation (winter heating season), the heat density that Solink PVT can provide is much higher than other technologies. This should make it possible to reduce the surface area needed to extract the thermal power required to feed a heat pump evaporator. With this new generation of PVT collectors, it should therefore be possible to equip existing buildings with more than 4 floors with a HP using a PVT collector field as heat source.

One of the TriSolHP project objectives is to confirm that this is indeed the case but also to specify how these PVT collectors should be installed on the roof to maximize their performance. In addition, the impact of snow and frost formation during the heating season on collector performance has also been investigated.

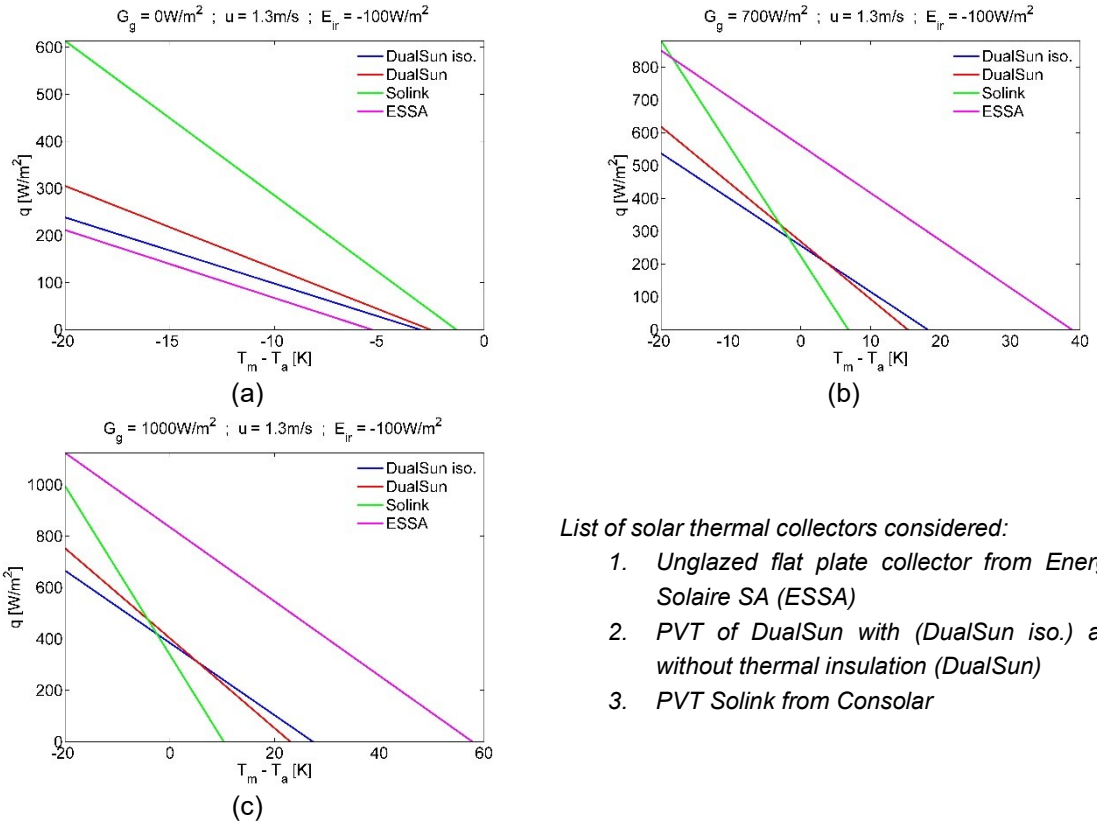

List of solar thermal collectors considered:

1. *Unglazed flat plate collector from Energie Solaire SA (ESSA)*
2. *PVT of DualSun with (DualSun iso.) and without thermal insulation (DualSun)*
3. *PVT Solink from Consolar*

Figure 3 Thermal power density for different single and hybrid solar thermal collector (PVT) technologies as a function of the difference between the average collector temperature and the air temperature calculated according to ISO 9806:2017 with radiative losses of 100 W/m2 (clear sky)

As mentioned above in the description of the TriSolHP heating system concept, the combination of an R744 heat pump for DHW production with an R290 heat pump for heating allows the range of effectively usable heat source temperatures to be maximized. This combination also guarantees good COPs over a wide range of heat source temperature. The complementarity between these two types of HP is illustrated in ***Figure 4*** below, which gives the COP of an R744 HP and an R290 HP as a function of the heat production temperature with a heat source at -10°C (winter operating conditions). In these conditions, the R290 HP is more efficient than the R744 HP up to a temperature of ~40-50°C. Beyond that, the R744 HP is more efficient (production of DHW or heating of buildings with high temperature heat emitters). Note that this figure also illustrates the importance for R744 HP to guarantee the lowest possible return temperatures at the gas cooler. By reducing the return temperature on the gas cooler from 30 to 10°C, the COP increases from 2.5 to 3.2 for a production temperature of 50°C. This shows that it is important to develop hydraulic integration schemes to ensure a large temperature difference at the gas cooler of the R744 heat pump. It should be noted that for buildings using high temperature heat emitters, it could be possible to produce heat for DHW and heating via a R744 heat pump alone. It is one of the objectives of the TriSolHP project to identify the building typologies whose heat demand allows to guarantee a large temperature differential. The heat demand of these types of buildings could in principle be met using an R744 heat pump while maintaining good performance.

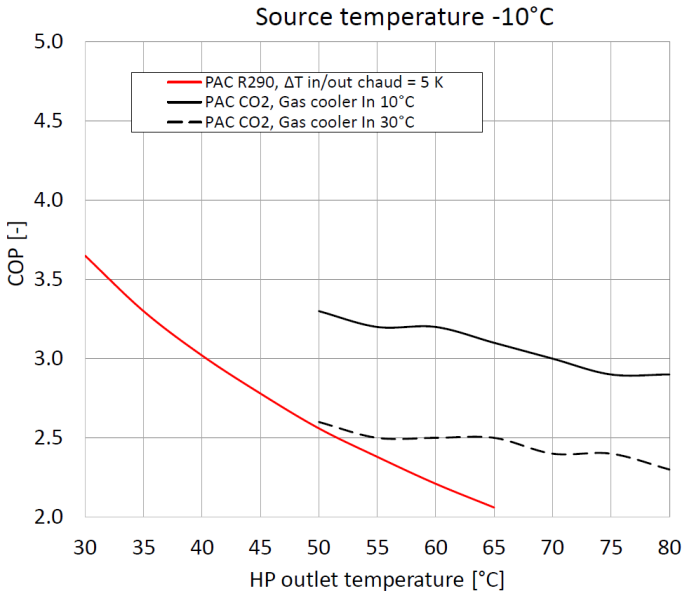

Figure 4 Comparison of the COP of a R744 HP (manufacturer's data for Enex Srl GeoHeat18 heat pump) and R290 (theoretical model) for a heat source temperature of -10°C as a function of the heat production temperature and for a return temperature on the gas cooler of 30 and 10°C

1.3 Objectives

The overall objective of the TriSolHP project is to develop a modular system coupling a PVT collector field with a heat pump system to satisfy the heating and DHW needs of different types of existing collective buildings with a COPa of 3.5. This modular system should require less than 0.25 m^2 of PVT surface per m^2 of heating space to be adapted to four-story and more building. Two different heat pump system are investigated. The first one is based on a R290 HP which provides heat for space heating and DHW production. The second one consists of a R744 HP for DHW production coupled with a R290 HP for space heating. The regulation of the system will be optimized in order to maximize the self-consumption of the electricity produced by the PVT collectors. The performance of this concept will be compared to the performance of a monovalent air-to-water heat pump operated in the same conditions.

In order to achieve this overall objective, the following intermediate objectives must be met:

1. Definition of hydraulic integration schemes as well as a sizing and regulation strategy of the system components for different building typologies (see **Section 4**)
2. Numerical modeling of the PVT collectors and the heat pump system with validation through experimental measurements (taking into account the formation of frost and water condensation on the PVT collectors) (see **Section 2**)
3. Energy and financial performances of the TriSolHP concept for different multifamily building typologies and comparison with an air-to-water heat pump (see **Section 6 & 7**)
4. Environmental performances of the TriSolHP concept compared to an air-to-water heat pump and estimation of the decarbonization potential of this concept (see **Section 6 & 8**)

2 PVT collectors - Performance measurements and numerical model

2.1 Solink PVT climatic room tests

To facilitate the adoption of the most convenient model for the performance simulations foreseen in the framework of the present project, a single Solink panel (depicted in **Figure 5**) placed under artificial environmental conditions of temperature, humidity and air velocity has been extensively measured in a climatic room hosted by the IGT Institute at the HEIG-VD premises in St.Roch à Yverdon-les-Bains. During those tests, the PVT collector was always operated without irradiation (dark conditions).

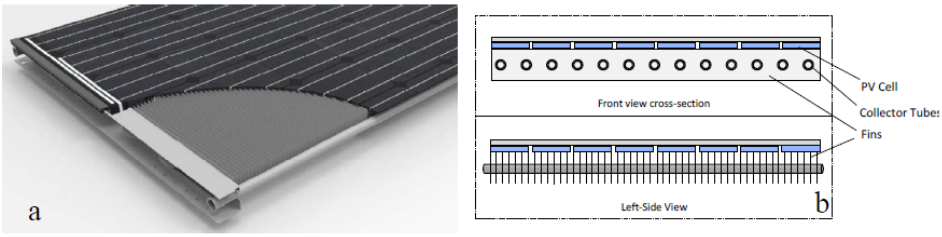

Figure 5 Solink PVT collector images, taken from [8]

2.1.1 Test set-up

The layout of the experimental set-up adopted in the climatic room is shown in **Figure 6**: a Solink PVT-solar collector was placed in the middle of an airflow, characterized by a series of probes.

Apart from the airflow speed, correlated to the fans power level, the climatic conditions in the climatic room were monitored by 4 sensors measuring the air temperature and by 2 sensors acquiring relative air humidity. A heat transfer fluid (a mixture of water and ethylene glycol at 40 % in volume) was circulated through the collector during the tests to quantify the corresponding collector thermal power through the measurement of the heat gain and the flow rate of the heat transfer fluid (HTF).

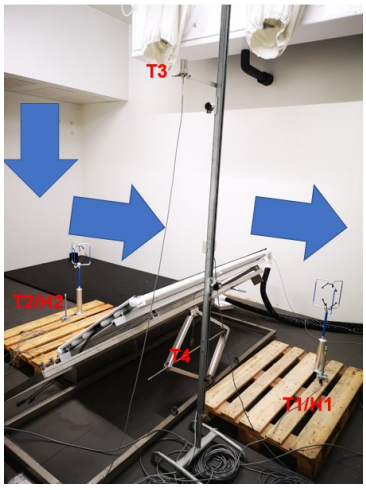

Figure 6 Test setup adopted in the climatic room and forced air ventilation mean direction over the collector.

To measure its performance once stable environmental conditions have been reached in the climatic room, a 40% v/v glycol mixture is circulated through the collector while measuring the volumetric flow rate of the heat transfer fluid (HTF) and its temperature at the circuit inlet and outlet. Environmental conditions are characterized by measuring the air speed over the collector pane at a distance of 5 cm and temperature and humidity of the circulating air inside the climatic room (see **Figure 6**). **Table 1** shows the main features of the measurement equipment together with their accuracy and the relevant process-control-related uncertainties.

Table 1 Measurement sensor accuracy and environmental control uncertainties.

Measurement	Sensor	Unit	Sampling, in [s]	Uncertainty @ 3σ	Process stability @ 3σ
Air temperature, T_{air}	pt100 Class B	°C	5	± 0.5 K	± 0.75 °C
Air relative humidity, H_{air}	combined temperature / humidity probe	%	5	± 10 %	± 10%
HTF temperature at inlet / outlet: T_{in}, T_{out}	pt100 1/3 DIN	°C	25	± 0.1 K @ 0°C	± 0.03 °C
HTF flow rate, $\dot{w}$	Khrone Optiflux 1050	l/h	25	± 1.5% @ 50 l/h ± 0.75% @ 125 l/h	± 1 l/h (@ +/-3 σ)

2.1.2 Air flow measurements

The airflow velocity over the collector was correlated to the rotation speed of the climatic room fans, as shown in **Figure 7**.

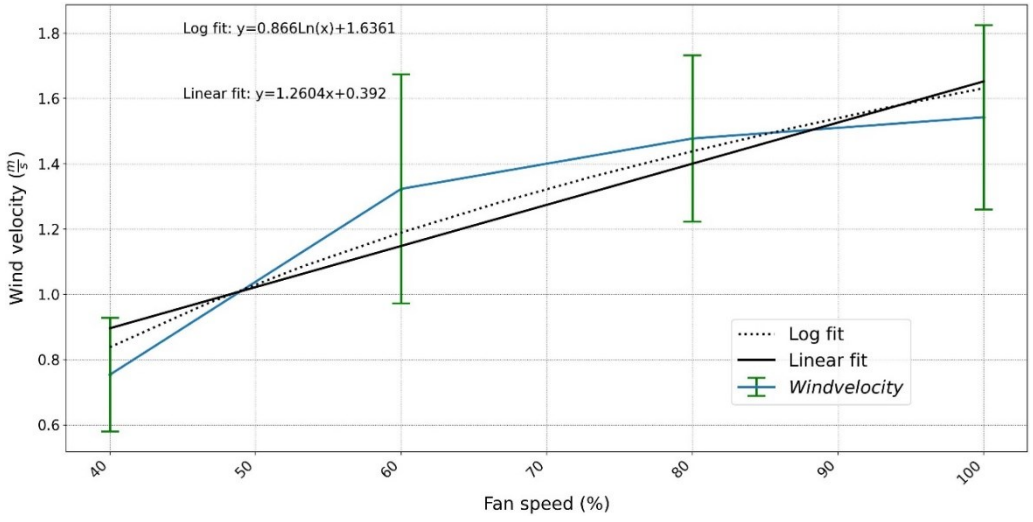

Figure 7 Results of the airflow velocity measurements performed over the collector plane.

Measurements were also performed to establish the homogeneity of the airflow velocity over the collector pane, which is quite limited, as shown in **Figure 8**. It is evident that the airflow velocity was higher over the left side of the collector front side.

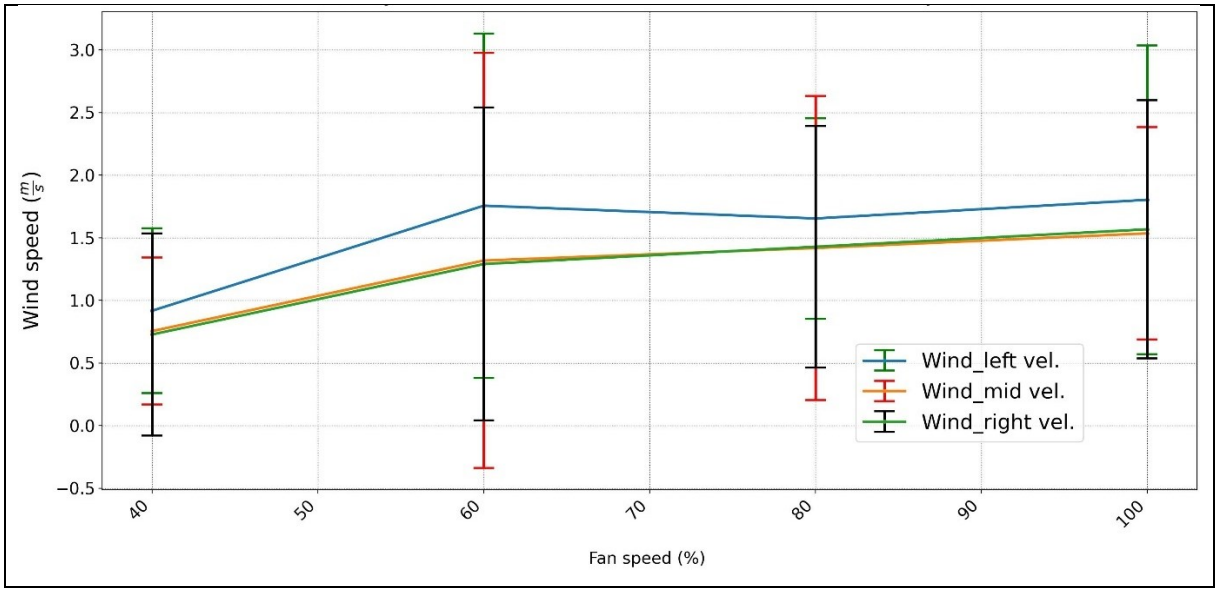

Figure 8 Air flow homogeneity across the collector plane: the air flow velocity over the collector is higher on one side of the climate room.

A comparison with the test conditions foreseen by most of the standards (see **Figure 9**) helps concluding that some conditions are far from ideal.

In the analysis that followed, the inhomogeneity of the airflow was neglected and its velocity parallel to the collector plane estimated with the following linear relationship for the average wind speed:

$$v = 1.26 * rpm + 0.4 \qquad \text{Eq. 1}$$

where:

- v is the air flow velocity, in [m/s];
- rpm is the fan speed, in [%].

The impact of differences related to the test conditions adopted in the climatic room with respect to those required during a certification performance test will be addressed in the future, possibly extending the test conditions to those required from standards. It needs to be stressed, nevertheless, that the Solink PVT collector performance of interest in the conservative design of a heat source would corresponds to environmental conditions with minimal air flow over the collector (i.e., at minimal thermal performance) rather than at conditions when the heat exchange between the collector and the environment is favorable (i.e., with high air flow).

Thermal performance	EN 12975	Collector B, pre-conditioning 5h with G > 700 W/m², diffuse fraction < 30 %. Steady State or Quasi-Dynamic Testing.
	ISO 9806-1	Collector A, tilt-angle latitude ± 5° but not less than 30°, diffuse fraction < 20 %. Collector area: 0,1 % accuracy, minimum global irradiation G >800 W/m². Wind speed 2 - 4 m/s. Volume flow 0,02 kg/(s*m²), max. drift +/- 10 %, deviation mass flow ± 1%, Deviation Irradiation ± 50 W/m². Deviation T_{amb} ± 1 K, deviation inlet temperature ± 0,1 K. T_{out}-T_{in} >1,5 K, T_m-T_{amb} at η_0 ± 3K. Conditioning phase minimum 15 min and measurement phase minimum 15 min.
	ISO 9806-2 [2]	Collector A according to ISO 9806-1
	SRCC Standard 100	Collector A, 5 minutes measurement points / 0,07 g/(s*m²) according to ISO 9806-1
	CAN/CSA-F378-87	Collector A according to ANSI/ASHRAE
	ANSI/ASHRAE standard 93	Minimum global irradiation G >790 W/m², deviation irradiation ± 32 W/m², diffuse fraction < 20 %. Max. T_{amb} 30 °C. Wind speed 2,2 – 4,5 m/s, volume flow 0,02 g/(s*m²). Deviation inlet temperature ± 2% or 1°C Deviation mass flow ± 2% or 0,000315 l/s. Deviation T_{amb} ± 1,5 K. Conditioning phase 2*times constant or minimum 10 minutes. Measurement phase minimum 0,5*times constant or minimum 5 minutes.
	AS/NZS 2735.1	Collector A, tilt-angle latitude ± 5° but not less than 30°, diffuse fraction < 20 %. Collector area: 0,1 % accuracy, minimum global irradiation G >800 W/m². Wind speed 2 - 4 m/s. Volume flow 0,02 kg/(s*m²), max. drift +/- 10 %, deviation mass flow ± 1%, Deviation Irradiation ± 50 W/m². Deviation T_{amb} ± 1 K, deviation inlet temperature ± 0,1 K. T_{out}-T_{in} >1,5 K, T_m-T_{amb} at η_0 ± 3K. Conditioning phase minimum 15 min and measurement phase minimum 15 min.

Figure 9 Test conditions foreseen by several test standards for solar thermal collectors.

During 2023, the air field around the collector placed inside the climatic room was better characterized thanks to the adoption of anemometers placed on the collector pane. **Figure 10** and **Figure 14** show, respectively, one of the adopted collector setups, with the position of the measurement instrumentation, and the air speed theoretical distribution based on 2D FEM modeling [9].

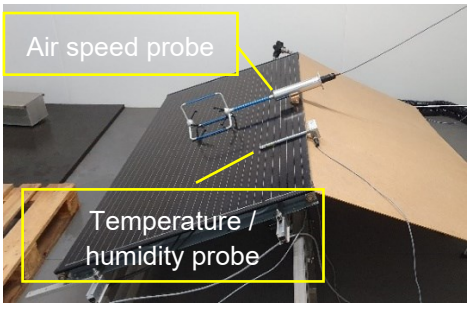

Figure 10 Measurement layout for an east-west structure upwind oriented inside the climatic room, showing the probe position.

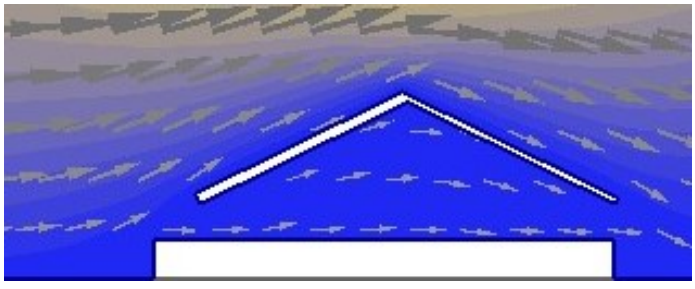

Figure 11 2D visualization of the air flow pattern around the collector when installed on an east-west structure.

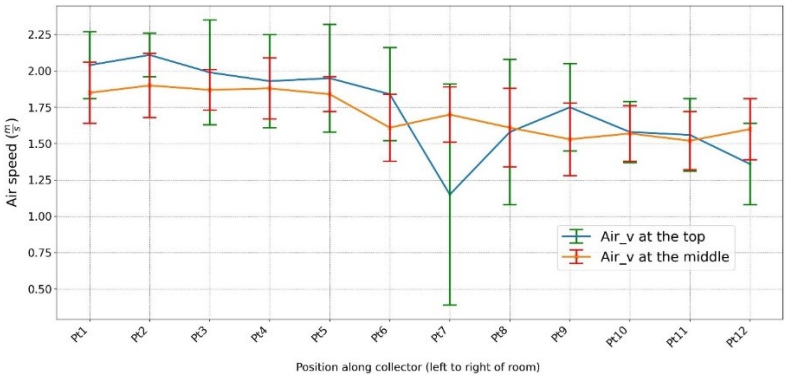

Figure 12 measured speed distribution of the air flowing over the collector pane.

Figure 12, on the other hand, shows the measured speed distribution of the air flowing over the collector pane, while **Figure 13** shows the speed of the air flow in the middle of the collector pane as a function of the control frequency of the room fan rotors.

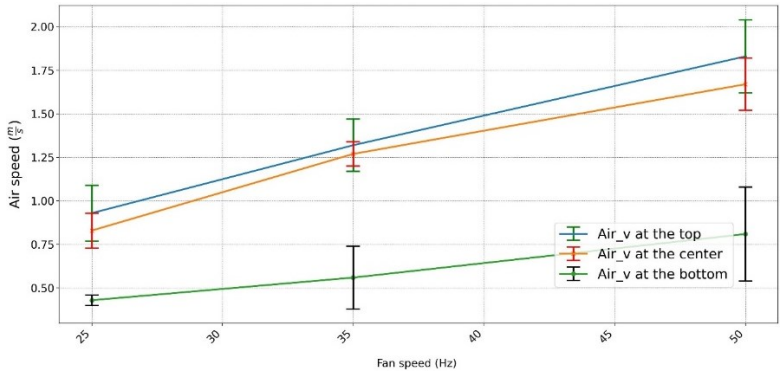

Figure 13 speed of the air flow in the middle of the collector pane as a function of the control frequency of the room fan rotors.

2.1.3 Testing conditions

During the measurement campaign, tests were carried out under several environmental conditions and with different collector layout and orientation:

- To evaluate the **influence of ice formation on the collector performance**, the temperature inside the climatic room was kept at 0°C, while the HTF inlet temperature and the air relative humidity were maintained at -10°C and over 85%, respectively. No water condensation was allowed, while the circulating HTF was kept constantly at around 50 l/h and the collector was installed on a standalone structure for installation on a flat roof with a tilt of 45° and oriented upwind;
- To evaluate the **impact of air speed on the collector performance,** measurements were carried out again on the standalone structure oriented upwind but with a 20° tilt, for air at 15 °C and 40-50% of relative humidity, an HTF inlet temperature of 5°C and a flow-rate of 78 l/h;
- To evaluate the impact of **collector orientation and type of installation**, the performance was measured for 3 installation layouts (standalone structure with 20° tilt, east-west structure at 25° tilt and slanted roof integration) and for 4 orientations (0°, 45°, 90° and 180°), as shown in **Figure 14**.

2.1.4 Data analysis

For the current study, measurement data were treated and analyzed under python environment, while to compare measurement data to simulation models a dynamic model was implemented under TRNSYS environment by adopting the “Type 203” [10], a model for uncovered liquid-cooled collectors which allows to simulate their performance based on model parameters derived from certification tests.

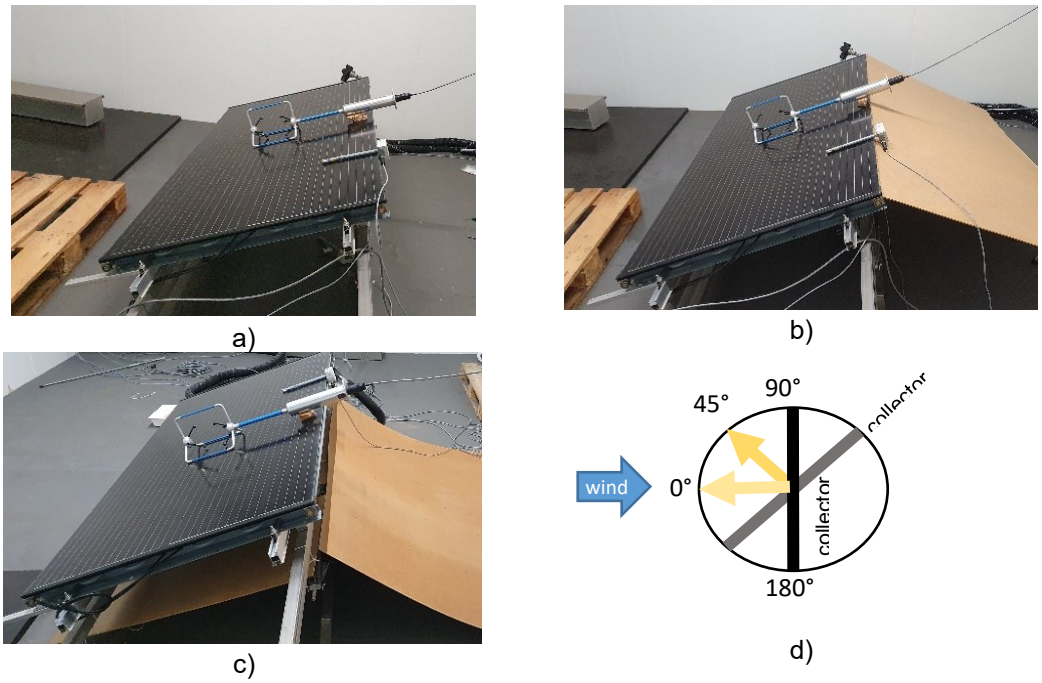

Figure 14 Collector layout and orientation tested during measurements: a) standalone structure at 25° tilt; b) east-west structure at 25° tilt; c) slanted roof integration; d) tested collector orientation (i.e., when at 180°, the air flows over the rear of the collector first).

From acquired data, the following indicators were calculated:

1. Collector thermal power (in [W]):

$$P = \dot{w} * \rho_{HTF} * cp_{HTF} * (T_{out} - T_{in}) + (Mcp)_{eq} \frac{\partial \overline{T_{cll}}}{\partial t} \quad \text{Eq. 2}$$

where:

- $\dot{w}$ is the HTF volume flowrate in [m³/sec]
- ρ_{HTF} (in [kg/m³]) et cp_{HTF} (in [kJ/kg/K]) are density and heat capacity of the HTF, respectively;
- $(Mcp)_{eq}$ is the equivalent heat capacity of the collector including the HTF content;
- $\overline{T_{cll}}$ is the mean temperature of the collector, calculated as

$$T_{cll} = \left(\frac{T_{in} + T_{out}}{2}\right)$$ Eq. 3

2. Mean logarithmic temperature difference in the collector (in [K]):

$$dTlm_{cll} = \frac{(T_{air} - T_{in}) - (T_{air} - T_{out})}{ln\left(\frac{(T_{air} - T_{in})}{(T_{air} - T_{out})}\right)}$$ Eq. 4

3. The collector equivalent "thermal conductance", expressed in $[\frac{W}{K}]$:

$$U_{cll} = \frac{P}{dTlm_{cll}}$$ Eq. 5

2.1.5 Measurement results

To visualize and compare measurement data for the different tests with their corresponding model estimations, the collected heat flux $\dot{q}_{\mathrm{cll}}$, expressed in [W/m^2], and the heat transfer capacity referred to the collector front area U_{cll}, in [W/m^2/K], have been calculated for the measurement intervals for which the collector temperature was stationary according to the following equations:

$$\dot{q}_{\mathrm{cll}} = \frac{\dot{m}c_p}{A_G}(T_{\mathrm{out}} - T_{\mathrm{in}})$$ Eq. 6

$$U_{\mathrm{cll}} = \frac{\dot{q}_{cll}}{(\vartheta_a - \vartheta_m)}$$ Eq. 7

where $\dot{m}$ in [kg/s] is the mass flow rate trough the collector, c_p is the HTF specific heat, in [J/kg/K], A_G is the collector pane gross area, in [m^2], T_{in} and T_{out} are, respectively, the HTF temperature at the inlet and at the outlet of the PVT collector, in [K], while ϑ_a and ϑ_m are the ambient and the mean collector temperatures in [K], respectively.

2.1.6 Ice formation test

During the ice formation test, the test room temperature was kept below zero in presence of high humidity (left pane in **Figure 15**). The extracted thermal power decreased during the test as the collector became more and more covered in ice, diminishing its heat transfer with the environment (right pane in **Figure 15**). Due to the ice formation, i.e., the PVT collector under test went from featuring a U value of more than 24 W/m^2/K to less than 19 W/m^2/K (+/- 2 W/m^2/K at 1 σ), featuring a 25% reduction. Given the extreme conditions at which the collector has been exposed together with the test duration, it can be concluded that the collector is capable of delivering a relevant fraction of the available environmental energy even when covered in ice. The influence of ice formation on the back of the Solink collector was also discussed in a paper presenter at 2023 CISBAT conference in Lausanne [11].

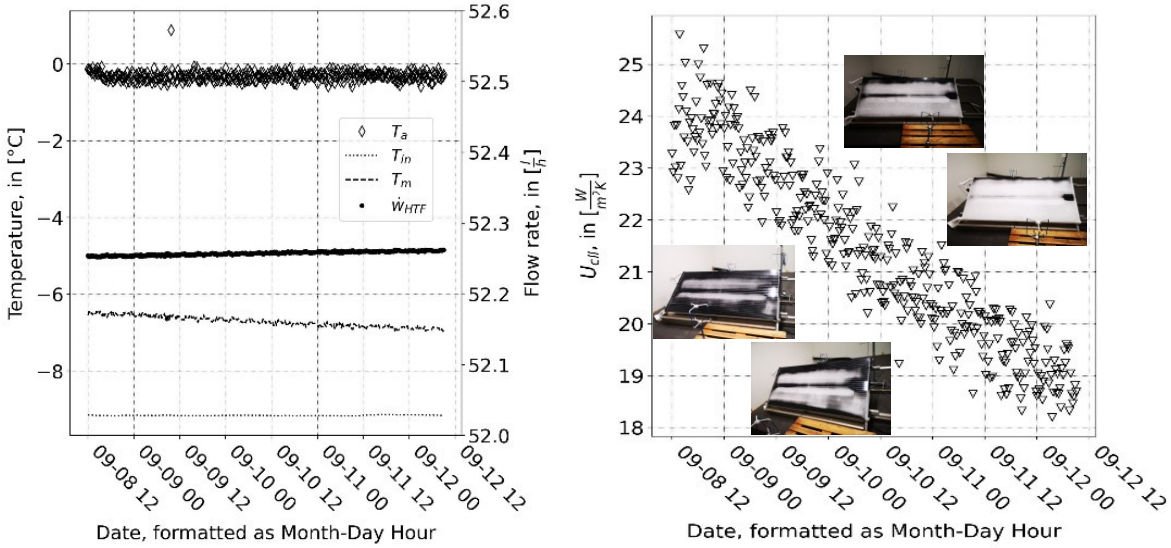

Figure 15 Test temperatures and flow rate (left) and overall heat exchange coefficient of PVT (right) during the ice formation test performed between the 8 and 12 of September (09-08 to 09- 12).

2.2 Influence of air velocity

The performance of the PVT collector was also tested in presence of varying air flow but with no irradiance to derive an insight on the impact of the air flow velocity over the overall heat exchange coefficient of the collector. **Figure 16** shows, as expected, that the energy transfer from the environment increases with increasing air velocity, as the heat exchange rate between the HTF in the collector and the external air increases.

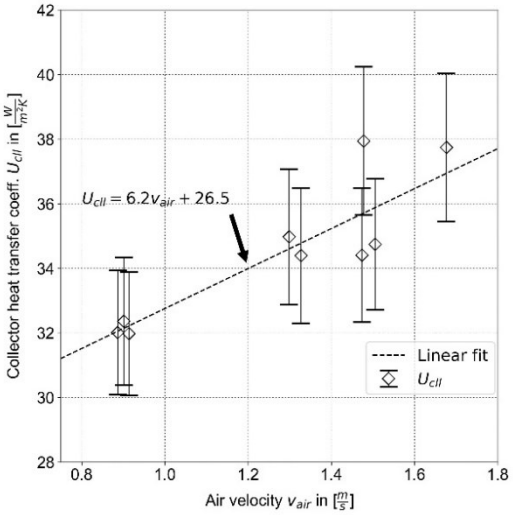

Figure 16 Dependence of the overall heat exchange coefficient from the air velocity measured on the collector front.

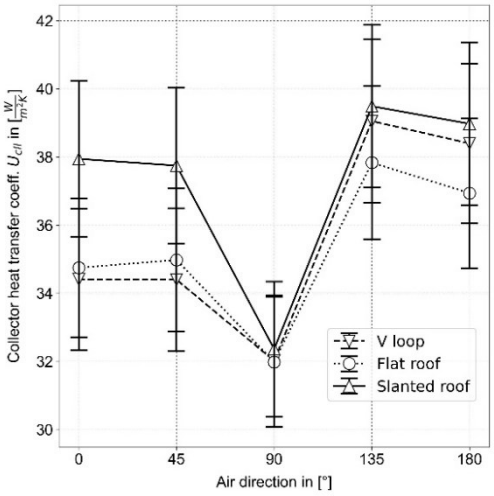

Figure 17 Dependence of the overall heat exchange coefficient on the air flow/PVT collector orientation

2.3 Influence of installation layout and collector orientation

As the air flow over the collector rear and front is affected by the installation layout, measurements were carried on 3 types of installations: a standalone support for flat roof installation; a structure for west-east installation; an integration layout for slanted roofs. In each case, 5 different orientations with respect to the air stream were tested, where 0° indicated that the air stream was over the front and 180° over the rear of the collector. As shown in **Figure 17**, the transfer coefficient between PVT collector and the environment increased with increasing incidence over the rear fins, with a minimum in every tested case happening when the air-flow is perpendicular to the fins over the back of the collector (i.e., 90° orientation). This arrangement, in fact, reduces considerably the air flow in the rear fin channels, hindering the exchange of the collector with the air. When the air stream arrives from the front, on the other hand, the air-is able to penetrate under the collector, increasing air turbulence on its back, especially in the case of roof integration for which an air-foil effect increases the air turbulence over the rear fins. For flat roof installation, instead, as the air-foil effect is reduced by geometry, the increase in exchange rate remains limited.

2.4 Solink PVT collector modelling

2.4.1 Reference model parameters

In literature, there exists three sets of performance model parameters for the Solink PVT panel manufactured by Consolar which are shown in **Table 2**:

- SET1: a first solar keymark performance measurement, performed on the 20.03.2019 by the ITW institute at the University of Stuttgart (license no 011-7S2894 P, 2019);
- SET2: a second SK measurement performed on the 23.03.2021 by the IGTE, the same institute under a new name, on the same PVT model (this latter substitutes the first SK measurement) (license no 011-7S2894 P, 2021);
- SET3: a field-test measurement performed by the ISFH and IGTE in 2019 on the same first-generation collector used in SET1 (see [8]).

Table 2 Solar Keymark model parameters set available in literature.

SET ID	**SET1**	**SET2**	**SET3**	**Units**
Model source	SK 16.01.2019	SK 23.03.2021	IGTE/ISFH	
$\eta_{0,b}$	0.468	0.137	0.532	
b_1	22.99	84.35	19.08	$W/m^2/K$
b_2	7.57	22.03	3.69	$J/m^3/K$
b_u	0.144	0.810	0.126	s/m
$(Mc_p)_{eq}$	26.5	41.58	26.5	kJ/K

To asses, which model offers a better reliability for the simulations foreseen in the current project, a simple TRNSYS model of the measurement setup realized in the climatic room has been implemented. By comparing the output of the same model with different parameters, one can judge which set in **Table 2** is the best.

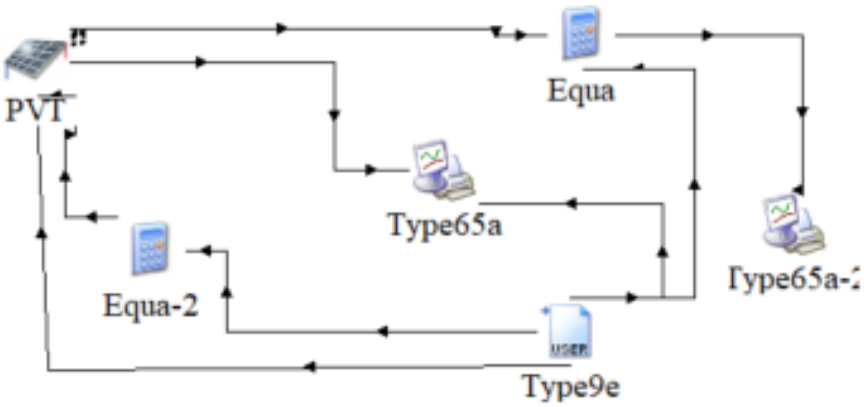

Figure 18 Layout of the TRNSYS simulation model adopted to validate the performance parameters to use in the present study.

2.4.2 TRNSYS model

A simple TRNSYS model, shown in **Figure 18**, was implemented in order to compare measurements to simulations based on several performance parameters. In particular, the TRNSYS model has been built around type 203, developed by the ISFH Institute of Hamelin in Germany. This “type”, a model of an unglazed photovoltaic-thermal solar collector, was originally validated based on roof test measurements and a measurement in a pilot plant over a period of one year (see [12], [13]).

By simulating the measurement setup adopted in the climatic room measurements, it is straightforward to compare the different parameter sets against the measurement performed in the climatic room.

Figure 18 shows the model used for calculations: the type 203 is used to process measurement data related to the environmental conditions in the climatic room, which are read by type 9e from an external file. Type 65a allows visualizing and saving simulation results, in particular the collector outlet temperature and its thermal power, for post-processing in a Jupyter-Lab Notebook.

Type 203 needs a series of inputs to model a PVT collector performance. Measurement data were used to provide the following inputs:

- environmental conditions (air temperature, air humidity, airflow velocity);
- process conditions (HTF inlet temperature, flowrate, thermodynamic properties);
- no irradiance on collectors;

while model parameters were introduced directly in the type 203 based on **Table 2**.

2.4.3 Comparison results and choice of model parameters

Figure 19 and **Figure 20** show the comparison between the measured collector overall heat transfer U and the simulated ones. It is evident how the new Solar Keymark certificate, issued in 2021, overestimates the parameter by a significant amount (more than 50%), while parameters derived from the preceding Solar-Keymark certificate (SK1, issued in 2019) and from the field test at the ISFH underestimate it by more than 20 and more than 40%, respectively. The parameters from the SK1 were hence chosen for implementation in the final system-wise simulations.

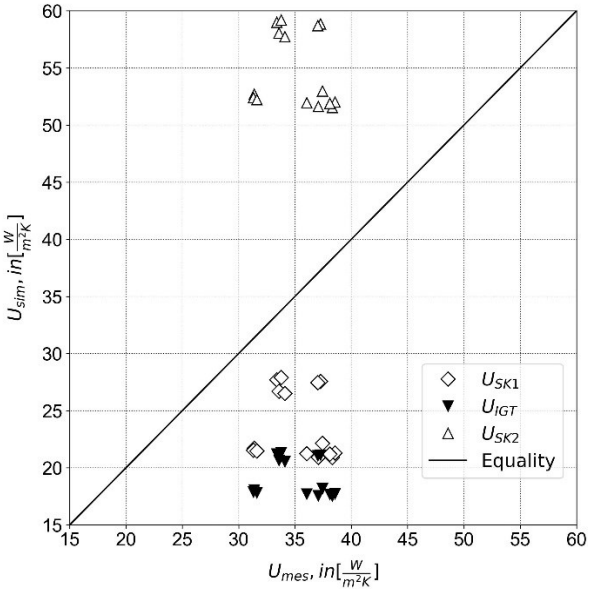

Figure 19 Simulated heat transfer capacity as a function of measured heat transfer capacity with the different Solar Keymark parameters sets given in **Table 2**

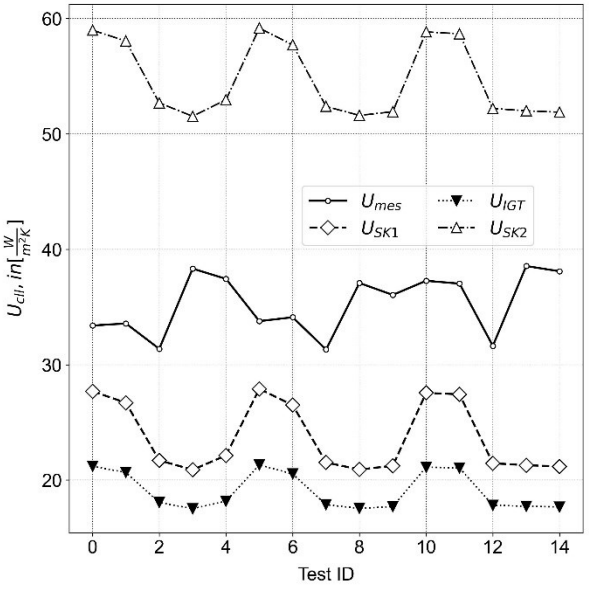

Figure 20 Comparison between measured and simulated heat transfer capacity with the different Solar Keymark parameters sets given in **Table 2**

The comparison of the model output with the measurements have been discussed in a paper presenter during the CISBAT conference in Lausanne in September 2023 [11]. One of the main conclusions of this paper is that the current Solar Keymark numerical model cannot reproduce accurately the effect of winds speed and direction on the efficiency production of WISC collector. This new family of solar thermal collector are more and more popular especially for applications with HP where they can act as heat source.

3 Heat pump numerical model description and validation

3.1 Introduction and targets

A python code for the theoretical modelling of vapor compression thermodynamic cycles has been developed by the Institute of Thermal Engineering IGT (now “Institute of Energies” IE), HEIG-VD. This model has been successfully implemented in previous research projects as a tool for the design of innovative Heat Pumps (HP) (ex. high-evaporating-temperature and low-charge n-butane HP, OFEN project HEAT/LOCH [6]) as well as a tool for the analysis of experimental measurements (see **Figure 21**).

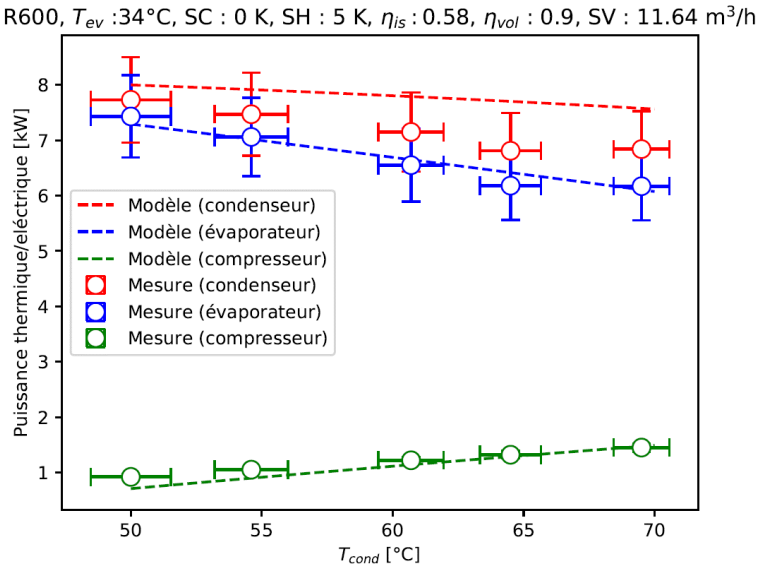

Figure 21 Example of comparison of the theoretical model against experimental data [6]

The code has been updated in order to take into account the use of propane (R290) or carbon dioxide (R744) as refrigerants. In particular, the need for a transcritical cycle when using R744 in HP, required a major modification of the code, since the control strategy and COP optimization are fundamentally different from the ones required by a classical (sub-critical) cycle.

The main targets in the framework of the present project are:

- Providing a realistic simplified model of heat pumps COP and heating capacity to be implemented in the TRNSYS simulations of the full system;
- Capturing the influence of the operating conditions (mainly temperatures at the heat source and the heat sink) on the thermal performance of the HP;
- Capturing the fundamental differences between the classical (sub-critical) thermodynamic cycle of R290 and the transcritical cycle of R744 in order to determine the conditions for optimal exploitation of each technology;
- Providing reliable results based on technical data of components currently available in the market (heat exchangers and compressors) without necessarily sticking to the datasheet of a specific HP manufacturer, thus being also able to evaluate the performance outside the range of nominal operating conditions;

- Providing a framework for a “fair” comparison between different refrigerants and cycles.

3.2 Theoretical model of classical (sub-critical) cycle

The modeling of the classical (sub-critical) cycle is based on the simplest possible machine configuration (see **Figure 22**) composed by:

- A single-stage compressor (1→2);
- A condenser (2→3) working with no or negligible outlet subcooling (SC);
- An Electronic Expansion Valve (EEV) (3→4) controlling the superheating (SH) at evaporator outlet;
- A dry evaporator (4→1).

Despite being the simplest possible machine configuration, this is what is commonly used in the vast majority of HPs available in the market for SH and domestic DHW production. The use of a more complex refrigeration cycle (ex. double-staged) would not be justified in terms of HP manufacturing cost and control complexity as compared to the energy efficiency improvement achievable, mainly because of the low heat-source to heat-sink temperature difference required in this kind of applications (in the order of ~35 K for nominal operation of space heating with floor heating up to maximum ~65 K for DHW production).

For the sake of simplicity, the use of an internal heat exchanger (IHX) has not been taken into account in this model. Despite from a theoretical point of view its use is supposed to increase the COP of the cycle, its influence on the overall HP efficiency is much less relevant as compared to the ones given by the temperatures of the heat sources and the efficiency of the compressor.

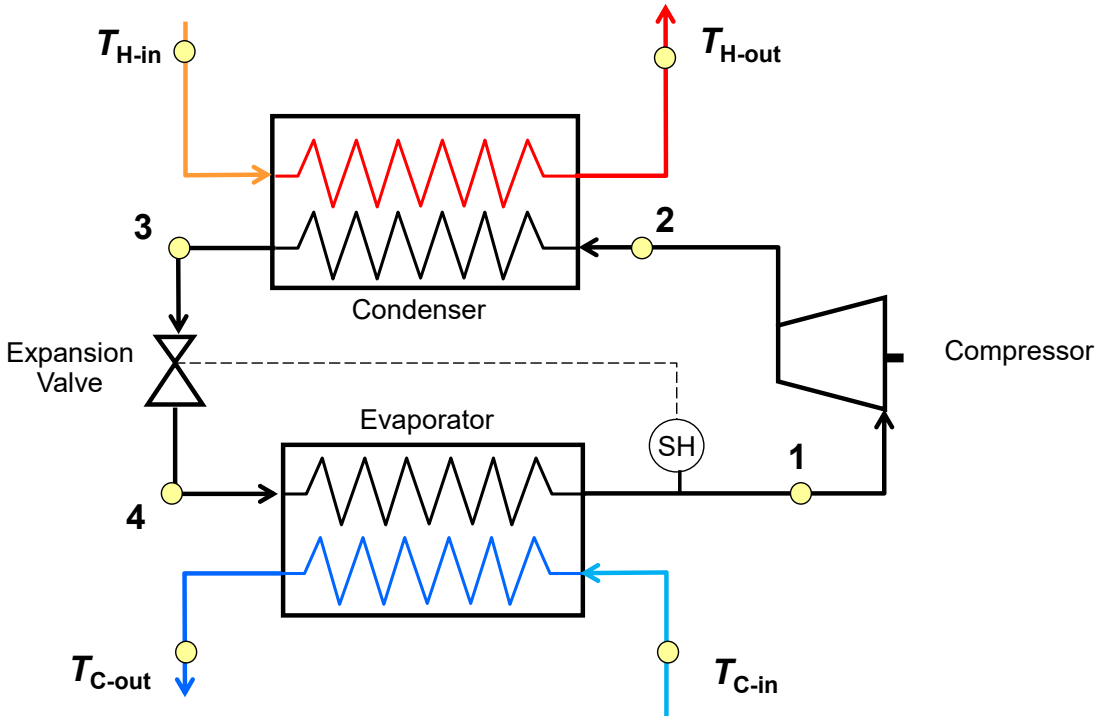

Figure 22 Machine configuration reference for the classical (sub-critical) cycle model.

3.2.1 Compressor sub-model

The compressor efficiency is the most critical parameter for the estimation the global efficiency (COP) and the heating capacity of the heat pump. The energy performance of the compressor can be described by its global isentropic efficiency η_{is} and its volumetric efficiency η_{vol}, defined as follows:

$$\eta_{is} = \frac{\dot{m}(h_{2-is} - h_1)}{W} \quad \text{Eq. 8}$$

where:

$\dot{m}$ [kg/s] is the actual refrigerant mass flow rate;

h_1 [J/kg] is the actual specific enthalpy of the refrigerant at the compressor suction;

h_{2-is} [J/kg] is the specific enthalpy at the compressor outlet in the case of ideal isentropic process;

W [W] is the actual electrical power consumption of the compressor.

$$\eta_{vol} = \frac{\dot{V}}{\dot{V}_{swept}} \quad \text{Eq. 9}$$

where:

$\dot{V}$ [m^3/h] is the actual refrigerant volumetric flow rate at compressor suction;

$\dot{V}_{swept}$ [m^3/h] is the ideal “swept volume”, depending only on the geometrical displacement of the compressor and its rotational speed.

In order to estimate some reference values for the volumetric and isentropic efficiency to be used in the theoretical model, the commercial semi-hermetic piston compressor HG56e/1155-4 S HC by the manufacturer Bock has been chosen as reference. This compressor is available in the market and is specifically designed to be used with propane as the refrigerant, as well as certified according to ATEX machine category 2.

The displacement of this compressor is 100.4 m^3/h at 50 Hz (1450 rpm). A picture and the overall dimensions are provided in Figure 23. The expected heating and electrical power provided by this compressor at 0°C evaporating temperature and 35°C condensing temperature are:

- Heating capacity: 65.5 kW
- Electrical power: 15.4 kW

The size of the compressor has been chosen in order to be representative for the range of heating power required by the heating building applications considered in this project.

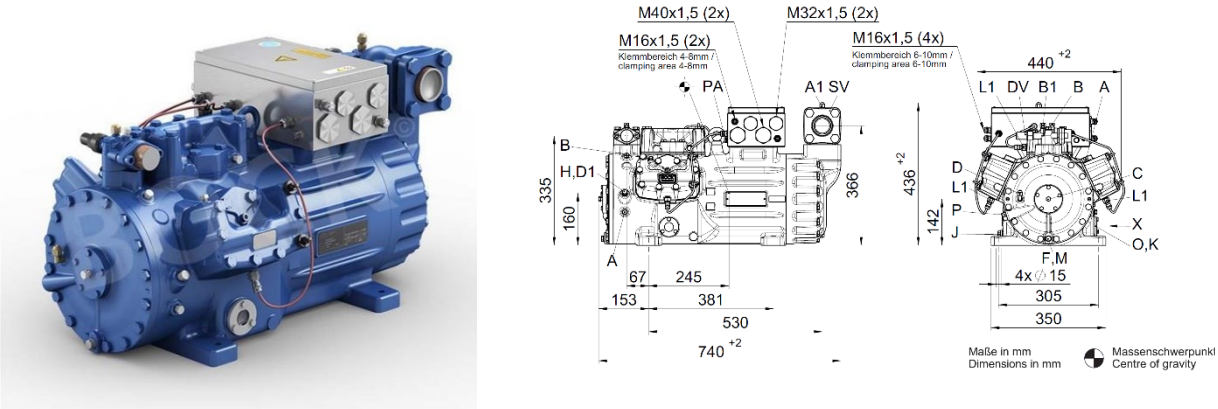

Figure 23 Picture and overall dimensions of the propane compressor used as reference [14]

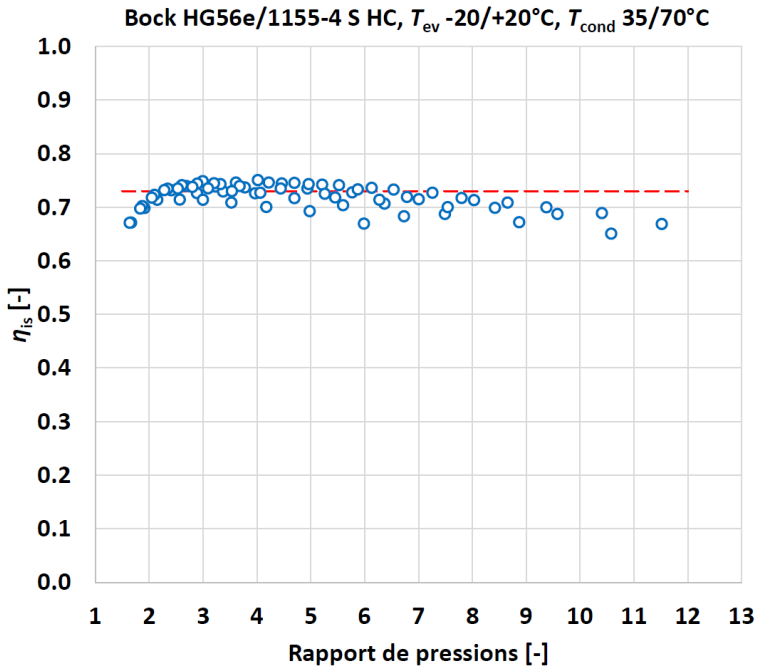

Figure 24 Global isentropic efficiency retrieved from manufacturer data (reference for classical cycle model).

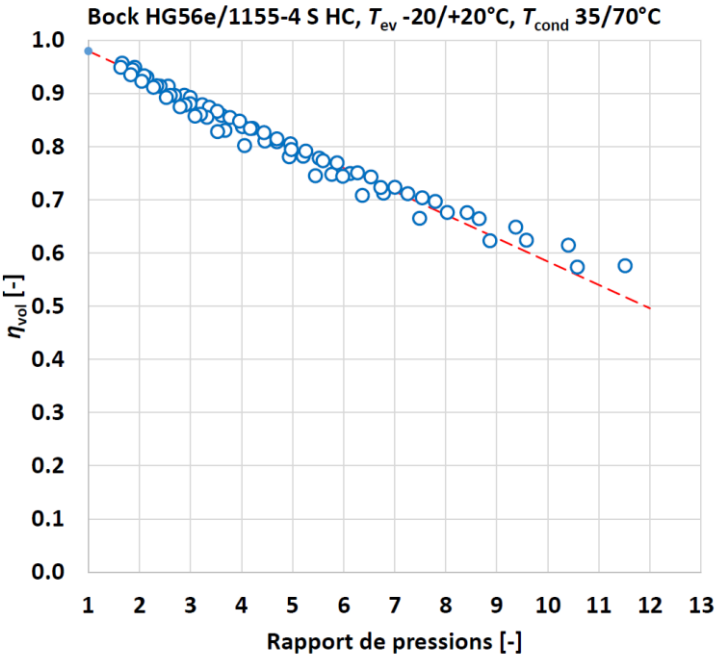

Figure 25 Volumetric efficiency retrieved from manufacturer data (reference for classical cycle model).

Technical performance data at evaporating temperature varying from -20°C up to + 20°C and condensing temperature varying from 35°C up to 70°C has been retrieved from the manufacturer selection software and is available in **Appendix 13.1.** Data has been reduced in order to plot the isentropic efficiency versus pressure ratio (see Figure 24) as well as the volumetric efficiency versus pressure ratio (see Figure 25). Based on these results the following assumption can be made for the theoretical model:

- Fixed global isentropic efficiency: $\eta_{is} = 0.73$
- Volumetric efficiency depending on pressure ratio r_p as follows: $\eta_{vol} = 0.98 - 0.042(r_p - 1)$

Figure 26 shows the operating envelope of the reference compressor. As compared to conventional semi-hermetic piston compressors for refrigeration applications, this machine recently available in the market can span a very wide range of evaporating temperatures, from -40°C up to 35°C. Such high upper limit, in particular, is extremely important for HP applications, since it allows the production of DHW all year-around.

The model takes into account the influence of the rotational speed of the compressor by adjusting the ideal displacement of the compressor (100.4 m³/h at 50 Hz) based on the inverter electrical frequency. For the sake of simplicity, the isentropic and volumetric efficiency are considered here independent from the inverter frequency. As a first approximation, one may consider this model reasonably accurate for the frequency range 30 – 60 Hz.

As a conclusion, the modelling of the compressor isentropic and volumetric efficiency based on this specific compressor for hydrocarbons recently available in the market, can be considered in our opinion as representative of the R290 heat pumps which will be available in the market in the next years for residential application. As a first order approximation, the present model could be considered representative for heating power in the range of 50 kW up to 200 kW.

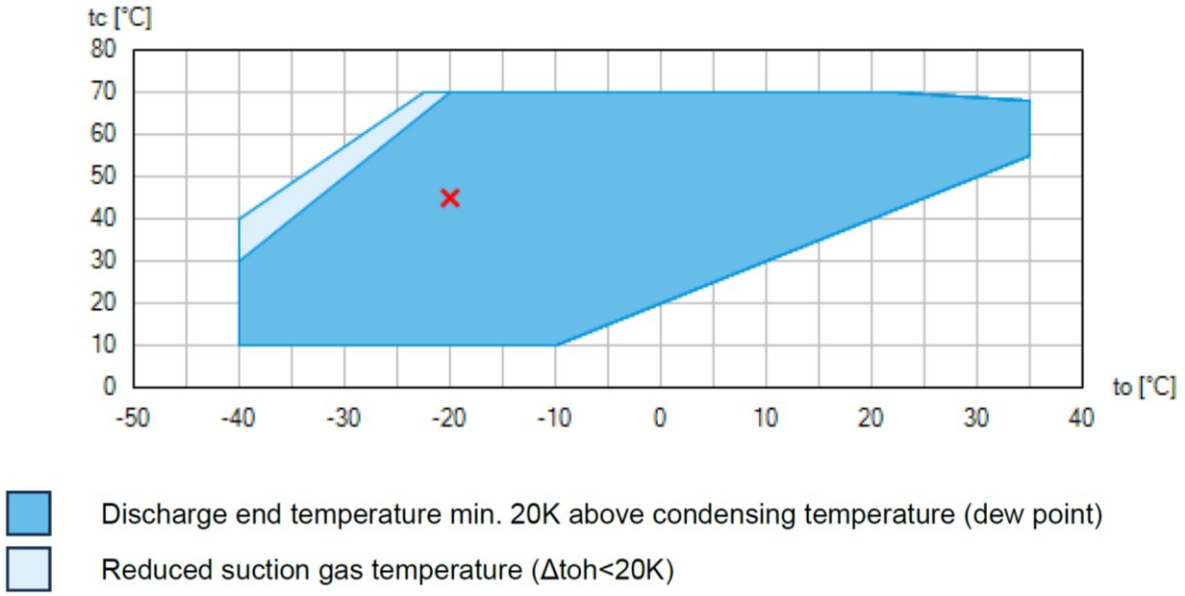

Figure 26 Operating envelope of the reference R290 compressor

3.2.2 Heat exchangers sub-model

The modelling of the thermal behavior of the condenser and the evaporator is based on a fixed value of the “approach” (i.e. the minimum temperature difference between refrigerant and water along the heat exchanger). Such approximation is not fully accurate, since the “approach” itself will indeed depend on the actual thermal power (which varies mainly with the compressor rotational speed and the operating

conditions, especially the evaporating pressure). However, in the case of “well designed” heat exchangers for COP optimization, the “approach” will be in the order of 1÷2 K; in this case, even a major relative variation of the “approach” will have a minor impact on the COP, since it will correspond to a variation of the actual evaporating or condensing temperature in the order of maximum 1 K (which roughly correspond to a variation of the order of 2-3% in terms of COP).

On the other hand, this model allows capturing well the impact of a variation of the water/brine flow rate on the thermal performance of the HP, which is extremely important in order to study the optimal hydraulic integration of the HP in the full system.

The water/brine outlet temperatures (T_{C-out}, T_{H-out}) are computed from the cooling and heating powers (Q_C, Q_H) provided by the calculation of the thermodynamic cycle, through the following equations:

$$Q_C = C_C(T_{C-in} - T_{C-out}) \quad \text{Eq. 10}$$

$$Q_H = C_H(T_{H-out} - T_{H-in}) \quad \text{Eq. 11}$$

where:

Q_C, Q_H [kW] are the cooling and heating powers

$$C = \dot{m}\, c_p \text{ [kW/K]} \quad \text{Eq. 12}$$

$\dot{m}$ [kg/s] is the water/brine flowrate

c_p [kJ/(kg K)] is the water/brine specific heat

If the inlet and outlet cold water temperatures and the superheating are known, the evaporating temperature can be directly determined by imposing a fixed “approach” value, as shown in Figure 27. At high evaporator brine flow rate (i.e. high C_C), the inlet-to-outlet brine temperature drop ($T_{C-in} - T_{C-out}$) will be low, and the minimum refrigerant-to-brine temperature difference will occur at a position along the evaporator corresponding to the brine inlet (see Figure 27 at left). By decreasing the brine flow rate, this position will switch to the brine outlet (see Figure 27 at left): at fixed brine inlet temperature T_{C-in}, any further decrease of the brine flow rate will decrease the brine outlet temperature and the actual evaporating temperature, thus decreasing both COP and heating power of the heat pump.

In the case of the condenser model, as first approximation, a fixed approach is imposed between the actual condensing temperature and the hot water outlet temperature. As one can see in Figure 28, at fixed condenser water inlet temperature T_{H-in}, any decrease of the hot water flow rate will increase the water outlet temperature T_{H-out} and the actual condensing temperature, thus decreasing the COP of the heat pump and, at a minor extent, the heating power (volumetric efficiency decreases).

Since the estimation of the thermodynamic cycle is based on the condensing and evaporating temperature, but these depend themselves on the water/brine inlet/outlet temperature, an iterating calculation is needed.

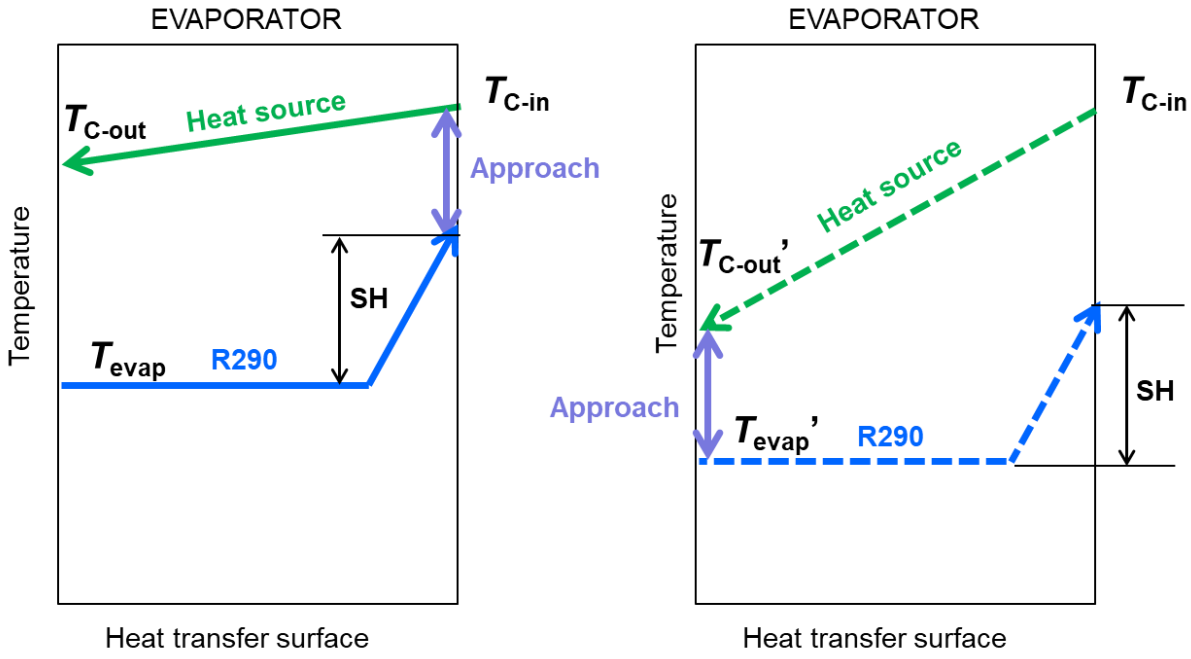

Figure 27 Schematics of the evaporator sub-model.

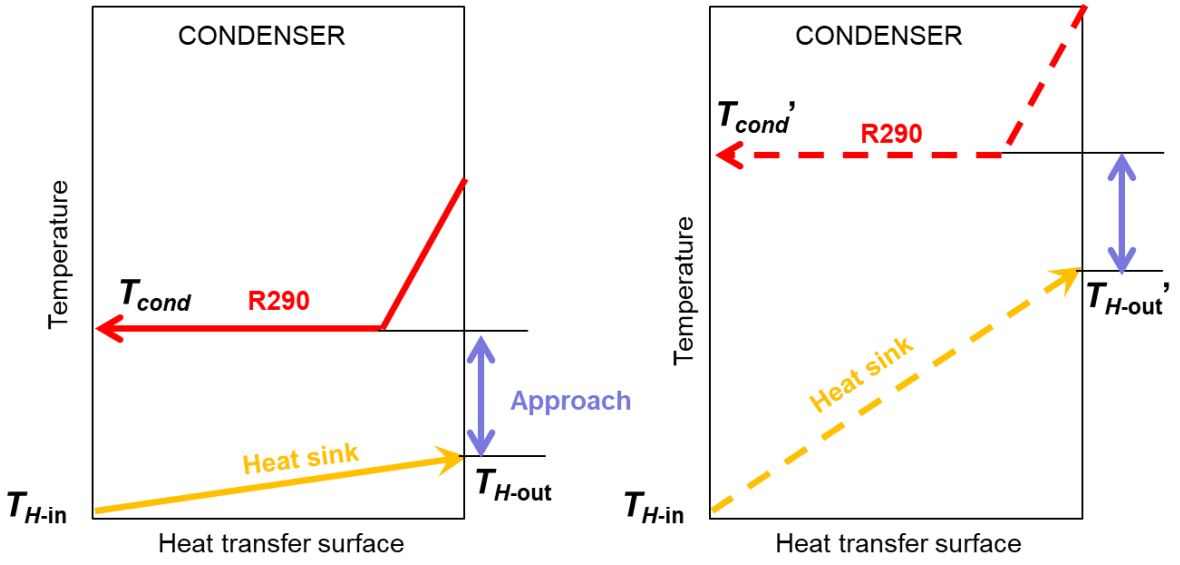

Figure 28 Schematics of the condenser sub-model.

3.2.3 Expansion valve sub-model

The expansion valve is modeled by imposing a fixed superheating (SH) value of 3 K. This can be considered as an optimized value nowadays achievable with modern electronic expansion valves (EEV) available in the market.

3.2.4 R290 heat pump model summary

The heat pump theoretical model can be summarized as follows:

$$COP, Q_H = f(T_{C-in}, C_C, T_{H-in}, C_H, freq) \quad \text{Eq. 13}$$

COP and heating power are computed as a function of cold and hot water flow rate and inlet temperature, as well as inverter frequency ($freq$ [Hz]).

The following parameters are adjustable:

- Refrigerant (nominal: R290);
- Compressor displacement;
- Compressor isentropic efficiency (nominal $\eta_{is} = 0.73$);
- Compressor volumetric efficiency as a function of pressure ratio r_p (nominal $\eta_{vol} = 0.98 - 0.042(r_p - 1)$);
- EEV fixed superheating at evaporator outlet (nominal: SH = 3 K);
- Inverter frequency;
- Fixed “approach” between refrigerant and water/brine in the heat exchangers (nominal 2 K);

Heat transfer fluid at heat source and heat sink (ex. different concentrations of glycol at the heat source can be modeled by modifying the value of C_C)

3.3 Theoretical model of transcritical cycle

The modeling of the transcritical cycle (see **Figure 29**) is based on a machine configuration similar to the one used for the modeling of the classical cycle (see **Section 3.2**):

- A single-stage compressor (1b→2);
- A gas-cooler (2→3) (the term “condenser” cannot be used since no phase-change occurs);
- An EEV (3→4) controlling the superheating (SH) at evaporator outlet and the high-pressure;
- A dry evaporator (4→1);
- An Internal Heat Exchanger (IHX) between the hot (high-pressure) CO_2 at the gas-cooler outlet (3) and the cold (low-pressure) CO_2 vapor at the evaporator outlet (1).

The use of the IHX, which has been discarded for the classical (sub-critical) model, has been taken into account in this model because of its very important role to increase the COP when the temperature of the water entering the gas-cooler ($T_{H\text{-}in}$) is high.

The impact of the IHX can be neglected in the model by simply forcing its efficiency ε to null.

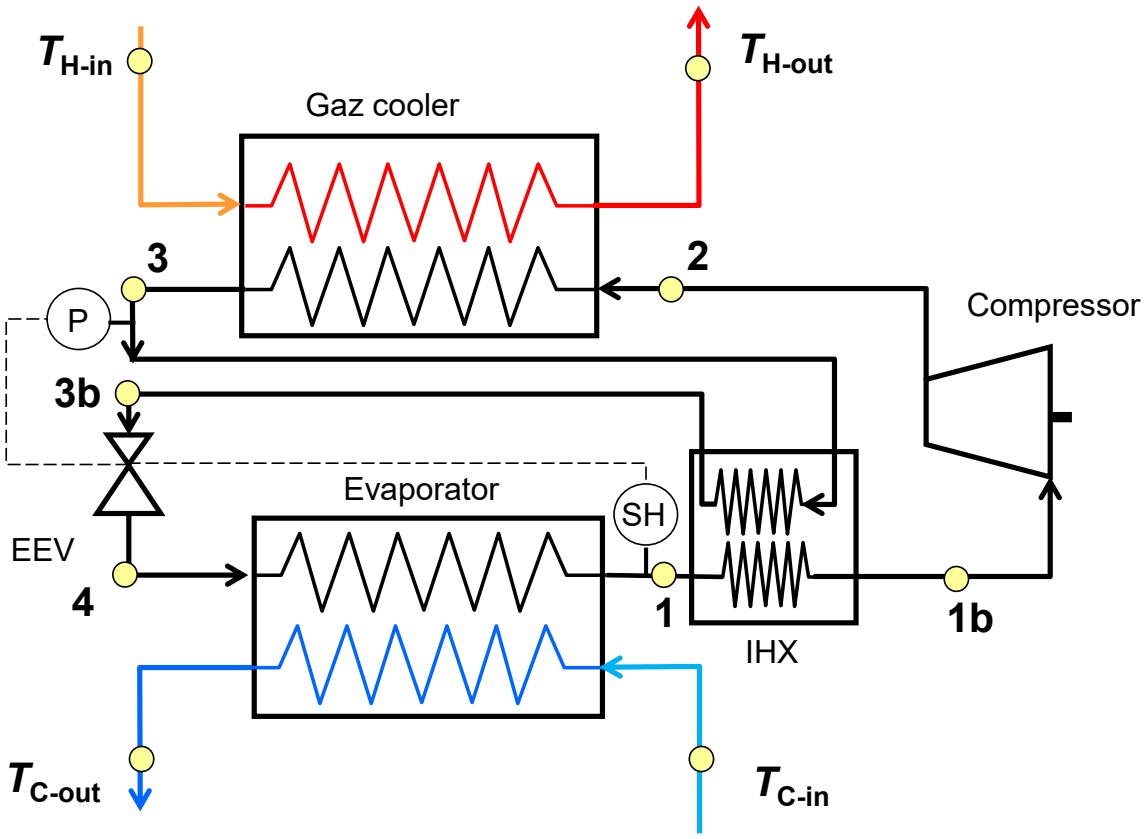

Figure 29 Machine configuration reference for the transcritical cycle model.

3.3.1 Compressor sub-model

For the sake of a fair comparison between the two models ('sub' and 'super'-critical) a very similar approach has been used for modeling the compressor of the transcritical model. A compressor for R744 transcritical applications of the same manufacturer (Bock HGX12/30-4 ML CO2 T) and similar power has been selected (see technical data in the **Appendix 13.2**).

Experimental data of η_{is} and η_{vol} has been retrieved from the compressor manufacturer data and plotted against pressure ratio in order to perform a linear interpolation. The dotted line curves in **Figure 30** and **Figure 31** have been used in the model.

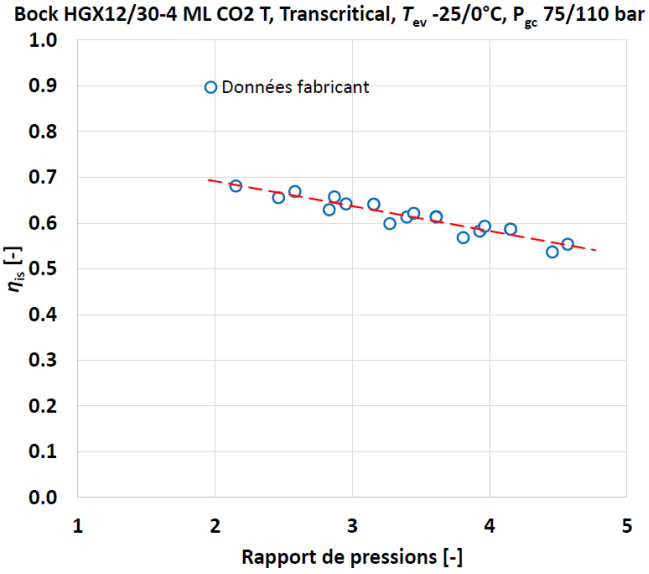

Figure 30 Global isentropic efficiency retrieved from manufacturer data (reference for transcritical cycle model).

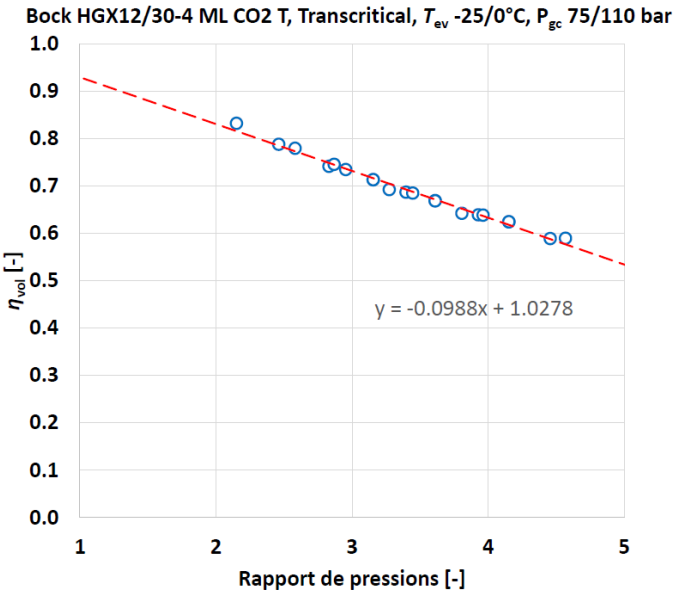

Figure 31 Volumetric efficiency data retrieved from manufacturer data (reference for transcritical cycle model).

3.3.2 Heat exchangers sub-models

The modelling of the thermal behavior of the gas-cooler and the evaporator is based, similarly to the classical-cycle model, on a fixed value of the “approach” (i.e. the minimum temperature difference along the heat exchanger between refrigerant and water).

The model for the evaporator is identical to the one of the classical HP model (see **Figure 27**).

Regarding the gas-cooler, a major difference is due in this case to the fact that no refrigerant phase-change occurs, hence the high-pressure supercritical CO_2 displays a continuous temperature drop from

inlet to outlet. The specific heat of CO_2 during this process is highly non-constant, and in particular this value rises when approaching the critical point (critical temperature ~30°C); as a consequence, the temperature profile of CO_2 is flatter in the central portion of the heat exchanger, therefore if the heat sink inlet-to-outlet temperature rise is high (which is the case for DHW production), the minimum approach between refrigerant and water occurs in the middle of the gas-cooler, as shown in the schematics in **Figure 32**. This implies that the model is more complex than the one of a classical condenser, since the full temperature profile must be accurately computed to determine the actual value of the approach (see example in **Figure 33**). Based on the authors' experience a nominal value of 10 K is used in this model.

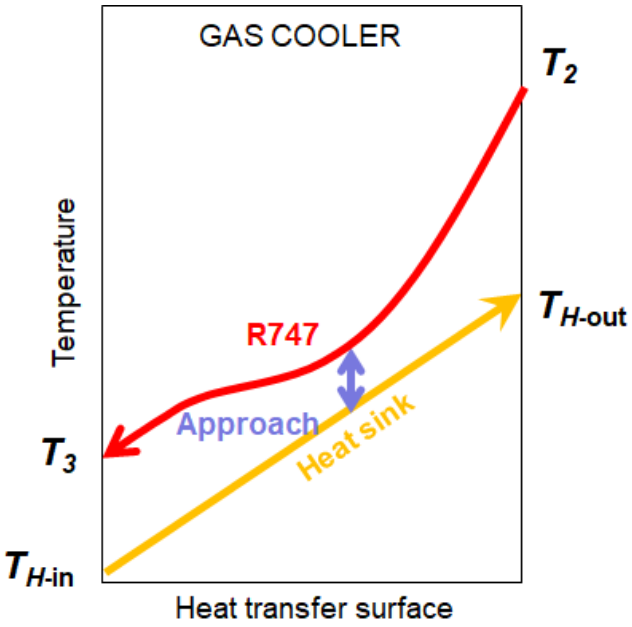

Figure 32 Schematics of the gas-cooler sub-model.

The second major difference of the modelling of the gas-cooler, as compared to the condenser for the classical cycle model, concerns the calculation of the heat sink flow rate. In the previous model the hot water outlet temperature is computed as a function of the inlet water and heating power as follows:

$$T_{H-out} = T_{H-in} + {Q_H}/{C_H} \qquad \text{Eq. 14}$$

On the contrary, in the present model both inlet and outlet DHW temperature are used as input, and the flowrate is computed as output:

$$C_H = \frac{Q_H}{(T_{H-out} - T_{H-in})} \qquad \text{Eq. 15}$$

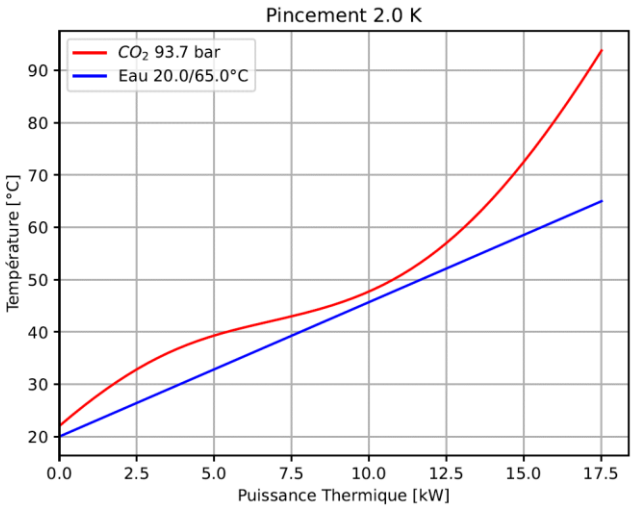

Figure 33: Example of actual temperature profiles in the gas-cooler as computed by the theoretical model.

This corresponds to the actual behavior of transcritical HPs available in the market, where the water flow rate through the gas-cooler is continuously adapted in order to react to any variations of T_{H-in}, and keep fixed T_{H-out} which is used a set-point for the control system.

Regarding the internal heat exchanger, it is modeled by imposing a fixed value of the heat exchanger thermal efficiency ε defined as follows:

$$\varepsilon_{IHX} = \frac{h_{1b} - h_1}{h_{1b-max} - h_1} \qquad \text{Eq. 16}$$

Where h_{1b-max} is the value of specific enthalpy that the vapor would have at its actual pressure and at the same temperature of the CO_2 exiting the gas-cooler (T_3).

A value of thermal efficiency ε_{IHX} = 1 corresponds to a counter-current IHX with infinite heat transfer area, which would allow to warm the low-pressure vapor up to the same temperature as the CO_2 exiting the gas-cooler.

A value of ε_{IHX} = 0.7 is used in the simulations, which can be considered as a “sound” sizing of this heat exchanger.

3.3.3 Expansion valve sub-model

As one can see in **Figure 29**, the expansion valve is modeled by imposing a fixed superheating value (SH = 3 K), as in the classical model.

The actual regulation strategy of an EEV in a well-designed transcritical HP for DHW, however, is not based on fixing the SH at the evaporator outlet, but to use the EEV as a “back-pressure-valve” to control the pressure in the gas-cooler. Indeed, for a given working condition (i.e. $T_{H\text{-}in}$ and $T_{h\text{-}out}$), an optimal high-pressure value exist, in terms of COP. This is very different from the condenser in a classical HP, where only one value of high-pressure is possible when $T_{H\text{-}in}$ and $T_{h\text{-}out}$ are fixed.

In current transcritical HP for DHW, the optimal high-pressure is computed by the control software; this value is then controlled through the EEV, and no actual direct control of the SH is possible. In this case, the SH is anyhow indirectly guaranteed by the design of the evaporator itself.

The model used in this project performs iterations of the thermodynamic cycle and the heat exchangers sub-models in order to assure, at the same time, the fulfillment of all the three following conditions:

- Superheating at the evaporator outlet according to the imposed SH value;
- Optimal high-pressure (pressure is varied till the COP maximum is found);
- Temperature approach between CO_2 and water in the gas-cooler.

As a conclusion, the present model can be considered to mimic the actual behavior of a well-designed transcritical HP for DHW.

3.3.4 R744 heat pump model summary

The heat pump theoretical model can be summarized as follows:

$$COP, Q_H = f(T_{C-in}, C_C, T_{H-in}, T_{H-out}, freq) \quad \text{Eq. 17}$$

COP and heating power are computed as a function of cold-water flow rate and inlet temperature, hot water inlet and outlet temperature, as well as inverter frequency ($freq$ [Hz]).

The following parameters are adjustable:

- Compressor displacement;
- Compressor isentropic efficiency (nominal as in **Figure 30**);
- Compressor volumetric efficiency as a function of pressure ratio r_p (nominal as in **Figure 31**);
- Fixed superheating at evaporator outlet (nominal: SH = 3 K);
- Fixed “approach” between CO_2 and hot-water in the gas-cooler (nominal 10 K);
- Fixed “approach” between CO_2 and cold-water in the evaporator (nominal 1 K);

Fixed IHX thermal efficiency (nominal ε_{IHX} = 0.7).

3.4 Validation against manufacturer and experimental data

3.4.1 R290 model validation

Manufacturer performance data of a R290 water-to-water heat pump available in the Swiss market (Regli NovaAqua [15]) is given in **Appendix 13.4**. The declared COP value, based on the EN14511 standard, at 0/-3°C inlet/outlet brine temperature and hot water production at 35°C, 52°C and 55°C are reported in **Figure 34**.

The water/brine flow rates and the compressor displacement values of the theoretical model has been adjusted in order to achieve 3 K inlet-to-outlet temperature drop at the evaporator and 5 K at the condenser, as required by the EN14511. The theoretical COP results are compared against these reference manufacturer data in **Figure 34** showing an excellent agreement.

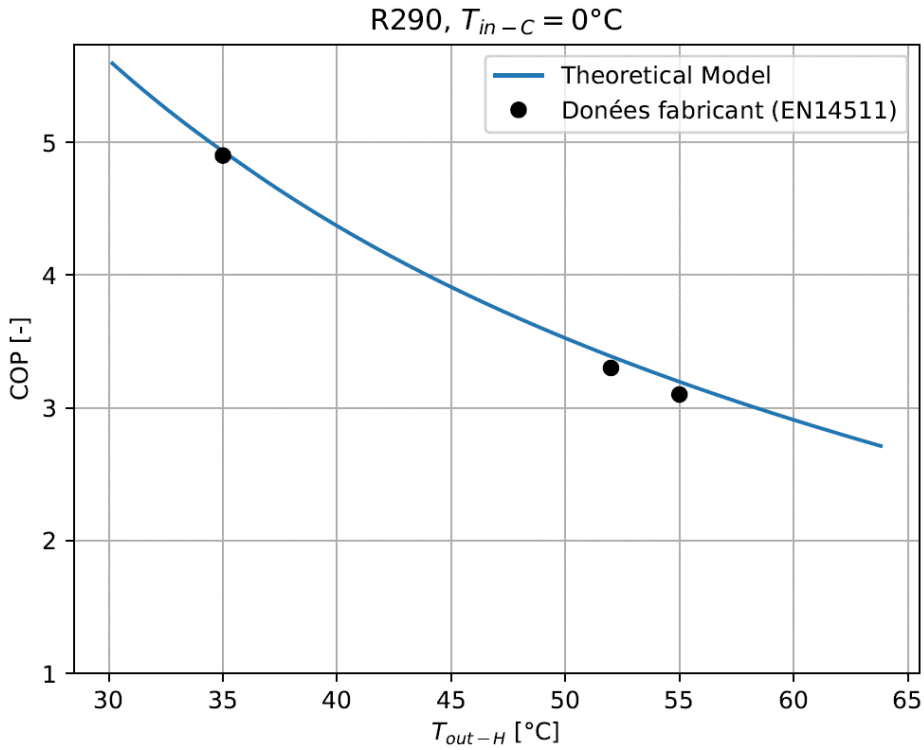

Figure 34 Comparison between theoretical model and manufacturer experimental data (**Appendix 13.3**).

3.4.2 R744 model validation

Experimental data of a transcritical R744 commercial geothermal HP for DHW production has been used for validation. The HP is the model "*Geoheat 18*" by manufacturer Enex [16] (see **Figure 35**).

The machine has been tested at the HP test bench of the HEIG-VD [17] (see **Figure 36**), which allows to experimentally measure the heating power, the cooling power and the electrical power of water/water and glycol/water HPs up to around 20 kW heating power. Flow rates and temperatures can be varied at both the heat sink and heat source independently. Measurements can be done at the testing conditions required by standards (ex. EN14511) or any other condition.

Figure 35 Transcritical HP Enex GeoHeat 18 under test in the HEIG-VD lab.

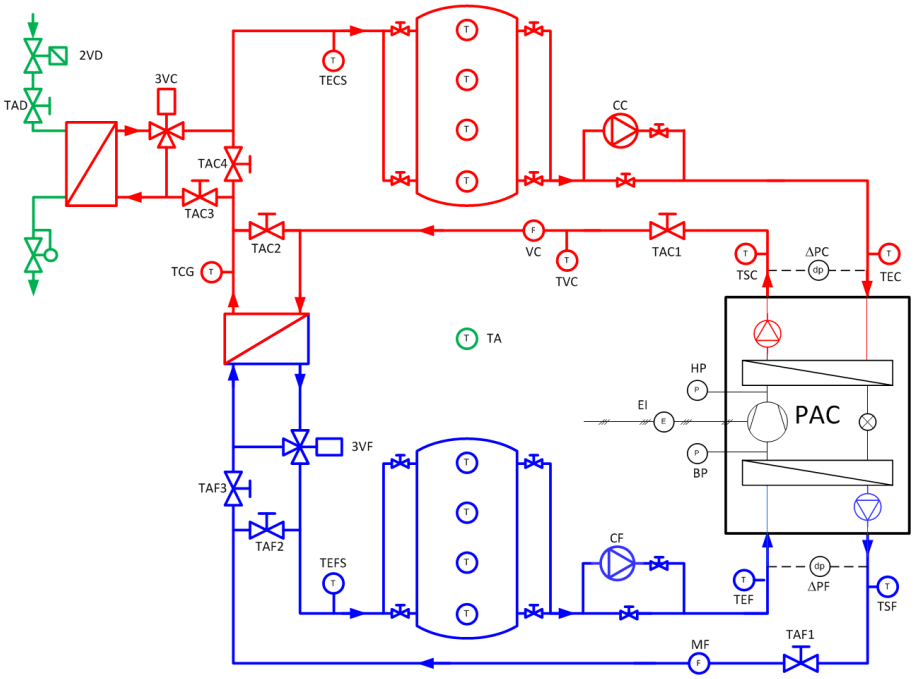

Figure 36 Heat pump test facility schematic.

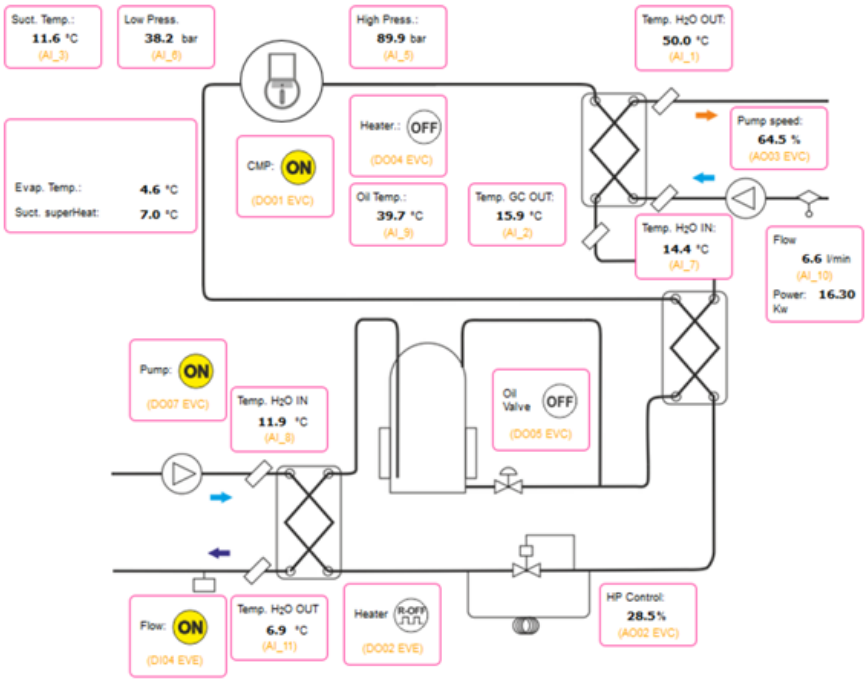

Figure 37 Screenshot of the heat pump proprietary monitoring and control system. Courtesy of Enex Srl.

A schematic of the HP proprietary control system is shown in **Figure 37**. The desired outlet DHW temperature is given by the user as set-point; the control system automatically computes the high-pressure for optimal COP and adapt the hot-water pump speed. Despite not being identical, the theoretical model developed in this project mimic this same behavior.

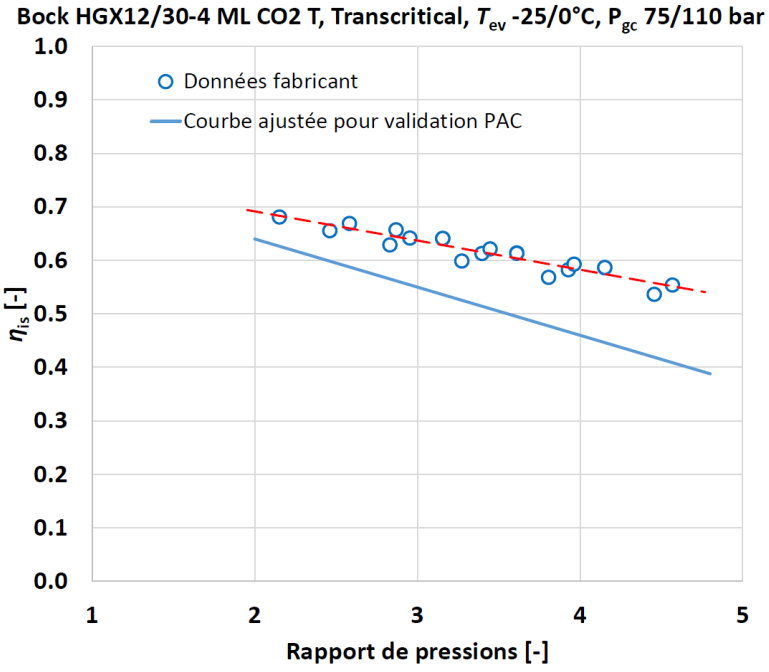

Figure 38 Compressor global isentropic efficiency used for the R744 model validation against Geoheat 18 experimental data.

This is one of the first machine of this type to have been available in the European market. For this reason, and also because of the quite low heating power (nominal 18 kW), the compressor displays a slightly lower efficiency than the higher-power and more recent and efficient compressor Bock HGX12/30-4 used for the theoretical model. The approximate adjustment shown by the blue linear trend in **Figure 38** has therefore been adopted in order to perform the present validation.

The following fixed parameters have been used for the theoretical model:

- Compressor swept volume 2.7 m^3/h;
- Compressor isentropic efficiency as shown by the blue line in **Figure 38** (adjusted as compared to nominal value in **Figure 30**);
- Compressor volumetric efficiency as shown in **Figure 31**;
- Fixed superheating at evaporator outlet SH = 3 K;
- Fixed "approach" between CO_2 and hot-water in the gas-cooler (nominal 10 K);
- Fixed "approach" between CO_2 and cold-water in the evaporator (3 K) [adjusted];
- Fixed internal heat exchanger thermal efficiency (nominal $\varepsilon_{IHX} = 0.7$);
- Cold water flow rate C_c = 2.0 kW/K (0/-3°C) or 2.7 kW/K (11/6°C)

Two different sets of experimental data have been considered:

- Fixed 13°C DHW inlet, variable DHW outlet (50°C to 65°C), two heat source conditions (0/-3°C and 11/6°C);
- Fixed heat source (12/6°C) and DWH 65°C outlet, variable DHW inlet (~20°C to ~40°C);

Experimental data of COP and heating power (with experimental uncertainty) of the two sets are compared against theoretical results in **Figure 39** and **Figure 40**. As one can see, despite the quite high complexity of the model, and the high amount of approximations and adjustable parameters, taking into account the experimental uncertainty, the model displays a remarkable agreement with experimental data.

In particular, results in **Figure 39** for the experimental set "A" show that the model is able to well predict the behavior of a transcritical HP at correct working conditions, i.e. low DHW inlet temperature, and high DHW outlet temperature.

On the other hand, results in **Figure 40** shows that the model is able to capture the actual behavior of a commercial HP even when operated at high inlet DHW. Such working conditions should be avoided to achieve optimal efficiencies, however this could happen because of a bad control of the hydraulic integration of the machine in the system. This feature of the theoretical model is very important for the present project, since the definition of proper hydraulic schemes and the analysis of the integration of the heat pumps in the whole space heating and DHW production system are very relevant topics.

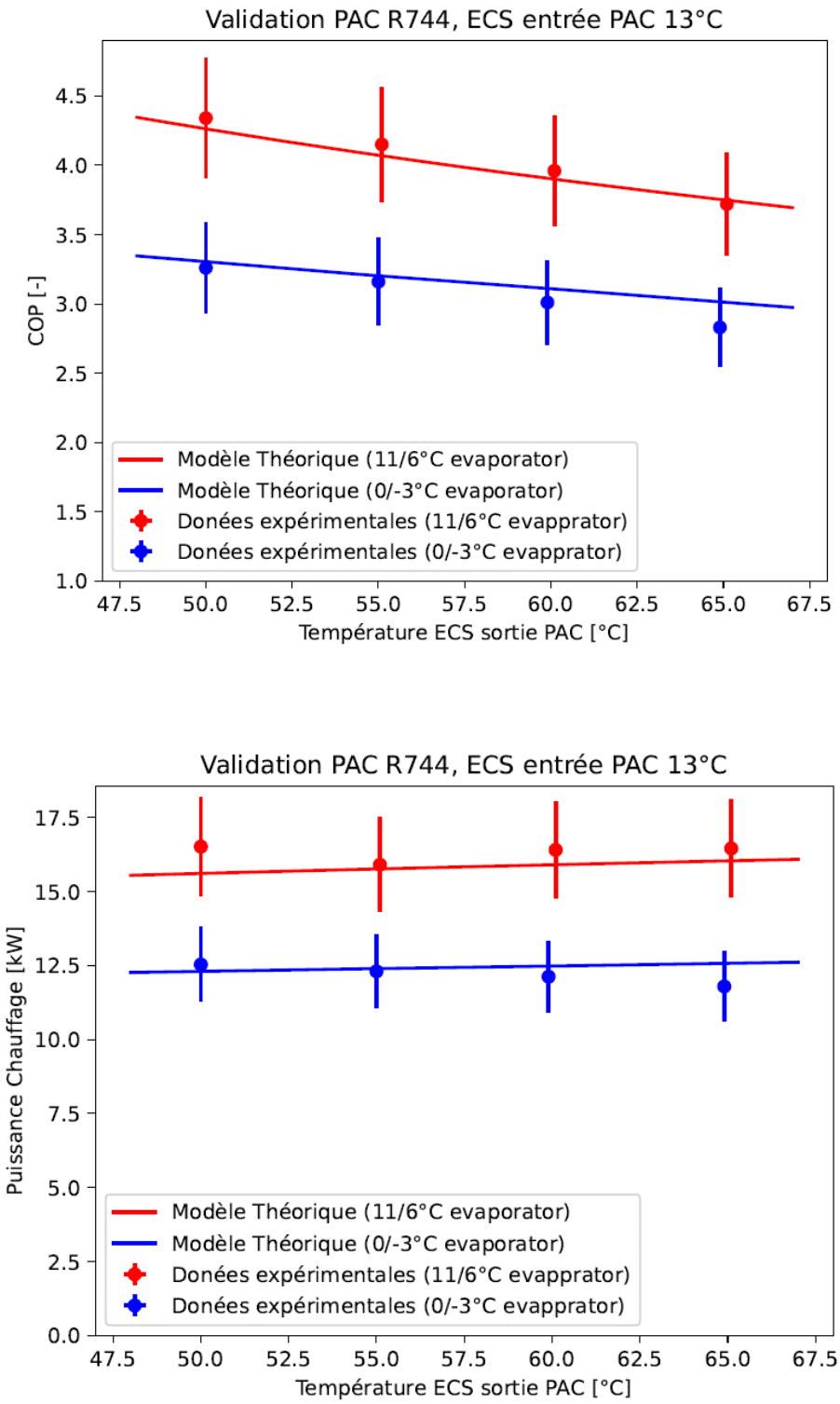

Figure 39 Comparison between theoretical and experimental data of COP and heating power at two different heat-source temperature, variable DHW production temperature, and fixed tap water inlet temperature.

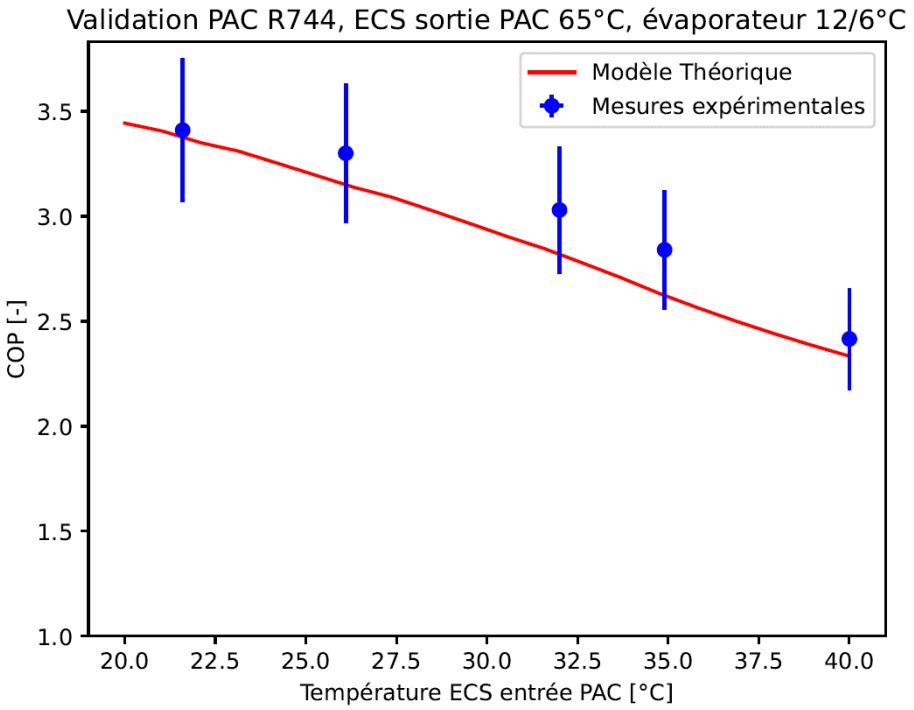

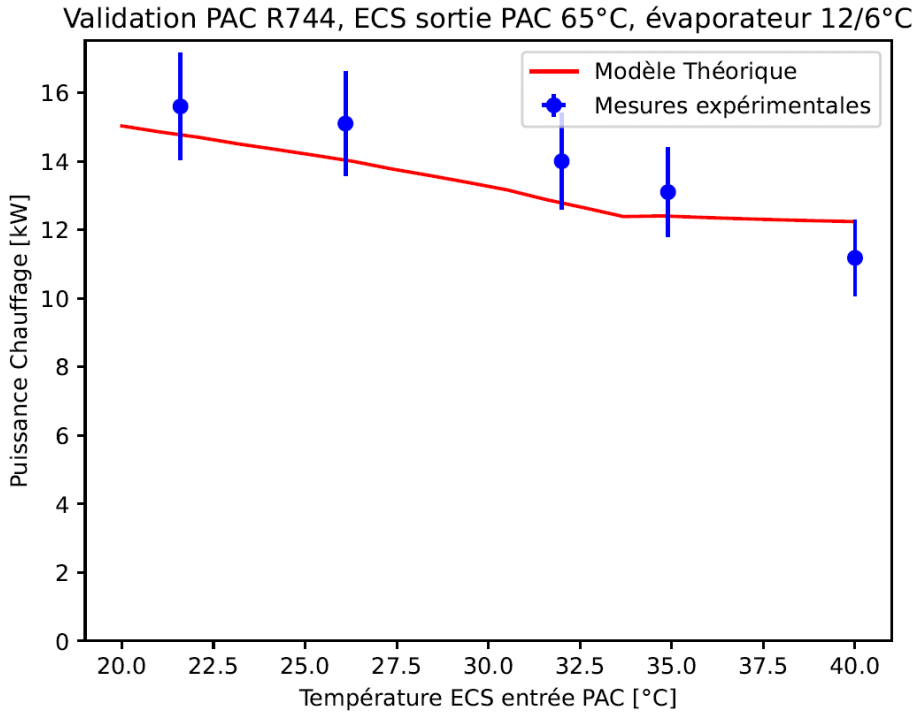

Figure 40 Comparison between theoretical and experimental data of COP and heating power at variable tap water inlet temperature and fixed heat-source and DHW production temperature.

3.5 Results of the theoretical models

3.5.1 R290 model results

Some sample results of COP and heating capacity for the R290 classical-cycle theoretical model are given in **Figure 41** and **Figure 42** at fixed heat-source and heat-sink flow rate (C_C = 20 kW/K, C_H = 20 kW/K), fixed inverter frequency (50 Hz), compressor swept volume (100.4 m^3/h) and variable heat-source inlet temperature (-15°C up to 20°C) and heat-sink inlet temperature (30°C up to 60°C).

As expected, the COP mostly depends on the source-to-sink temperature lift and the computed COP varies from COP ~ 2 (T_{in-C} = -15°C, T_{in-H} = 60°C) up to COP ~ 8 (T_{in-C} = 20°C, T_{in-H} = 30°C). Therefore, as already well-known, the most efficient use of a classical HP is the production of hot water for Space Heating at the lowest possible temperature (ex. floor heating), while a relevant efficiency drop is to be expected when producing high temperature DHW, especially in winter when the heat-source is cold. The results are in line with the COP expected by HPs already available in the market, which is expected to be, according to EN14511 operating conditions B0W35 (which roughly corresponds in **Figure 41** to T_{in-C} = 0°C, T_{in-H} = 30°C) in the order of 4.5~5 (see [18]).

In a common air/water HP application, the refrigerant in the evaporator is in direct thermal contact with the exterior air, which is blown through the evaporator by a fan. In the present application, an intermediate glycol loop is used between the heat source (i.e. air) and the refrigerant in the evaporator. Besides, the air flow over the PVT (Photovoltaic thermal hybrid solar collector) is due to natural convection and wind, which provides a lower heat transfer coefficient as compared to the one in a common evaporator of an air/water HP where a fan is used. As a consequence of both previous points, for a given exterior air temperature, in the present application the actual evaporating temperature (on which the COP actually deepens) will be lower than the one in a common air/water HP application. This could also reduce the application range of the HP if the lowest possible evaporating temperature is reached and this point should be carefully checked when selecting the HP.

The previous drawback can be counterbalanced by generously sizing the total PVT heat transfer surface. On the other hand, as compared to a common air/water HP application, the present system clearly provides some major advantages such as the combined production of electricity and the reduction of noise because of the absence of fans.

The above considerations about the comparison against a classical ASHP application applies to both the R290 and R744 HPs.

Another important performance parameter of an HP is the heating power provided. As one can see in **Figure 42**, this mostly depends on the heat-source temperature, and to a much lower extent on the heat-sink temperature. As an example, for a fixed theoretical swept-volume of 100 m^3/h, fixed nominal electrical frequency (50 Hz) and fixed heat-sink inlet temperature of 30°C, the heating power of a R290 HP is expected to vary from around 50 kW at -15°C heat-source inlet temperature, up to around 130 kW at +20°C. This implies that if a heat pump is capable to provide the required heating power in the coldest day of the winter, hence it will be oversized during all the rest of the heating season. This is only partially counterbalanced by the use of an inverter which allows to control the rotational speed of the compressor motor, hence directly controls the refrigerant flow rate and the heating power.

Regarding the impact of the heat production temperature, as one can see in **Figure 42**, at 0°C heat-source temperature, if the heat-sink inlet temperature is increased from 30°C (i.e. floor heating) up to 60°C (DHW production for anti-legionella constraint), the corresponding heating power decreases from ~80 kW down to ~60 kW.

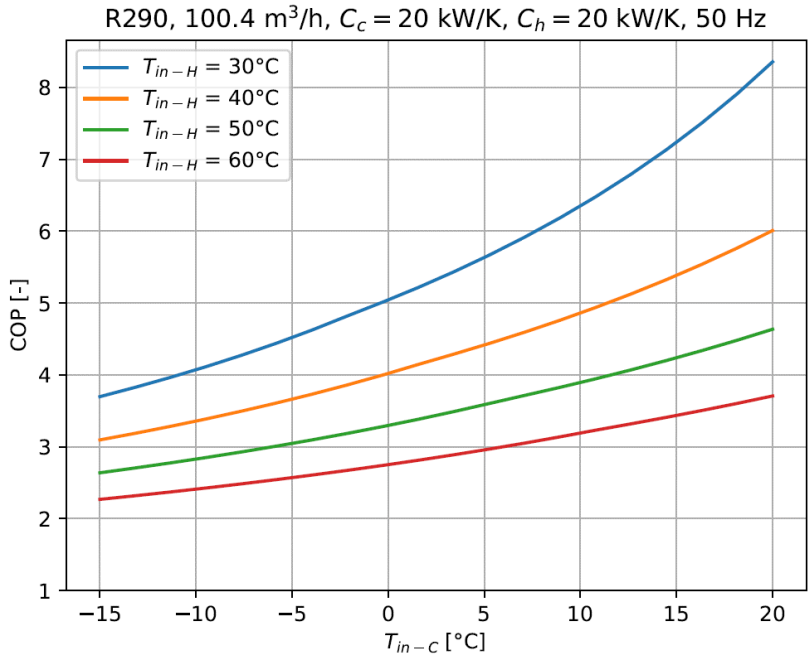

Figure 41 Example of COP theoretical estimation, as a function of heat source and heat sink temperatures (R290 classical cycle).

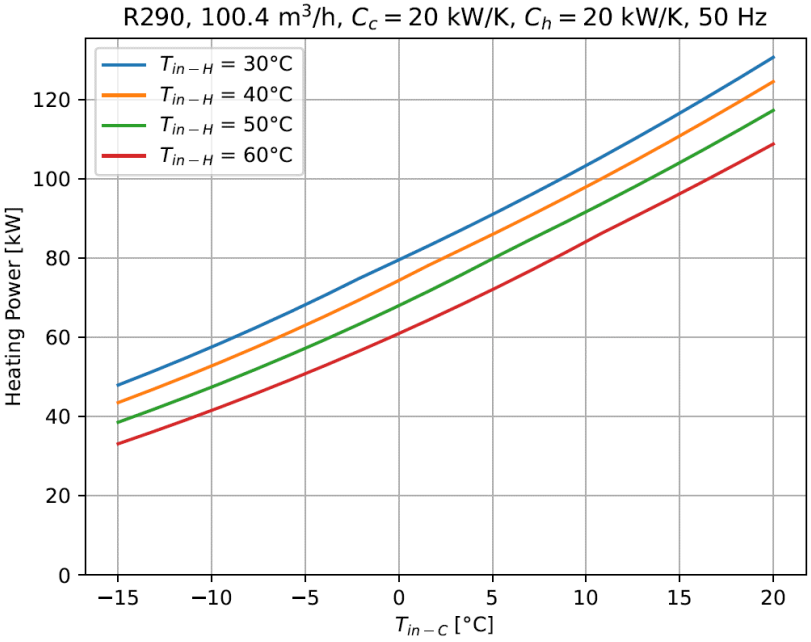

Figure 42 Example of heating power theoretical estimation, as a function of heat source and heat sink temperatures (R290 classical cycle).

Figure 43 shows an example of impact of the heat-source flow rate on the HP performance. As one can see, if in the case of **Figure 43** the flow rate drops below a value corresponding to C_C ~ 10 kW/K, both the COP and the heating capacity are degraded by the drop of evaporating temperature (see example in **Figure 27**). The abrupt drop of performance at lower flow rate and the flat behavior at higher flow rates clearly is a non-physical consequence of the approximate evaporator sub-model, which is based

on a fixed value of the approach between refrigerant and water; however, as first approximation, this behavior is pretty similar to the actual experimental one.

In order to avoid any relevant performance loss due to the low flow rate at the evaporator, it is suggested to adopt a water-glycol flow rate at the evaporator corresponding to an inlet-to-outlet temperature drop in the order to 3 K (this would correspond to C_C ~ 16 kW/K). Any increase of the flow rate above this value, would provide no actual improvement of the COP, but will mostly provide high pressure drop, therefore also a useless increase of the pumping power.

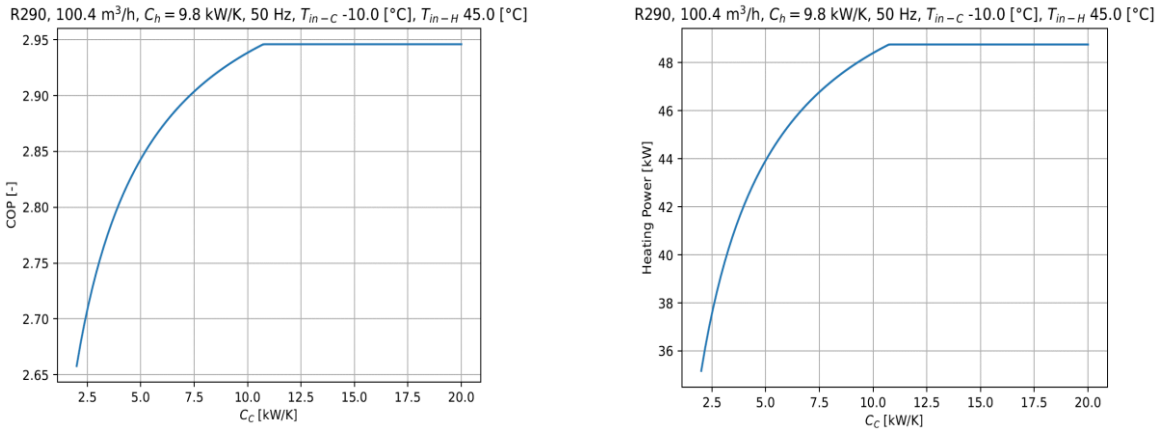

Figure 43 Example of the impact of the heat source flow rate on COP and heating capacity.

3.5.2 R744 model results

Some sample results of COP and heating capacity for the R744 transcritical-cycle theoretical model are given in **Figure 44** and **Figure 45** at the following fixed conditions:

- Heat-source flow rate: C_C = 20 kW/K;
- Inverter frequency: 50 Hz;
- Compressor swept volume: 20 m³/h;
- Compressor isentropic and volumetric efficiency as in **Figure 30** and **Figure 31**;
- Superheating at evaporator outlet: SH = 3 K;
- Evaporator approach: 1 K;
- Gas-cooler approach: 10 K;
- Internal heat exchanger efficiency: ε = 0.7.

The following variable conditions are considered for the two plots:

- Heat source (i.e. water/glycol) inlet temperature varying from -15°C up to 20°C;
- Four different inlet/outlet heat sink (i.e DHW) temperature conditions:
    - 10°C/65°C, corresponding to optimal exploitation for DHW production;
    - 20°C/65°C;
    - 30°C/65°C, corresponding to DHW production with degraded hydraulic control;
    - 40°C/50°C, corresponding to a possible (but not suggested) use for space heating.

In the simulations, the water flow rate in the gas-cooler is adjusted in order to correspond to the required inlet and outlet temperatures, in the same way as it is done by the control system of an actual transcritical HP for DHW, where the use of a variable speed pump is mandatory (see **Figure 37**).

As one can see, the use of a transcritical HP for space heating at 40°C/50°C inlet/outlet gas cooler temperatures make no sense from a thermodynamical point of view, since the achievable COP is much lower than the one of a classical-cycle HP.

As an example, according to the present theoretical models, at 0°C water-glycol inlet temperature the COP would be slightly above 2 for the transcritical cycle (see **Figure 44**) while this would be roughly in the order of ~3.5 for the classical cycle (see **Figure 41**, $T_{in\text{-}C} = 0°C$ $T_{in\text{-}H} = 40°C$ and $T_{in\text{-}H} = 50°C$). Besides, such working conditions represents already an extreme working point for a transcritical cycle, achievable only thanks to the use of the IHX. Depending on the actual design of each specific machine, gas cooler inlet temperature above ~40°C and gas-cooler outlet temperature below ~50°C are not possible. Beside the relevant efficiency drop, the operation at 40°C/50°C can therefore be very problematic in terms of reliability, since any variation of the temperature may lead to the stop of the HP.

As a final consideration regarding the possible use for space heating, it's worth stressing that, based on the above considerations, the use for a classical floor heating application (i.e. typically 30/35°C inlet/outlet) would be impossible with a R744 transcritical HP.

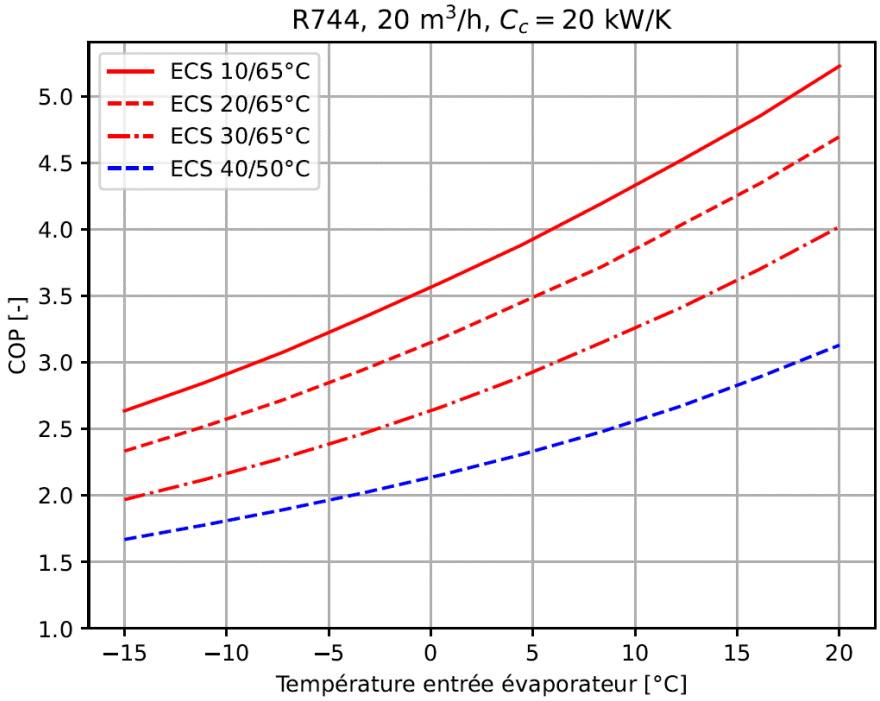

Figure 44 Example of COP theoretical estimation, as a function of heat source and heat sink temperatures (R744 transcritical cycle, ECS = DHW).

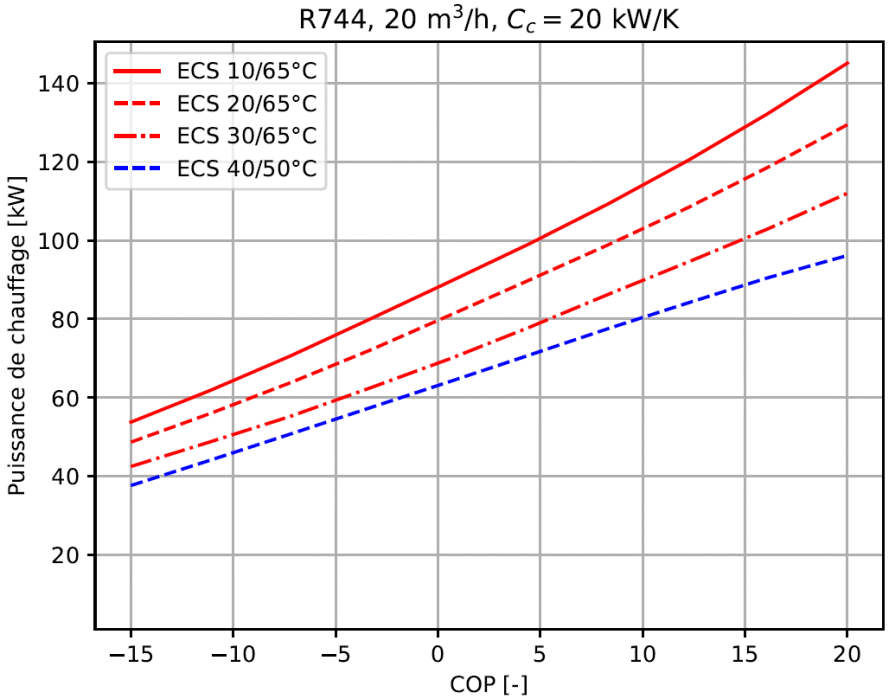

Figure 45 Example of heating power theoretical estimation, as a function of heat source and heat sink temperatures (R744 classical cycle, ECS = DHW).

On the other hand, the R744 transcritical-cycle becomes more efficient than the classical cycle when dealing with the production of DHW. As one can see in **Figure 44**, at 0°C water-glycol inlet temperature, water can be heated from 10°C (i.e. tap water network temperature) up to 65°C with a COP in the order of 3.5. This is done in a single passage of the water through the gas-cooler (see **Figure 46** on the right).

The optimal inlet-to-outlet temperature rise of water through the condenser of a classical-cycle HP is in the order of 5 K. In order to reach 65°C, the hot water must therefore be flown several times through the condenser and the increase of DHW temperature in the tank is achieved by a gradual rise (see Figure 46 on the left). The global COP of DHW production with a classical HP depends on the hydraulic control of the system: In order to increase the COP, one may let the tank to fully empty all the stored hot water and fill with cold tap water before starting a new DHW production DHW, however this would be totally not acceptable from an application point of view.

As one can see in **Figure 41**, the COP of the classical cycle at $T_{in\text{-}C}$ = 0°C and $T_{in\text{-}H}$ varying from 50°C to 60°C, varies from ~2.8 up to ~3.2, which is considerably lower than the COP~3.5 achievable with the transcritical cycle for a direct 10°C-to-65°C DHW production.

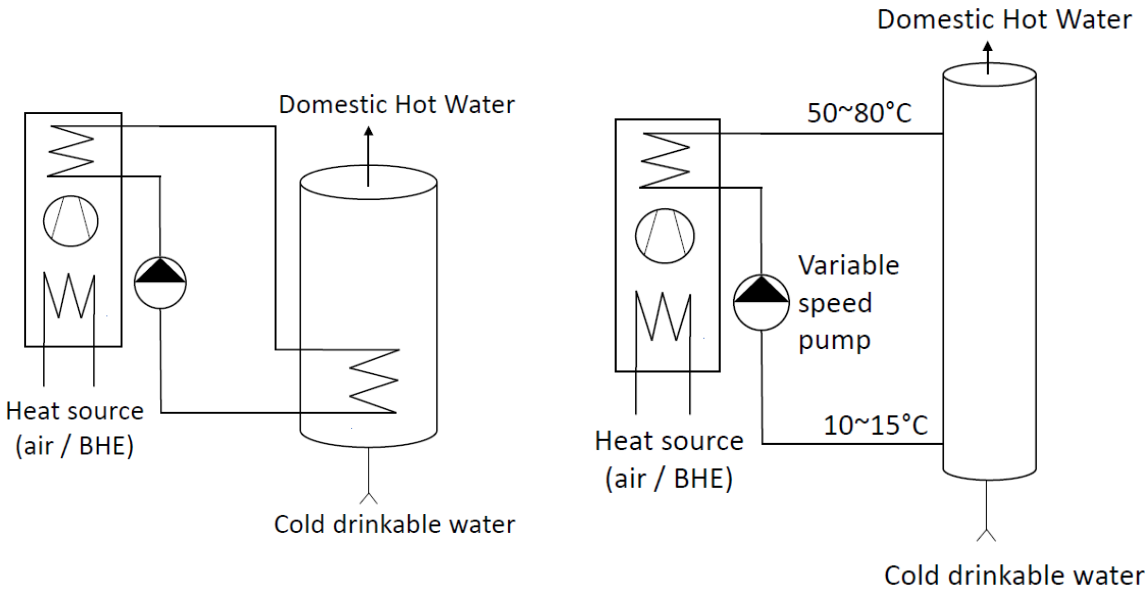

Figure 46 Comparison between the typical hydraulic integration for DHW production of a classical HP (on the left) and a transcritical HP (on the right) [17]

As one can see in **Figure 44**, at fixed 65°C gas-cooler outlet temperature, if increasing the inlet temperature from 10°C up to 20°C and 30°C, the COP drastically drops. Providing the lowest possible temperature (i.e. the temperature of the tap water network) is absolutely fundamental in order to properly exploit a transcritical HP. If tap water entering the system from the network is mixed with the hot water already present in the DHW, the energy efficiency easily drops below the one of a classical HP (as an example, COP~2.6 at $T_{in\text{-}C}$ = 0°C and gas cooler inlet/outlet 30/65°C). Besides, if this temperature rises above the maximum allowable gas cooler inlet temperature (~40°C) the operation of the HP becomes impossible, which can lead to reliability problems and possibly reduced life time of the HP.

An example of possible proper hydraulic integration, as suggested by the manufacturer of the tested HP manufacture is shown in **Figure 47**. This topic will be further discussed in details in the **Section 4**.

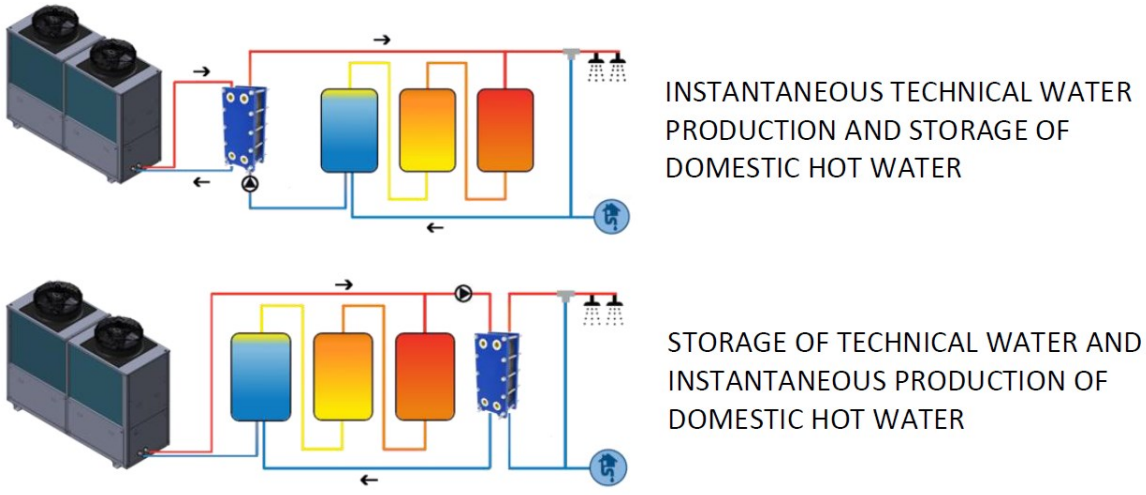

Figure 47 Example of proper hydraulic integration of a transcritical HP for DHW production, as suggested by a manufacturer [16]

Regarding the heating capacity results of the transcritical HP shown in **Figure 45**, its dependence on the heat source temperature is the same as the one of the classical cycle, since no actual difference applies to the heat transfer process in the evaporator.

When increasing the gas-cooler inlet temperature, the heating capacity drops, while the electrical power consumption keeps roughly constant (see [17] for further details), which explains the relevant COP drop.

3.6 Theoretical comparison between refrigerants

The classical-cycle theoretical model can be used to perform a "fair" comparison among different refrigerants in terms of thermodynamic cycle. The following refrigerants have been chosen[1]:

- Propane (R290), natural refrigerant, GWP = 3, flammable (A3), as reference;
- Ammonia (R717), GWP = 0, slightly flammable but toxic (B2L), as possible natural refrigerant alternative;
- R410A, synthetic HFC refrigerant mixture (R32/R125), GWP = 2088, non-flammable (A1), nowadays largely the most used refrigerant in domestic HPs in Switzerland, it will be banished at European level because of its global warming effect in new application starting from 1 January 2025, depending on the type and size of application[2];
- R32, synthetic HFC refrigerant, GWP = 675, slightly flammable (A2L), it will most probably temporarily replace R410A in small domestic split HPs;
- R1234ze(E), GWP = 0, slightly flammable (A2L), latest generation HFO synthetic refrigerant.

It's worth mentioning that this comparison refers only to the thermodynamic cycle performed assuming a fixed approach at heat exchangers. The difference in terms of heat transfer properties is therefore neglected.

The volumetric flow rate at compressor suction required to achieve a reference value of 100 kW heating power at $T_{in\text{-}C}$ = -10°C and $T_{in\text{-}H}$ = 45° has been computed, and results are shown in **Table 3**. This parameter gives a rough idea of the size of the compressor and therefore also of the refrigerant circuit. As one can see, there are no major differences among the refrigerants selected. R410A and R32 are the most compact solutions, which is not a surprise since this is one of the reasons why these refrigerants are adopted by HP manufacturers. As compared to R410A, the compressor would be around 70% bigger with R290, 50% bigger with R717 and almost 4 times bigger with R1234ze(E).

The biggest component in a HP application is typically the evaporator if a direct exchange with air is done. In the present case, brine/water HP are used, therefore in our opinion, whatever is the refrigerant among the ones selected, the HP itself would be reasonably compact. Besides, in terms of space occupation, the critical point for the present application would clearly be the solar panels and not the heat pump.

Results of COP and heating power at fixed heat sink inlet temperature 45°C and variable heat source inlet temperature from -20°C up to 20°C are shown in **Figure 48** and **Figure 49**, respectively. At the reference condition $T_{in\text{-}C}$ = -10°C and $T_{in\text{-}H}$ = 45°, as compared to R410A which can be considered the

---

[1] Office fédéral de l'environnement OFEV, Vue d'ensemble des principaux fluides frigorigènes, État septembre 2020, https://www.bafu.admin.ch/dam/bafu/fr/dokumente/chemikalien/fachinfo-daten/uebersicht_ueberdiewichtigstenkaeltemittel.pdf.download.pdf/liste_des_principauxfluidesfrigorigenes.pdf, last visit the 29.11.2023

[2] Amendments adopted by the European Parliament on 30 March 2023 on the proposal for a regulation of the European Parliament and of the Council on fluorinated greenhouse gases, amending Directive (EU) 2019/1937, https://www.europarl.europa.eu/doceo/document/TA-9-2023-0092_EN.html, last visit the 29.11.2023

present industrial reference, the COP is around 5% higher with R290, R32 and R1234ze(E), and around 10% higher with ammonia.

Table 3 Compressor displacement values used for the refrigerant comparison simulation

	$\dot{V}_{swept}$ [m³/h]
R290	208
R410A	125
R32	109
R1234ze(E)	490
R717	187

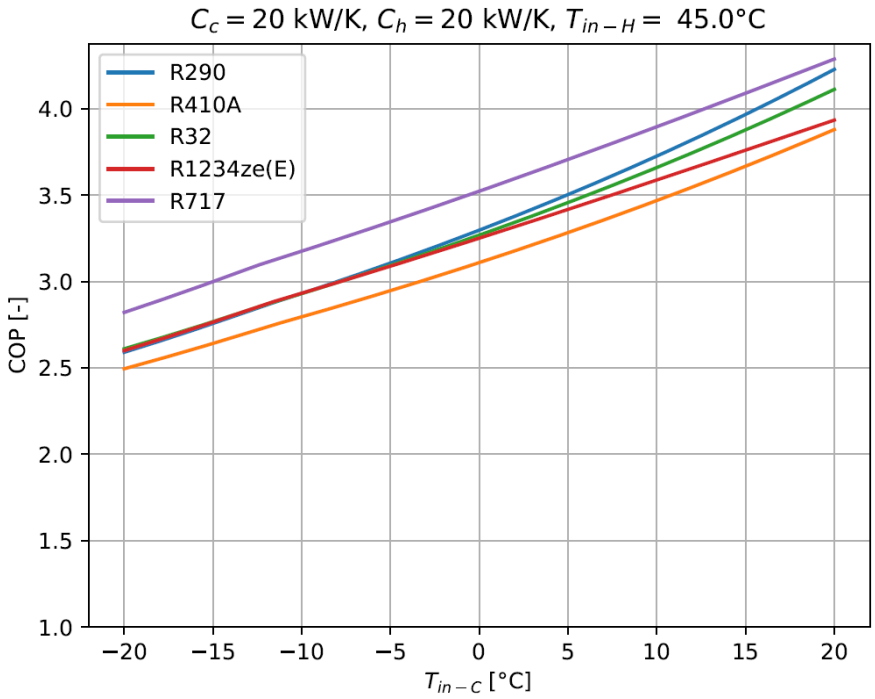

Figure 48 Theoretical comparison of COP between different refrigerants at heat sink inlet temperature 45°C.

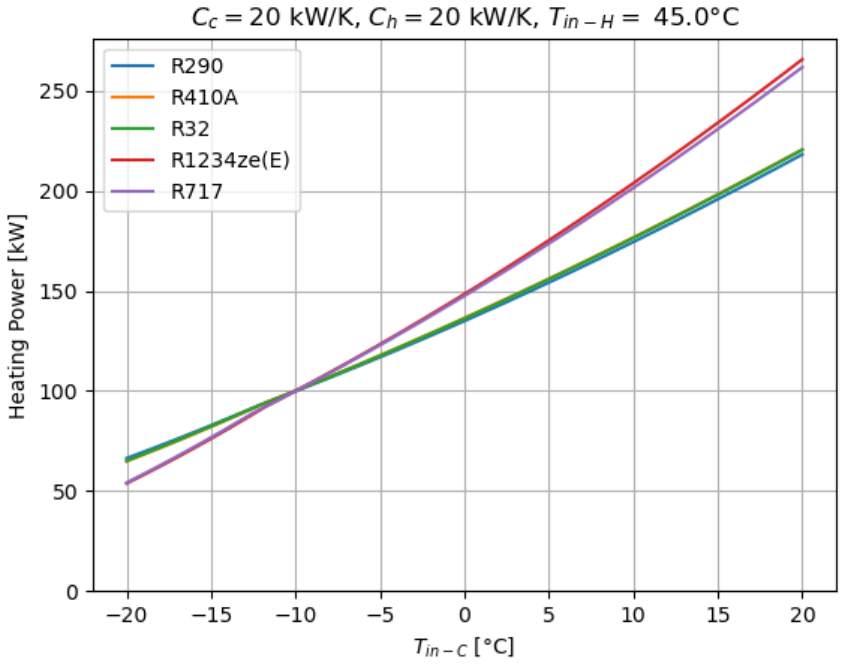

Figure 49 Theoretical comparison of heating capacity between different refrigerants at heat sink inlet temperature 45°C (swept volumes according to **Table 3**).

At higher evaporating temperatures, these ratios change. In particular, the COP of R1234ze(E) and R717 in **Figure 48** tend to drop relatively to the other refrigerants. This behavior, however, is due mostly to the fact that all the simulations are run at fixed water flow rates C_C ~ 20 kW/K and C_H ~ 20 kW/K, which correspond to an inlet-to-outlet temperature difference of 5 K at the reference conditions. As one can see in **Figure 49**, the heating power of R1234ze(E) and R717 rises with evaporating temperature more than with other refrigerants, which implies that, based on the assumptions of the heat-exchangers sub-model, the difference between heat-sink inlet temperature and actual evaporating temperature diverges more (see **Figure 27**). This behavior could easily be counterbalanced by increasing the water flown rate.

The most important conclusions of the present analysis are:

- The use of propane as refrigerant (R290) does not provide any efficiency loss as compared to the nowadays industrial reference for HPs (i.e. R410A); on the contrary, a slight improvement of COP is provided in terms of thermodynamic cycle;
- As expected, ammonia (R717) provides even better COP.

This comparison is based merely on thermodynamic cycle considerations and the analysis of the integration in the building and of the financial constraints due to the toxicity or flammability levels of each refrigerant are outside the scope of the present work.

Nevertheless, it's worth rapidly focusing on the availability of R290 HP and R744 HP on the market.

Hydrocarbons, in particular iso-butane (R600a) but also propane (R290), are nowadays used in the vast majority of domestic refrigerators, thanks to the fact that the actual risk linked to flammability is almost null because of the very low amount of refrigerant (< 150 g) needed in these systems. In the field of HP, despite the fact that R290 is well known to be an excellent refrigerant for this kind of application and the technical feasibility has been proven (see, for example [19]), the actual market penetration has been

much smaller, in particular because of the higher amount of refrigerant needed. However, in recent years small and medium capacity R290 heat pumps are becoming more and more available. An indirect index of this trend can be retrieved from the public bulletin of the WPZ "*Wärmepumpen-Testzentrum*": while the number of air/water R290 HP listed in it was 0 in 2018, and just one in 2019, this increased up to 6 in the latest one (30.10.2023) [20].

An example, among others, of available R290 HP is provided in the **Appendix 13.4**.

Regarding transcritical R744 HP, this is already a mature technology, as confirmed by the fact that at least 5 million units (so-called "EcoCute") have been installed at commercial domestic level in Japan [21], certainly also pushed by state incentives and by the fact that in this country the average ratio of the annual thermal energy demand for DHW is in the order of 50%. Despite this, transcritical HPs are still very seldom used at Swiss level, but they are available on the market. An example, among others, of an available product is the HP experimentally tested for this project [16].

4 Systems definition, sizing and control strategy

This section presents the different hydraulic diagrams selected for the TriSolHP system, as well as their control strategies and sizing method. In the following sections, the two configurations selected are then simulated for different building loads to assess the energy, environmental and economic performance, as well as the potential application of such a system.

System sizing and control strategy are partially based on previous work on air-source HP systems [22], which have been developed based on an extensive literature review, discussions with experts in the field, and long-term in-situ monitoring of two pilot projects with large air-source HP.

4.1 Systems definition

As mentioned previously, the TriSolHP concept combines natural refrigerant heat pumps (propane and/or CO_2) with PVT collectors as heat source. In order to limit the scope of the investigation to cases significant to the current study, two hydraulic configurations have been selected:

- **System 1:** a single propane HP (R290) producing heat for both SH and DHW preparation, with SOLINK PVT collectors as heat source; this configuration has been selected because it requires less space and volume in the boiler room than the second configuration (only one HP and less DWH storage volume required). In addition, this configuration is also simpler to install and control.
- **System 2:** a propane HP (R290) for SH and a CO_2 HP (R744) for DHW preparation, both connected to a SOLINK PVT collector field as a common heat source. This second configuration has been selected for cases with sufficient volume available. Moreover, in this configuration heat required for space heating and DHW will each be produced by a HP using a refrigerant well adapted to its operating conditions: R290 for space heating and R744 for DHW production (large temperature difference on the heat sink side of the HP).

These two configurations are illustrated in **Figure 50**. Symbols used in the hydraulic diagrams are described in **Figure 51**.

The following elements have been considered for the development of the configurations:

- DHW production should be separated from SH in order to operate the HP at the lowest temperature possible.
- A buffer tank in the SH loop ensures a minimum run time for the HP, limiting the on/off cycles, and allows providing heat continuously for SH when the system is producing DHW. A 3-pipe connection to this buffer tank is usually recommended (rather than a 4-pipe connection) to supply heat with the HP at the lowest temperature possible and to limit heat losses.
- In System 2, a series of buffer tanks enhances stratification and allows the recirculation water to be fed back into the system at the correct temperature level. This is necessary to ensure a low return temperature to the CO_2 HP. The COP of this latter type of refrigerant is, in fact, negatively impacted by low temperature difference on the heat sink side of the HP. Indeed, on the heat sink side, a R744 provide heat to the system by transcritical gas cooling (instead of refrigerant condensation).
- An external, rather than internal, heat exchanger is used for DHW to provide enough heat transfer area between the HP loop and the DHW tank.
- A mixing valve on the evaporator side of the HP prevents high inlet temperatures during the summer (critical mainly for the R744 HP).

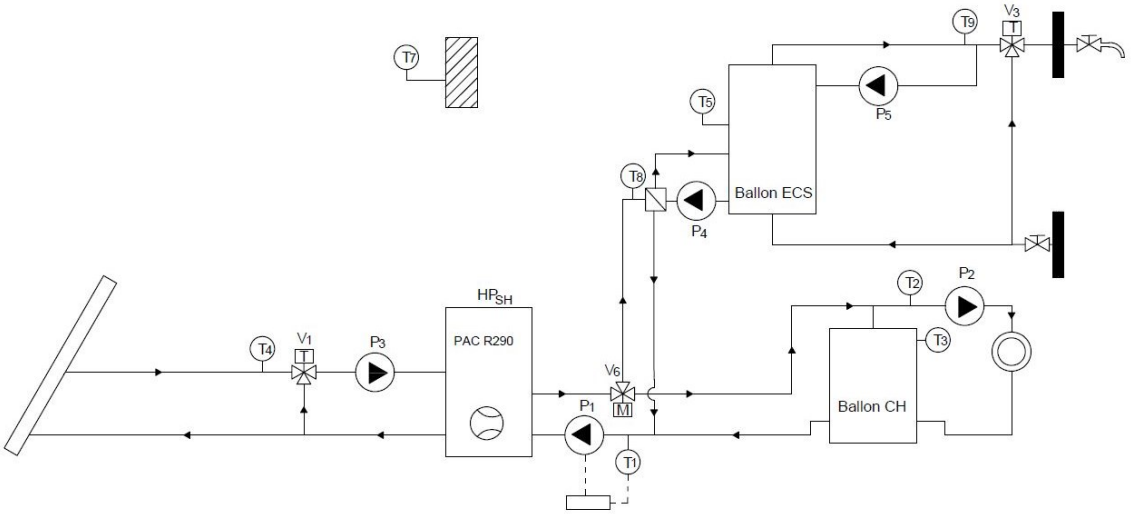

System 1: Propane/R290 HP for both SH and DHW preparation

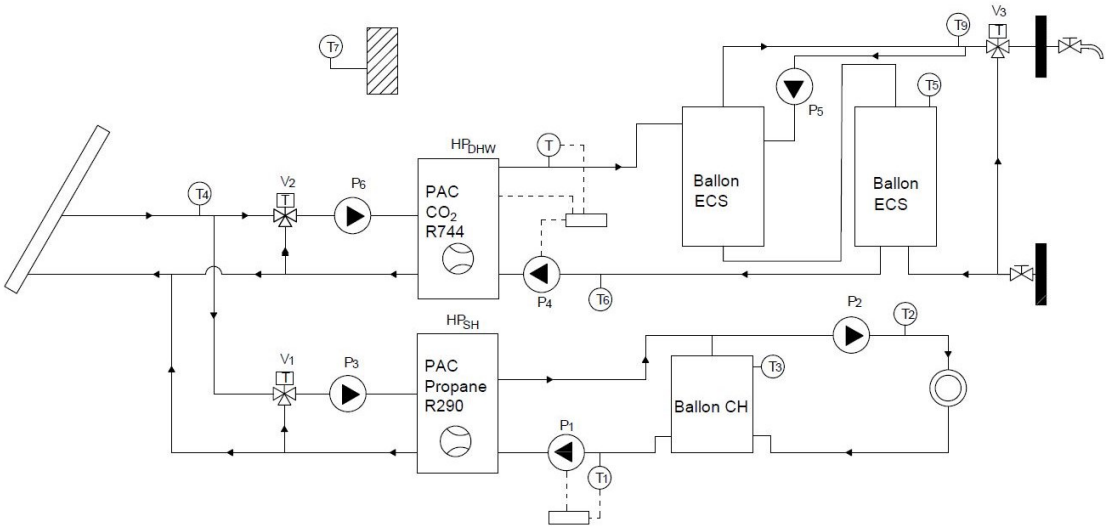

System 2: Propane/R290 HP for SH and CO_2/R744 HP for DHW preparation

Figure 50 Hydraulic diagrams of the two reference systems adopted in the present study for SH and DHW preparation.

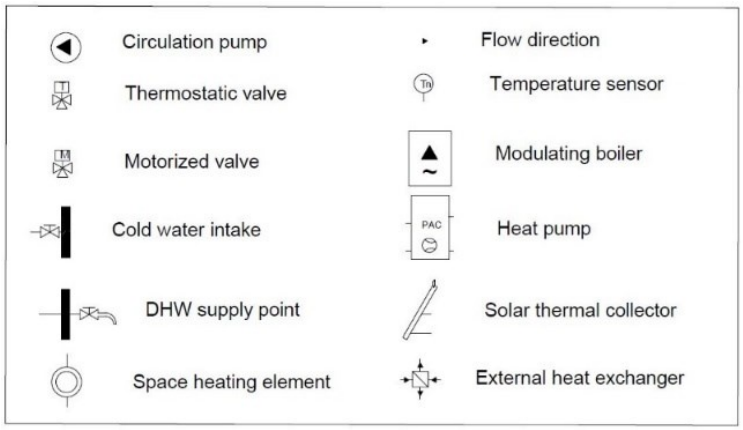

Symbol	Description
T1	HP return temperature on SH loop
T2	SH supply temperature
T3	SH tank top layer temperature
T4	Heat source supply temperature
T5	DHW tank top layer temperature
T6	HP return temperature on DHW loop
T7	Outdoor temperature
T8	HP supply temperature on DHW loop
T9	DHW supply temperature
HP_{SH}	Heat Pump for Space Heating
HP_{DHW}	Heat Pump for Domestic Hot Water preparation
P1	HP circulation pump on SH loop
P2	SH loop circulation pump
P3	Heat source circulation pump for HP_{SH}
P4	DHW loop circulation pump
P5	DHW recirculation pump
P6	Heat source circulation pump for HP_{DHW}

Parameter	Description
$T_{min,SH}$	Outdoor temperature for SH loop activation
$T_{set,SH}(T7)$	SH loop target temperature (based on outdoor temperature and the heating curve)
$T_{c,max,HP}$	HP condenser maximum outlet temperature
$T_{e,min,HP}$	HP evaporator minimum inlet temperature
$T_{set,DHW}$	Nominal temperature for the DHW production loop
$TR_{set,DHW}$	Nominal temperature for the DHW recirculation
T_{biv}	Bivalence point: temperature at which the active heating generator is changed.
PW_{bl}	Modulating boiler power
ρ	Density of circulating water
$\hat{w}$	volumetric flow rate of circulating water
c_p	specific heat of circulating water

Figure 51 Symbols and parameters used in the hydraulic diagrams in **Figure 50**.

4.2 Control strategy

For both system configurations, the following control strategy and design features are considered:

- The system switches between SH and DHW production to maintain the tanks at their respective setpoint temperatures. In the case of simultaneous demand, priority is given to DHW.
- Space heating:
    - SH is enabled when the outdoor air temperature (T7) is below 16°C. If SH is enabled, circulation pump P2 is set ON to distribute heat to the building.
    - The production temperature of the HP for SH is set according to the heating curve of the building (1K above), so as to operate at the lowest possible temperature. The heating curve is available in **Appendix 13.5**. It is based on the monitoring of an existing non renovated multifamily building.
    - When the temperature at the top of the tank (T3) is lower than the setpoint defined by the heating curve and there is no DHW demand, the HP, as well as its circulation pumps (P1 and P3), are switched ON. The SH tank is then charged until the HP return temperature (T1) becomes higher than its setpoint temperature, at which point the HP and circulating pumps (P1 and P3) are switched OFF.
    - The circulating pump on the condenser side (P1) operates with a variable flowrate based on the HP heating output.
- DHW:
    - The HP supply temperature reaches 65°C for DHW preparation to prevent legionella proliferation in agreement with SIA 385/1:2020.

- The DHW system operates based on a temperature at an intermediate level of the DHW storage (T5: top third of the tank in System 1, top of the coldest tank in System 2). If this temperature is lower than the setpoint temperature, the system switches to DHW preparation (in System 1: R290 HP and associated pumps ON; in System 2: R744 HP and associated pumps ON), until the HP return temperature reaches its setpoint temperature or the HP condenser limit temperature.
- In System 1, the condenser circulation pump (P1) operates with a variable flowrate based on the HP heating output, and the circulation pump between the DHW tank and the heat exchanger (P4) operates with a constant flow rate. In System 2, the gas cooler circulation pump (P4) has variable flowrate to maintain the supply temperature at the setpoint.
- DHW recirculation pump (P5) is operated at a constant flowrate according to a schedule (12 hours per day between 6 AM and 11 PM).

- Heat source (PVT):
  - The circulating pumps (P3 and P6) on the PVT collector loop are ON whenever their corresponding HP is ON. They operate with a constant flowrate, as defined in section 4.3.
  - If necessary, the mixing valve (V1 and V2) recirculates part of the flow to keep the working fluid below 20°C (HP evaporator maximum inlet temperature).
  - The back-up heater located at the inlet of the HP evaporator maintains the working fluid above -10°C if the PVT collectors heat gain is not sufficient. This prevents freezing of the working fluid in scenarios with low PVT collector area (minimum temperature of the working fluid with 40% propylene glycol is -22°C).

Note that for modeling purposes, the system control strategy is simplified in the numerical model presented in **Section 6**. Instead of using two temperature sensors for the activation of the heat pumps (one at the top and one at the bottom of the SH and DHW tanks), only one sensor is used, with the following setpoints and hysteresis: heating curve setpoint + 5K for SH and 50°C + 10K for DHW. Since the temperature at the bottom of the tank is not taken into account for control in the model, return temperatures to the heat pump could be higher than expected in practice, which might have an impact on the heat pump efficiency.

4.3 Sizing

The components of the system are sized according to the following procedure.

Heat pumps

For DHW, the HP capacity is sized according to the SIA 385/2 [19], assuming a typical demand of 45 L/day/person (as used by engineering companies when the DHW demand is unknown), storage and distribution losses of 30%, as well as 6 daily charging cycles with a duration of 1 hour each. The HP has to ensure the total DHW demand, it must therefore be able to produce at 60-65°C in the most critical conditions (outside air temperature of -10°C for the Swiss plateau, i.e. inlet evaporator temperature of approximately -15°C).

For SH, the HP capacity is defined to be able to provide the maximum daily SH demand within 18 hours (the 6 remaining hours being reserved for 6 DHW cycles of 1 hour each), with a distribution temperature of 55°C (as per the heating curve) and an outdoor air temperature of -10°C (i.e. an inlet evaporator temperature of approximately -15°C).

In System 1 (R290 HP for SH & DHW), the HP capacity is the highest of the two HP capacity selected (SH and DHW). In System 2 (R290 HP for SH & R744 HP for DHW), each HP capacity corresponds to the HP capacity selected for the specific production it is dedicated to (SH or DHW).

The nominal flowrate on the condenser (or gas cooler) side depends on the HP:

- **R290 HP:** This type of HP operates with a rather low temperature lift. The nominal condenser flowrate is chosen to achieve an inlet-to-outlet temperature difference of 5K in SH at design conditions (outside air temperature of -7°C for the Swiss plateau).
- **R744 HP:** This type of HP requires a higher temperature lift than R290 HP. The nominal gas cooler flowrate is chosen to achieve an inlet-to-outlet temperature difference of 40K at the DHW design conditions described above.

The nominal flowrate on the evaporator side depends on both the HP capacity and the size of the PVT collector field. These elements each have their own recommended flowrate, namely:

- **HP:** Inlet-to-outlet temperature difference of 3K at the conditions described above for SH and DHW
- **PVT collector field:** Nominal flowrate of 0.1 m³/h per collector, as per Consolar's recommendations. To prevent excessively high or low flowrates in the collectors, we have established an acceptable range for the flowrate, namely half (minimum) to twice (maximum) the nominal flowrate, i.e. 0.05 m³/h to 0.2 m³/h per collector.

If the HP evaporator flowrate falls within the PVT collectors flowrate range, it is used as is. However, if it falls outside this range, the selected flowrate is the closest acceptable flowrate for the PVT collectors field (i.e. either the minimum or the maximum PVT flowrate).

Back-up heater

In this project, the back-up heater has an infinite capacity, ensuring that the heat source of the HP is always sufficient to meet the building demand. The aim is to more easily identify and quantify situations where the PVT heat source is undersized to meet the load.

SH and DHW tanks

For DHW, the tank is sized according to the SIA 385/2 standard (i.e., in relation with the DHW demand), assuming the same conditions used for HP capacity sizing.

For SH, the tank is sized based on the HP capacity to ensure that the HP operates at least 20 minutes every time it is switched on. The aim is to prevent short cycling and preserve the lifespan of the HP compressors. Critical conditions correspond to mid-season operation where the HP capacity is high compared to the SH demand. Therefore, tank sizing is calculated for a distribution temperature of 45°C (as per heating curve) and an outdoor air temperature of 15°C (i.e. an inlet evaporator temperature of approximately 17°C).

SOLINK PVT collector field

Consolar and SOLTOP Energie SA recommends a PVT collector field area of approximately 3.5 m² per HP kW (condenser), for an evaporator inlet temperature of -15°C [23].

In **Section 6**, the reference systems are first simulated with the recommended PVT area. Then, for the sensitivity analysis, the PVT area is varied to observe the influence of the installed PVT area on the system energy performance and GHG emissions.

5 Building typologies

This section defines the typology of buildings studied in the sensitivity analysis by numerical simulation in Section 6. These typologies are the same as the ones studied in the AirBiVal project [22], related to the fuel-switch from fossil fuel boilers to air-to-water heat pumps in existing buildings. Thus, it is possible to compare the results of the air-source heat pump system to the TriSolHP system.

Building typologies studied in this project are defined based on several parameters, namely: i) global characteristics, such as the heated floor area or occupant density; ii) heat demand for space heating and domestic hot water, and iii) available roof area. These parameters allow to cover a wide variety of building typologies without getting into details (number of stories, form factor…) which are not necessary for this study. For example (**Figure 52**), two buildings with the same shape, and thus the same roof area, can have different heat demand. In addition, two buildings with a different shape can have the same heat demand, but different roof area. Therefore, the roof area and the heat demand provide enough information on the building typology for this study.

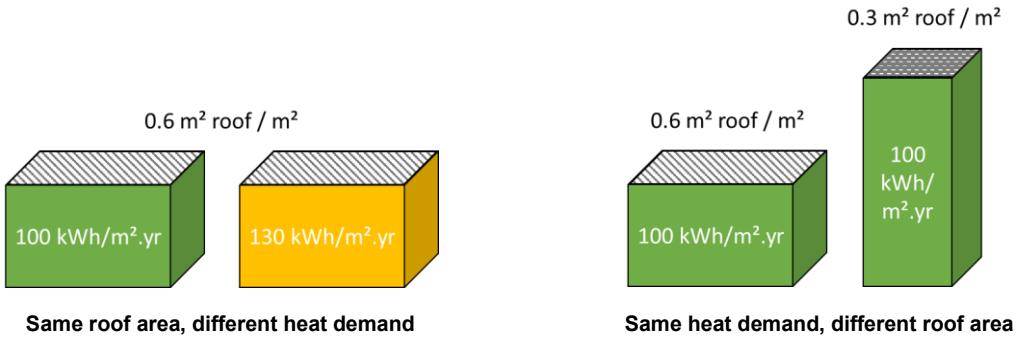

Figure 52 Schematic comparison of different building typologies

5.1 Global characteristics

The building heated floor area and number of inhabitants align with those of a non-renovated multifamily building located in Geneva, built in 1974. This building underwent a comprehensive energy analysis as part of the AirBival project and served as basis for numerical simulations of various air-source HP systems [22]. The total heated floor area of the building is about 4'000 m², accommodating 114 inhabitants, which results in a density of 35.1 m² per person. The building features three entrances, each entrance serving a heated floor area of about 1'330 m². This value is close to the median (1'225 m²) and average (1'448 m²) heated floor area per building entrance for multifamily buildings in Geneva (see **Appendix 13.6**).

5.2 Space heating demand

The SH demand is based on a statistical analysis of the SH demand of Geneva's multifamily building stock [24]. Even though this benchmark corresponds to Geneva's building stock, a recent study has shown that the SH demand distribution is similar at the national level [25]. The SH demand chosen for this study are the following:

- **Low:** 78 $kWh_{th}/m^2.y$, i.e. 281 MJ/m².y (median for 1981-2010 period, 1st decile for 1946-1980 period)
- **Medium (reference):** 101 $kWh_{th}/m^2.y$, i.e. 363 MJ/m².y (9th decile for 1981-2010 period, median for 1946-1980 period)
- **High:** 130 $kWh_{th}/m^2.y$, i.e. 468 MJ/m².y (9th decile for 1946-1980 period)

- The benchmark and selected space heating demand levels are available in **Appendix 13.6.**

- As for AirBiVal, the building is simulated with an hourly load curve, calculated from the annual SH demand and hourly outdoor air temperature using the following hypothesis: i) SH system cut-off temperature of 16°C; ii) SH system forced to a stop between June 1st and September 1st, regardless of the outdoor air temperature.

5.3 Domestic hot water demand

The DHW demand correspond approximately to the minimum, median, and 9th decile of a benchmark of DHW demand for nearly one million m² of heated floor area of MFB located in Geneva [26] :

- **Low:** 25 L/d per person (21.7 $kWh_{th}/m^2.y$) [3]
- **Medium (reference):** 35 L/d per person, corresponding to the average value for multifamily buildings according to SIA 385/2 standard [27], (30.4 $kWh_{th}/m^2.y$)
- **High:** 50 L/d per person (43.5 $kWh_{th}/m^2.y$)
- To obtain an hourly DHW load, we apply the hourly schedule provided in SIA 385/2 standard [27] to the daily DHW volumes.

5.4 Roof area and PVT collector configuration

In order to simulate a system equipped with a realistic PVT collector area, we perform a statistical analysis of the available roof area for Geneva's multifamily building stock, for which a large amount of data is available. Two different roof areas are available from georeferenced data layers, namely:

- the gross roof area, from [28]
- the useful roof area, from [29], taking into account solar irradiation (> 800 $kWh_{th}/m^2.y$), presence of technical equipment/obstacles on the roof and a 1 m margin along the roof edges.

Figure 53 shows an example of the gross and useful roof area provided by these databases. On one hand, the gross roof area overestimates the available roof area because it does not consider technical equipment/obstacles on the roof nor a safety margin on the edge of the roof. On the other hand, the useful roof area only considers surfaces with solar irradiation higher than 800 $kWh_{th}/m^2.y$. Such limit might lead to an underestimation of the available roof area, since the PVT collectors used for the present study are more sensitive to the outside air temperature than the solar radiation. Nevertheless, it is important to note that the roof surface areas provided in this second database (useful area) do not take into account the layout of PVT panels. The actual PVT panels area that can be installed depends on the shape of the available roof surface. For instance, if the roof surface provided by the database is 10 m long, but only 0.5 m wide, the roof area will be equal to 5 m², even though installing PVT panels is not feasible on such a narrow surface. This can result in an overestimation of the PVT surface area that can actually be installed. For further details on the assessment of the available roof area, please refer to **Appendix 13.7**.

[3] Estimation based on a temperature difference of 50 K (from 10°C to 60°C) and 30% storage and distribution losses.

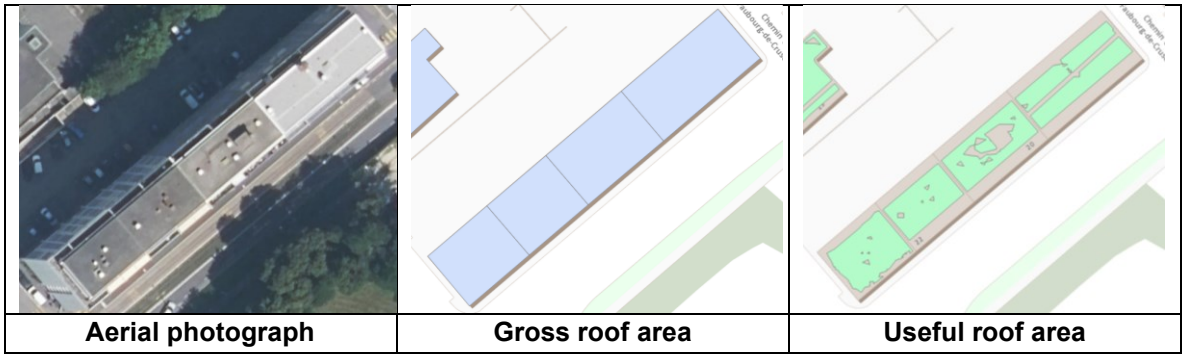

Figure 53 Example of gross and useful roof area given by the databases

The useful roof area is combined with other building characteristics such as the heat demand, resulting from a study on the heat demand of Geneva's building stock [30]. The aim is to calculate indicators to describe the existing building typologies and evaluate the TriSolHP system potential application. Results of the benchmark for the canton of Geneva are presented in **Figure 54** (in m² of PVT area per MWh_{th} of total heat demand), considering a ratio of PVT to roof area of 70% for flat roofs and 90% for sloped roofs.

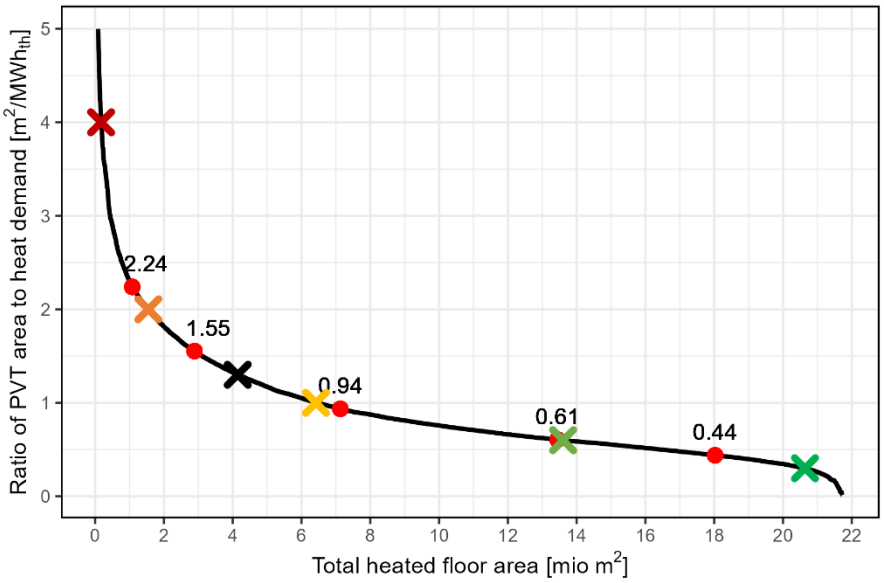

Figure 54 Ratio between available PVT area and heat demand (SH + DHW) for Geneva's multifamily building stock. The red dots from left to right correspond to: 1st decile, 1st quartile, median, 3rd quartile and 9th decile. Crosses correspond to values chosen for the sensitivity analysis.

To examine the TriSolHP system for a wide range of roof areas, the following PVT areas to total heat demand ratios have been considered for the analysis:

- **Very low:** 0.3 m² PVT/ MWh_{th}
- **Low:** 0.6 m² PVT/ MWh_{th}
- **Medium:** 1.0 m² PVT/ MWh_{th}
- **Reference:** 1.3 m² PVT/ MWh_{th}
- **High:** 2.0 m² PVT/ MWh_{th}

- **Very High:** 4.0 m² PVT/ MWh_{th}

- For the reference case, the value of 1.3 m² PVT/MWh_{th} comes from sizing recommended by Consolar and SOLTOP Energie AG: 3.5 m² PVT per kW_{th} HP at B-15/55°C for a flat roof and an inverter/multi-stage HP [31].

In the numerical simulations presented in **Section 6**, the PVT collectors are considered mounted on a flat roof, in an east-west configuration with a slope of 20°, as usually installed by experts in the field. The heat transfer fluid circulating in the loop between the PVT and the HP evaporator is propylene glycol, with a concentration of 40% to prevent freezing during the coldest days of the years.

5.5 Summary of the sensitivity analysis scenarios

Table 4 presents a summary of the sensitivity analysis on the building typology, which is performed separately for each of the two systems (see system definition in section 4). In total, 4 variations in SH and DHW demand are analyzed, in addition to the reference case. Each heat demand variation is evaluated with five distinct PVT collector areas (0.3, 0.6, ..., 4 m² PVT/MWh_{th}), corresponding to various roof sizes and available roof area. This results in a total of 25 cases per system.

Table 4 Summary of the sensitivity analysis on the building typology. Values in blue highlight changes compared to the reference case

Case	Description	SH demand [$kWh_{th}/m^2_{floor}.y$]	DHW demand [L/day.pp]	DHW demand [$kWh_{th}/m^2_{floor}.y$]
1	Reference	101	35	30
2	Low SH demand	**78**	35	30
3	High SH demand	**130**	35	30
4	Low DHW demand	101	**25**	**22**
5	High DHW demand	101	**50**	**44**

6 Thermal and environmental performance of the systems

This section presents simulation results regarding the energy and environmental performance of the two TriSolHP systems (see **Section 4**), designed for existing multifamily buildings. First, we examine a reference case for each system and compare the results between the two systems. Then a sensitivity analysis is conducted to assess the impact of building typology on system performance. Lastly, the TriSolHP systems are compared to an air-source HP system in terms of energy performance and greenhouse gas emissions.

Using the results from this section, the minimum and optimal ratio of PVT area to the total heat demand is defined. Those results are used in section to evaluate the TriSolHP system potential application in the Geneva building stock, based on geo-referenced data (see **Section 8**).

6.1 System modeling

To assess and compare the performance of the proposed systems (see description in **Section 4**), energy models are developed using TRNSYS 18 [32] with a 1-minute time step over a whole year of operation.

Heat source

PVT collectors are simulated using Type 203 [33], analyzed in **Section 2**. It is configured based on the parameters obtained from the Solar Keymark certificate delivered in 2019 (SET1 in **Section 2**), which gives results closest to experimental results than the 2021 certificate. Heat losses in the PVT collector loop are not considered.

The HP numerical models (R290 and R744) incorporate performance maps detailed in **Section 3**. These models account for the impact of operating conditions, such as flowrates and temperatures at the heat source and the heat sink, on the thermal output and COP of the HP. HP sizing is based on the method described in **Section 4**.

An infinite-capacity heating rod located at the inlet of the HP evaporator maintains the working fluid above -10°C in case PVT collectors heat gains are insufficient. The aim is to easily quantify the heat source deficit (i.e. undersized PVT area) from the energy supplied by the electrical backup. Additionally, it will indicate the minimum PVT area required to cover the building heat demand without the need of a heating rod (monovalent system). The efficiency of this heating rod is assumed to be equal to 100%. Another option would have been to shut down the HP when the working fluid temperature is too low, and quantify the resulting decrease in comfort. However, this approach would have been complex since the building is simulated with an hourly load curve, not a detailed building model. There is therefore no interaction between the building and the system.

The HP and the backup heater are switched on and off based on the heat demand. There is no specific control strategy implemented to optimize the self-consumption rate of PV electricity production by the HP.

Heat demand

The SH demand is provided as inputs to the simulation in hourly values, as described in **Section 5**. For both systems, the monitored temperature is located at the top third of the SH tank. The setpoint is determined based on daytime and night time heating curves, with a 5 K hysteresis. These heating curves are derived from in-situ measurements conducted during the St-Julien pilot project and are detailed in **Appendix 13.5**.

The DHW demand is simulated using an input DHW tapping flow rate as described in **Section 5.3**, and a constant mains water temperature of 10°C. In System 1, the monitored temperature is located at the

top third of the tank. In System 2, which employs two DHW tanks to enhance thermal stratification, the monitored temperature is located at top of the tank with the mains water inlet (“cold” tank). In both cases, the setpoint is set to 50°C with a 10 K hysteresis. DHW recirculation is activated intermittently between 6 a.m. and 11 p.m. for a total of 12 hours per day.

Heat losses from the SH and DHW tanks are taken into account, as well as DHW recirculation losses. The latter are calibrated to reach about 30% for a DHW draw-off of 45 L/pers.day (value used for sizing). DHW recirculation losses are included activating the circulation pump intermittently between 6 a.m. and 11 p.m. for a total of 12 hours per day. This frequency corresponds to simulated storage and distribution losses of around 30% for a DHW draw-off of 45 L/pers.day, the value used for sizing ([22]).

Weather conditions

Weather data such as the outdoor temperature and solar radiation come from SIA 2028 standard for the location of Geneva (1’318 HDD[4] and global horizontal radiation of 1’277 kWh/m².y), representative of the Swiss plateau.

6.2 Performance indicators

In order to evaluate and compare the performance of the different systems, following energy, comfort and environmental performance indicators are used.

Energy performance

Figure 55 shows a simplified diagram of the electricity and heat flows. The nomenclature from this figure will be used for the performance indicators and results in the following sections.

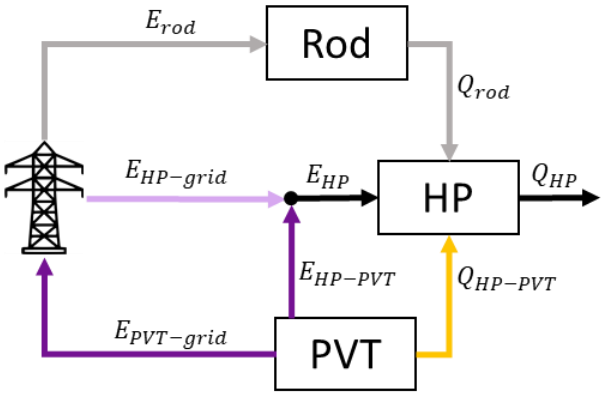

Figure 55: Simplified diagram of the heating system’s electricity (E) and heat (Q) flows.

The annual HP performance is evaluated by the seasonal performance factor (SPF_{HP}) according to Eq. 18. It is defined as the ratio of annual heat production (Q_{HP}) to annual HP electricity consumption (E_{HP}).

$$SPF_{HP} = \frac{\sum Q_{HP}}{\sum E_{HP}} \qquad \text{Eq. 18}$$

The SPF_{HP_Rod} evaluates the energy performance considering the annual electricity consumption of the heating rod (see Eq. 19). Finally, the $SPF_{grid.sys}$ considers the self-consumed PVT electricity by the HP as defined in Eq. 20. The HP self-consumption is calculated with a time step of 1 min.

[4] HDD correspond to the “Écarts de température cumulés (ETC)” defined in SIA 2028-C1:2015, with a base temperature of 12°C.

$$SPF_{HP\_Rod} = \frac{\sum Q_{HP}}{\sum E_{HP} + \sum E_{Rod}}$$ Eq. 19

$$SPF_{grid.sys} = \frac{\sum Q_{HP}}{\sum E_{HP} + \sum E_{Rod} - \sum E_{HP-PVT}}$$ Eq. 20

These indicators do not take into account the electricity consumption of the auxiliaries (circulation pumps, valves, etc.) and de-icing of the PVT.

Comfort

The DHW comfort is evaluated based on the number of tapping hours with a distribution temperature above 50°C (top of storage tank), divided by the total number of tapping hours to obtain an annual percentage.

The comfort in space heating is defined as the ratio of the heat supplied to the building to the total space heating demand (simulation input).

Emissions

Emissions related to the HP and rod electricity consumption from the grid are calculated using Eq. 21, where $E_{HP-grid}$ and E_{rod} are the hourly electricity consumption (in kWh_e). The $f_{elec.h}$ is the hourly CO_{2eq} content of Swiss electricity, averaged over the years 2016 to 2019 (in gCO_{2eq}/kWh_e). The latter is taken from [34], which considers domestic generation and imports from neighbouring countries. The CO_{2eq} electricity content has an overall average of 99 gCO_{2eq}/kWh_e, but daily peak values in the winter reaching 300 gCO_{2eq}/kWh_e.

$$C_{grid} = \sum_{h} (E_{HP-grid} + E_{rod-grid}) \cdot f_{elec.h}$$ Eq. 21

Emissions associated to the PV electricity production self-consumed by the HP (C_{PVT-HP}) are evaluated by a constant emission factor of 42 gCO_{2eq}/kWh_e [35]. The total CO_{2eq} emissions of the system (in gCO_{2eq}) are evaluated by Eq. 22 and are finally related to the HP production (gCO_{2eq}/kWh_{th}) using Eq. 23.

$$C_{global} = C_{grid} + C_{PVT-HP}$$ Eq. 22

$$C_{th} = \frac{C_{global}}{Q_{HP}}$$ Eq. 23

Note that the total emissions of the *system do not include emissions savings related to injection of excess PV electricity production into the grid. In addition, we only consider emissions related to the electricity consumption of the heating system. Embodied energy of the system (e.g. heat pump, PVT collectors, etc.) is not included.*

6.3 Reference systems

Description

The main parameters of the two reference systems are summarized in **Table 5**. Components sizing (HP, tank, pumps, etc.) and control strategy is based on the method described in **Section 4**. The choice of the reference conditions in terms of building demands (SH and DHW) and PVT area are detailed in **Section 5**.

For the reference cases, the PVT area is based on the value recommended by Consolar (3.5 m² PVT per kW_{th} at the HP condenser at B-15/55°C) for a flat roof and an inverter/multi-stage HP [31]. In this case, it corresponds to 1.3 m² PVT per MWh_{th} of heat demand.

It is interesting to note that, for the chosen sizing method, the total installed HP capacity is a lot greater in System 2 than in System 1. Indeed, in System 1, the R290 HP provides both SH and DHW by switching between each production, with approximately 6 h / 24 h for DHW and 18 h / 24 h for SH. Given the high SH demand compared to the DHW demand, it is sized to meet the SH demand. In System 2, each HP is sized to meet the demand to which it is dedicated to (SH or DHW). However, since they have a common heat source, they also have to operate alternately. Therefore, the HP for SH has the same capacity in both systems, but System 2 also has an additional HP capacity installed for DHW. Hence the higher total HP capacity in System 2. This results in higher investment costs for System 2 (see **Section 7**). In addition, given space constraints on the roof and boiler room, it might be more difficult to implement in existing buildings.

Table 5 Main parameters of the reference systems

		System	
Parameters	**Units**	**System 1 (R290 for SH & DHW)**	**System 2 (R290 for SH & R744 for DHW)**
SH demand	kWh/m².yr	101	101
DHW demand	L/day.pers	35	35
	kWh/m².yr	30*	30*
HP capacity - R290 (B0/W35)	kW	377	377
HP capacity - R744 (B0/W10-65°C)	kW	-	134
Volume of SH tank	m³	3.7	3.7
Volume of DHW tank	m³	2	2
Setpoint temperature	SH	Heating curve+5K	Heating curve+5K
	DHW	50°C + 10K	50°C + 10K
PVT area	m² PVT/kW_{th}	3.5	3.5
	m² PVT/MWh_{th}	1.29	1.29
PVT orientation	-	West-east	West-east
PVT tilt angle	-	20°	20°

*Energy for DHW preparation. Estimation based on a temperature rise of 50 K (10°C to 60°C) and storage and distribution losses of 30%.

Results

The energy balances, performances, and CO_{2eq} emissions of the two reference systems are presented in **Figure 56** and summarized in **Table 6**. Detailed daily profiles and typical days from both winter and summer are provided in **Appendix 13.8** for further insight.

Both systems effectively meet the building's heat demand. They ensure 100% comfort rate in SH and maintain a DHW distribution temperature above 50°C most of the time (89-97%).

The energy supplied by the rod accounts for a very small fraction, constituting only 0.1% of the total building heat demand. This indicates that the PVT area is large enough for the system to operate as a monovalent system, with the heating rod as emergency backup only.

When examining individual HP performance for SH production (R290 in both systems), both systems have a similar SPF of about 3.4, due to identical SH configurations (building demand, sizing, setpoint, etc.).

For the DHW production, System 1 uses a R290 HP, while System 2 relies on a R744 HP. As described in **Section 3,** the latter is expected to lead to higher efficiency than the R290 HP for production temperatures above 50°C (if the return temperature to the gas cooler is low enough). However, simulation results show that both systems achieve a SPF_{HP} of 3.26 for the DHW production. The efficiency of the R744 HP, lower than expected, can be attributed to high gas cooler inlet temperatures, which can reach up to 40°C (see typical days in **Appendix 13.8)**. As explained in **Section 3**, the gas cooler inlet temperature has a major impact on the COP of such HP. To ensure a return temperature to the gas cooler as low as possible (System 2), the buffer tanks must be stratified. Many parameters can influence it, such as the control strategy, sizing of the HP and buffer tanks, DHW demand, etc. Next section explores an alternative version of this reference system to try to optimize the energy performance of the R744 HP. Nevertheless, achieving an SPF of 3.26 for DHW production represents a significant improvement compared to air-source heat pumps (ASHP) using HFC refrigerants. The latter typically have an SPF of about 2.8 for DHW, as simulated in the AirBival project.

Both systems display remarkably similar global energy performance, achieving a SPF of about 3.3 without considering the self-consumed PV electricity ($SPF_{HP\text{-}rod}$). When it is taken into account, the SPF of the system ($SPF_{grid.sys}$) reaches approximately 4.1 for both systems.

Table 6 Results for the reference systems

		System	
	Indicators	**System 1 (R290 for SH & DHW)**	**System 2 (R290 for SH & R744 for DHW)**
System	SPF_{HP}	3.33	3.37
	$SPF_{HP\text{-}rod}$	3.31	3.35
	$SPF_{grid.sys}$	4.05	4.15
	PV self-consumption rate (HP only)	22%	22%
	PV coverage rate (HP only)	18%	19%
	PVT electricity production efficiency	17%	17%
SH	SPF_{HP}	3.35 (R290)	3.40 (R290)
	Comfort	100%	100%
DHW	SPF_{HP}	3.26 (R290)	3.26 (R744)
	Comfort (supply > 50°C)	97%	89%
Rod	Share of total heat production	0.12%	0.15%
CO_{2eq} emissions	HP - grid [gCO_{2eq}/kWh_{th}]	32.7 (92.7%)	32.6 (92.4%)
	HP - PVT [gCO_{2eq}/ kWh_{th}]	2.3 (6.5%)	2.4 (6.6%)
	Rod [gCO_{2eq}/ kWh_{th}]	0.3 (0.9%)	0.4 (1.0%)
	Total [gCO_{2eq} / kWh_{th}]	35.3	35.4

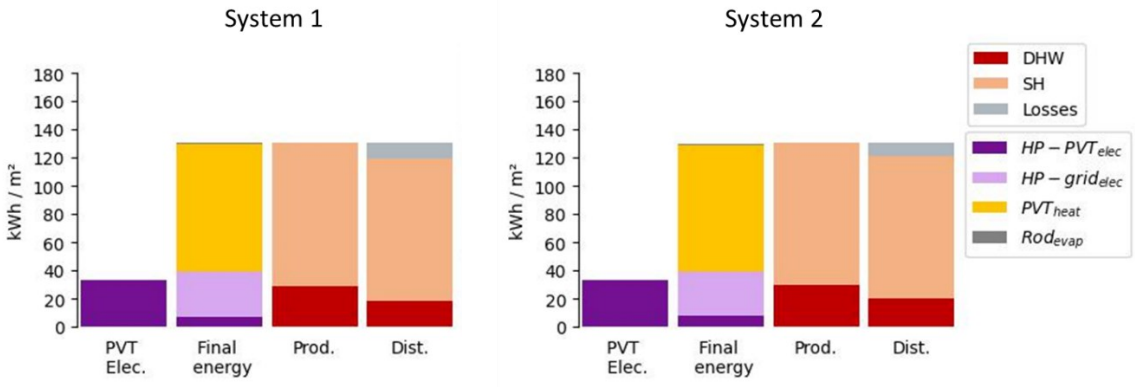

Figure 56 Energy balance of the reference systems

Annual PV electricity production efficiency is equal to 17% in both cases. In addition, both systems achieve an annual self-consumption rate of the PV electricity production of 22%. This self-consumed PV electricity covers about 18% of the HP electricity consumption. Even though most of the PV electricity production occurs during the summer months (June-September), most of the HP's self-consumption happens in winter due to the higher heat demand during daytime (more details in **Appendix 13.8**).

The total CO_{2eq} emissions of both systems are around 35 gCO_{2eq}/kWh_{th}, of which 92% are related to the HP electricity consumption from the grid, about 7% to the self-consumed PV electricity by the HP and only 1% to the heating rod electricity consumption from the grid. Most emissions occur during the winter (see daily profiles in **Appendix 13.8** for more details), because the high building heat demand coincides with a period where the grid's CO_{2eq} content is at its highest.

Alternative version of System 2

To enhance thermal stratification in the DHW tanks in System 2 and thereby improve the efficiency of the R744 HP, this section presents simulation results for an alternative version of System 2, with a lower DHW setpoint.

As mentioned in the previous paragraph, the efficiency of the R744 HP in System 2 is lower than expected. The use of a R744 HP was motived by the high COP for production temperatures above 50°C compared to the R290 HP (providing that temperature to the gas cooler is low enough). The COP of R744 heat pumps is however very sensitive to the gas cooler inlet/outlet temperature difference: for a given gas cooler outlet temperature, the lower the inlet temperature, the higher the COP (**Figure 44**). For the reference system presented in **Table 6**, the average gas cooler inlet temperature is 28°C.

Considering that the mains water temperature is supplied at 10°C at the bottom of the “cold” tank, it appears that there is room for optimization of the system. To ensure that the condenser inlet temperature is as low as possible, the buffer tanks must be highly stratified. Many parameters can influence this, such as the control strategy, sizing of the HP and buffer tanks, DHW demand, etc.

This system configuration and control strategy has already been studied in the literature with an air-source R744 HP and led to relatively low return temperatures to the HP condenser [36]. However, several parameters differ from our system: higher DHW demand, higher volume of the storage tanks compared to the DHW demand and lower DHW setpoint.

To evaluate the influence of these parameters on the proposed TriSolHP system, we ran several simulations on System 2 using values for these parameters similar to the ones of that study. The lower DHW setpoint had the greatest impact on the efficiency of the R744 HP. By maintaining a lower temperature at the top of the "cold" tank, the HP stops before the temperature at the bottom of this tank reaches high levels.

Table 7 shows the results of System 2 for two different DHW setpoints: one with a setpoint of 50°C (as previously presented in the **Table 6**), and the other at 40°C. Both scenarios incorporate a 10 K hysteresis and a HP production temperature of 65°C.

Table 7 Results of System 2 for two different DHW setpoint temperatures, with the reference heat demand and PVT surface area

	DHW setpoint	
Indicators	**50°C + 10K**	**40°C + 10K**
$SPF_{grid.sys}$	4.15	4.19
SPF_{HP}	3.37	3.42
SPF_{HP} for SH (R290)	3.40	3.35
SPF_{HP} for DHW (R744)	3.26	3.72
HP-R744 inlet brine T°C - Evaporator*	11°C	11°C
HP-R744 inlet water T°C – Gas cooler*	28°C	20°C
Comfort (supply > 50°C)	89%	64%

* Weighted average temperature

As shown in **Table 7**, the average inlet temperature at the evaporator of the R744 HP is equal to 11°C in both cases as the PVT area and HP capacity is unchanged. The primary difference lies in the inlet water temperature at the HP gas cooler. The average reaches 28°C with a setpoint at 50°C, while it decreases to 19°C with a setpoint at 40°C. In fact, with a setpoint at 50°C, the HP often stops because its inlet temperature hits the high limit of 40°C (see **Section 3**), while with a setpoint at 40°C, the heat pump stops before the bottom of the "cold" tank reaches such levels. As a result, the SPF of the R744 HP increases considerably from 3.26 to 3.72 when the setpoint is lowered.

Figure 57 illustrates the influence of the gas cooler inlet temperature on the COP of the R744 HP. For a given evaporator inlet temperature of about 10°C, the COP can vary from 2.5 to more than 4.0. Since it is unlikely for the gas cooler inlet temperature to consistently remain as low as 10°C, it can be concluded that the SPF of the alternative version of System 2 (with DHW setpoint at 40°C) is near the maximum achievable performance.

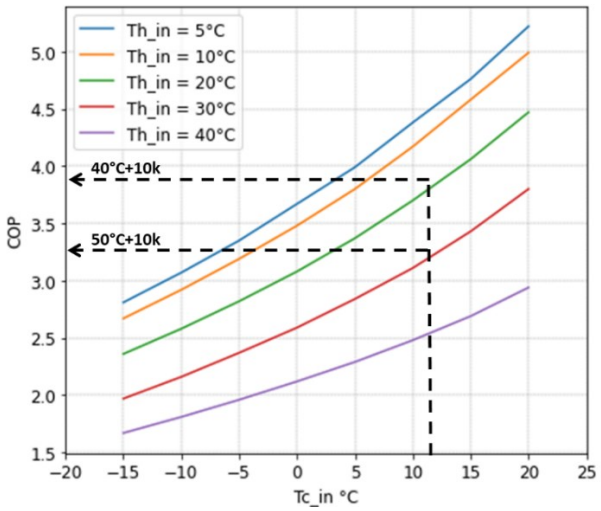

Figure 57 COP of the R744 HP as a function of inlet brine temperature at the evaporator (Tc_in °C) and inlet water temperature at the gas cooler (Th_in °C)

However, when the setpoint is reduced to 40°C, there is a significant reduction of the DHW comfort: the distribution temperature exceeds 55°C only 65% of the time, whereas it reaches 89% when the setpoint is set to 50°C. Therefore, reducing the DHW setpoint at the top of the "cold" tank is not an ideal solution. A more detailed analysis of the system is necessary to determine the optimal configuration (HP and tanks sizing, setpoint etc.), which would allow to achieve high energy performance and DHW comfort.

In addition, it is important to note that there are several limitations to the energy model which can lead to lower thermal stratification of the tanks:

- The tank model is not a detailed computational fluid dynamics model. It is a simplified thermal model (Type534), in which the volume is vertically divided into thermal nodes (20 nodes in our simulations). It does not take into account hydraulic phenomenon such as turbulence or the influence of the type of injection pipes, obstacle plates or other devices designed to enhance thermal stratification.
- As mentioned previously in **Section 4**, the control strategy is simplified in the numerical model since it uses a single temperature sensor, placed at the top of the "cold" tank. In contrast, the recommended approach employs two temperature sensors: one placed at the top of the "hot" tank (containing the distribution outlet) to maintain the distribution temperature above setpoint, and another sensor at the bottom of the "cold" tank (containing the cold-water inlet) to prevent high return temperatures to the heat pump. With two sensors, it is therefore easier to meet DHW comfort and achieve high HP efficiency. Nevertheless, the simulated control strategy is very similar to the one simulated for the air-source R744 HP system [36], which led to relatively low gas cooler inlet temperatures.
- Consequently, simulated return temperatures to the HP could be higher than expected in practice, leading to unexpectedly low SPF.

It should be noted that even with the R744 HP increase in efficiency with the lower DHW setpoint, the overall HP performance for SH and DHW (SPF_{HP}) only increases slightly, from 3.37 to 3.42. This can be attributed to fact that the DHW demand represents only 22% of total demand. Any improvement in the DHW performance will have a minor impact on the overall performance compared to an improvement of the SH production efficiency.

In the following sensitivity analysis, System 2 will be simulated with a setpoint temperature of 50°C + 10 K. This choice ensures a consistent comparison with System 1 and an air-source HP system from a previous study, as they all meet similar DHW comfort.

6.4 Sensitivity analysis

As a complement to the reference cases, the following sensitivity analysis is conducted on various building typologies (described in **Section 5**) to evaluate the impact on the TriSolHP systems:

- Three levels of SH demand: 78, 101 (reference), and 130 kWh_{th}/m^2.year
- Three levels of DHW consumption: 25, 35 (reference), and 50 L/d per person
- Five PVT areas: 0.3, 0.6, 1.0, 2.0, and 4.0 m^2 PVT per MWh_{th} of heat demand

A total of 25 different variants per system are simulated. It is important to note that, in all instances, sizing of the HP and storage tank follows the methodology described in **Section 4**. Detailed information regarding the key parameters (HP capacity, volume of the tanks, etc.) of each case can be found in **Appendix 13.9**.

System 1: R290 HP for SH and DHW

Figure 58 illustrates the CO_{2eq} emissions (gCO_{2eq}/kWh_{th}) and energy performance ($SPF_{HP\text{-}rod}$ and $SPF_{grid.sys}$) results of the sensitivity analysis for System 1.

For a given PVT area, changes in heat demand have a small impact on emissions. For example, in scenarios with a low PVT area of 0.3 m² PVT/MWh$_{th}$, the total emissions range from 49 to 53 gCO$_{2eq}$/kWh$_{th}$. However, the installed PVT area has a significant influence on the CO$_{2eq}$ emissions and energy performance of the system. Indeed, due to an increase in SPF, emissions drop from 50 gCO$_{2eq}$/kWh$_{th}$ with 0.3 m² PVT/MWh$_{th}$ to about 30 gCO$_{2eq}$/kWh$_{th}$ with 4 m² PVT/MWh$_{th}$. This represents a reduction in emissions of about 40% between the least and most efficient systems. In all cases, emissions are mainly due to the HP electricity consumption from the grid, which accounts for 78% to 93% of total emissions.

For each of the heat demand variants ("Low SH", "High SH", etc.), emissions related to the use of the heating rod increase when the PVT area decreases. For low PVT areas, the heat source (i.e. PVT heat gains) is too limited to compensate for the amount of heat extracted by the heat pump. Consequently, the heating rod is activated to keep the working fluid temperature at the evaporator inlet above -10°C. The heat production of the heating rod reaches up to 6% for cases with 0.3 m² PVT/MWh$_{th}$, and represents up to 20% of total emissions. The use of an electrical backup heater therefore has a significant impact on the emissions of the system. It is important to note that the setpoint temperature of the backup heater (-10°C) has an influence on the energy consumption of the system. Lowering the setpoint temperature would reduce the need for backup, but may increase the amount of glycol necessary to prevent freezing of the working fluid, thereby increasing pumping energy consumption.

Increasing the PVT area not only reduces the need for the backup heater, but also results in higher self-consumption of the PV electricity production by the HP. PV coverage of the HP electricity consumption ranges from about 6% with 0.3 m² PVT/MWh$_{th}$ to about 28% with 4 m² PVT/MWh$_{th}$. Emissions due to the HP consumption from the PV production remain relatively low, reaching about 10% of the total emissions with the highest PVT area of 4 m² PVT/MWh$_{th}$.

Across all heat demand variants, it is evident that increasing the PVT area above 1 m²/MWh$_{th}$ (which is close to Consolar's sizing recommendations) does not yield a significant reduction in emissions. For example, doubling the PVT area from 2 to 4 m² PVT/MWh$_{th}$ only reduces emissions by 1.8 gCO$_{2eq}$/kWh$_{th}$ (about 5%). Indeed, the thermal efficiency (SPF$_{HP\text{-}rod}$) and the self-consumption from the PV production do not improve significantly.

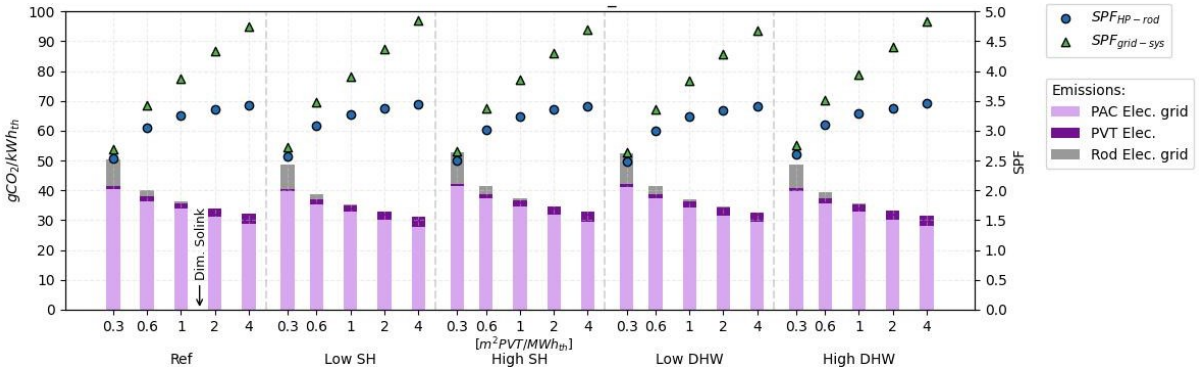

Figure 58 Results of the sensitivity analysis for System 1. Left axis: gCO$_{2eq}$ emissions per kWh$_{th}$ of heat demand (bars). Right axis: SPF_{HP-rod} and $SPF_{grid-sys}$ (points)

To better compare the energy performance between the different scenarios, **Figure 59** shows the energy performance indicators (SPF) in relation to the PVT area in m² PVT/MWh$_{th}$ and m² PVT.

We can observe that for the same m² PVT/MWh$_{th}$ (top part of the figure), there is no significant difference in the energy performance when the heat demand changes. This is because the PVT area and HP capacity are sized based on the building heat demand, using the same sizing method. However, we must not lose sight that as demand varies, the installed PVT area (in m²) changes, as shown on the bottom part of **Figure 59**.

In this figure, we observe that improvements of the heat production efficiency (HP and heating rod) are marginal for PVT area above 1-2 m² PVT/MWh$_{th}$ or 500-1000 m² of PVT. Specifically, the SPF$_{HP}$ and SPF$_{HP\text{-}rod}$ reach a limit at approximately 3.5. Nevertheless, increasing the PVT area still improves the SPF$_{grid.sys}$ (up to about 4.8), as the HP self-consumption of electricity from the PV increases. Like SPF$_{HP}$ and SPF$_{HP\text{-}rod}$, there is also a limit, but the system has not reached it yet with 4 m² PVT/MWh$_{th}$.

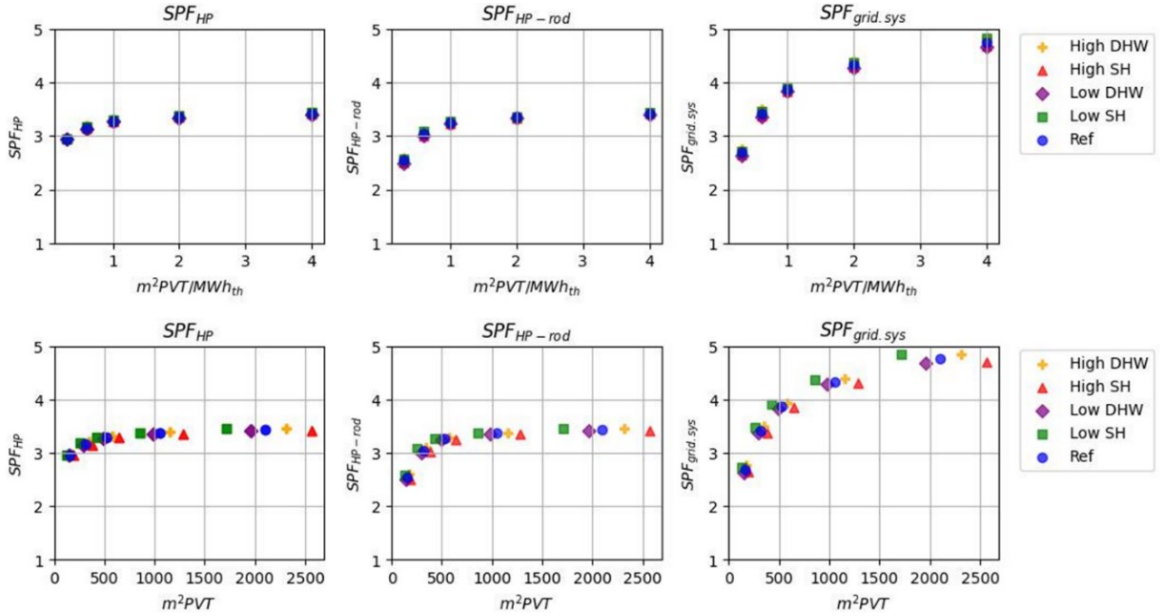

Figure 59 System 1 - Seasonal performance factor (SPF) as a function of the PVT collector area in m²PVT/MWh$_{th}$ (top) and m²PVT (bottom) for different building heat demand.

Figure 60 shows the distribution of the heating rod (top) and R290 HP (bottom) electricity consumption calculated on a 15-min basis. We can note that for low PVT areas (0.3-1.0 m² PVT/MWh$_{th}$), the power usage of the heating rod is greater than or equal to the R290 HP power usage. It is not cost-effective to install an electrical backup heater with the same or greater electrical capacity than required by the HP. In addition, the practice shows that on-site maximum connection power is often limited in large existing buildings and, in some cantons, the use of direct electric heating is subject to restrictions. For low PVT areas, it could therefore make more sense to implement a bivalent system with a gas boiler (on the condenser side of the HP), but this might increase CO_2 emissions of the system.

Above 0.6 m²PVT/MWh$_{th}$, there is minimal need for the heating rod. Over a whole year, the heating rod operates during only 3 to 66 hours. These systems may even operate without the heating rod or use it solely as an emergency backup (monovalent system). To confirm this assumption, it would be necessary to simulate these systems without the heating rod, or with a heating rod of limited capacity.

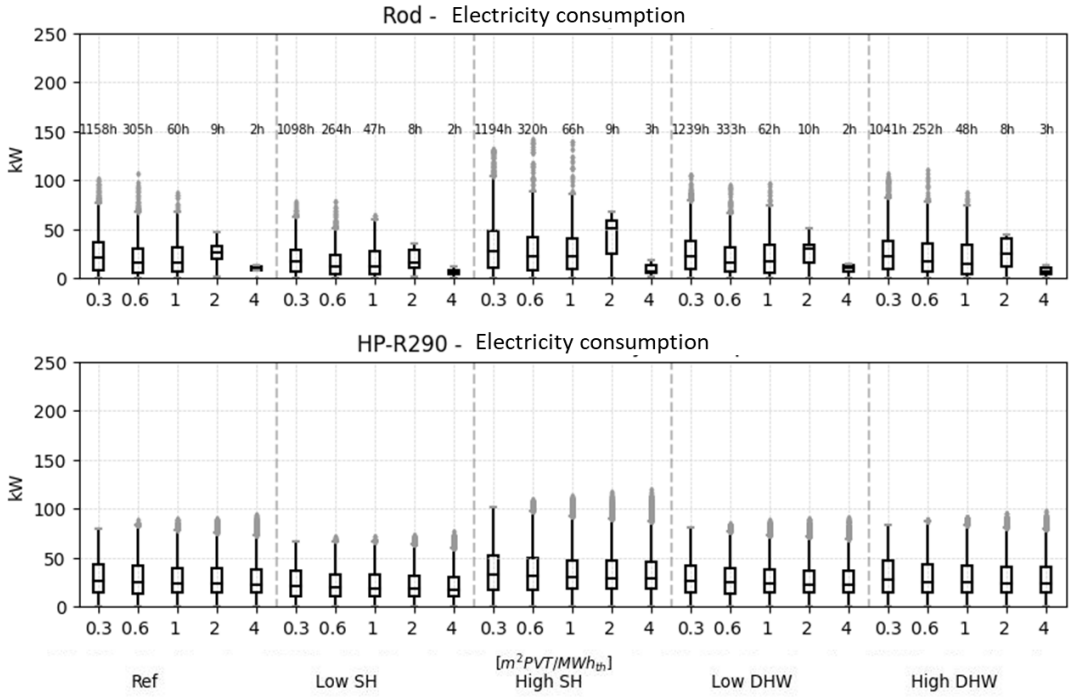

Figure 60 System 1 - Distribution of the power consumption by the rod (top) and the HP-R290 (bottom) for different building heat demand. Power consumption calculated from 15-minute average.

System 2: R290 HP for SH & R744 HP for DHW

Figure 61 illustrates the CO_{2eq} emissions (gCO_{2eq}/kWh_{th}) and energy performance ($SPF_{HP\text{-}rod}$ and $SPF_{grid.sys}$) results of the sensitivity analysis for System 2.

In comparison to System 1, System 2 shows similar trends and closely aligned indicators in terms of both emissions and SPF. System 2 shows a slight increase in performance compared to System 1 of maximum 4% for $SPF_{HP\text{-}rod}$, and maximum 5% for $SPF_{grid.sys}$. Total emissions are very similar in both systems, with less than 3% difference.

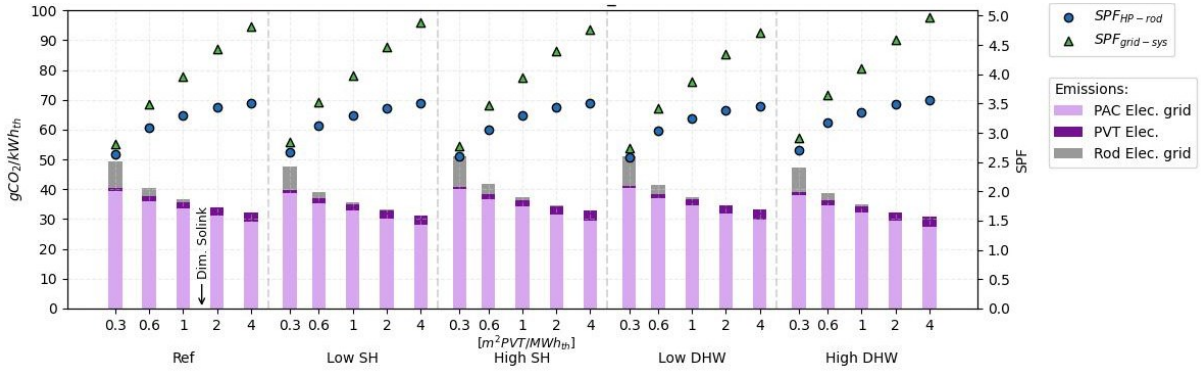

Figure 61 Results of the sensitivity analysis System 2. Left axis: gCO_{2eq} emissions per kWh_{th} of demand (bars). Right axis: SPF_{HP-rod} and $SPF_{grid-sys}$ (triangles and circles points)

Like System 1, we observe in **Figure 62** that improvements of the heat production efficiency (HP and heating rod) and CO_2 emissions savings are marginal for PVT area above 1-2 m² PVT/MWh_{th} or 500-1000 m² of PVT. Specifically, the SPF_{HP} and $SPF_{HP\text{-}rod}$ reach a limit at approximately 3.5.

Nevertheless, increasing the PVT area still improves the $SPF_{grid.sys}$ (up to about 4.9), as the HP self-consumption of electricity from the PV increases. Like SPF_{HP} and $SPF_{HP\text{-}rod}$, there is also a limit, but the system has not reached it yet with 4 m² PVT/MWh_{th}.

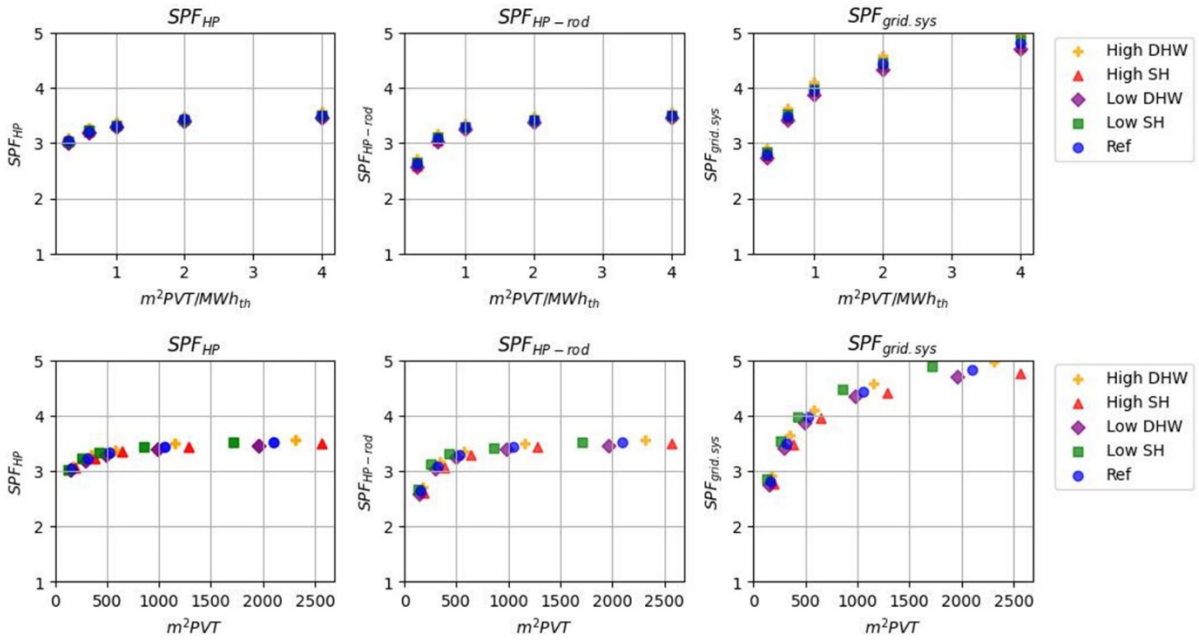

Figure 62 System 2 - Seasonal performance factor (SPF) as a function of the PVT collector area in m²PVT/MWh_{th} (top) and m²PVT (bottom) for different building's demand

Also like System 1, for small PVT areas (0.3-0.6 m² PVT/MWh_{th}), the heating rod power usage reaches or even exceeds the HP power usage, which is unrealistic from both economical, practical and legal perspectives. However, with larger PVT areas (above 0.6 m² PVT/MWh_{th}), the need for the heating rod is minimal, as it operates during only 3 to 82 hours per year. These systems might even operate without the heating rod or with the heating rod as an emergency backup only (monovalent system). Additional simulations without the heating rod or with a heating rod of limited capacity would be required to confirm this assumption.

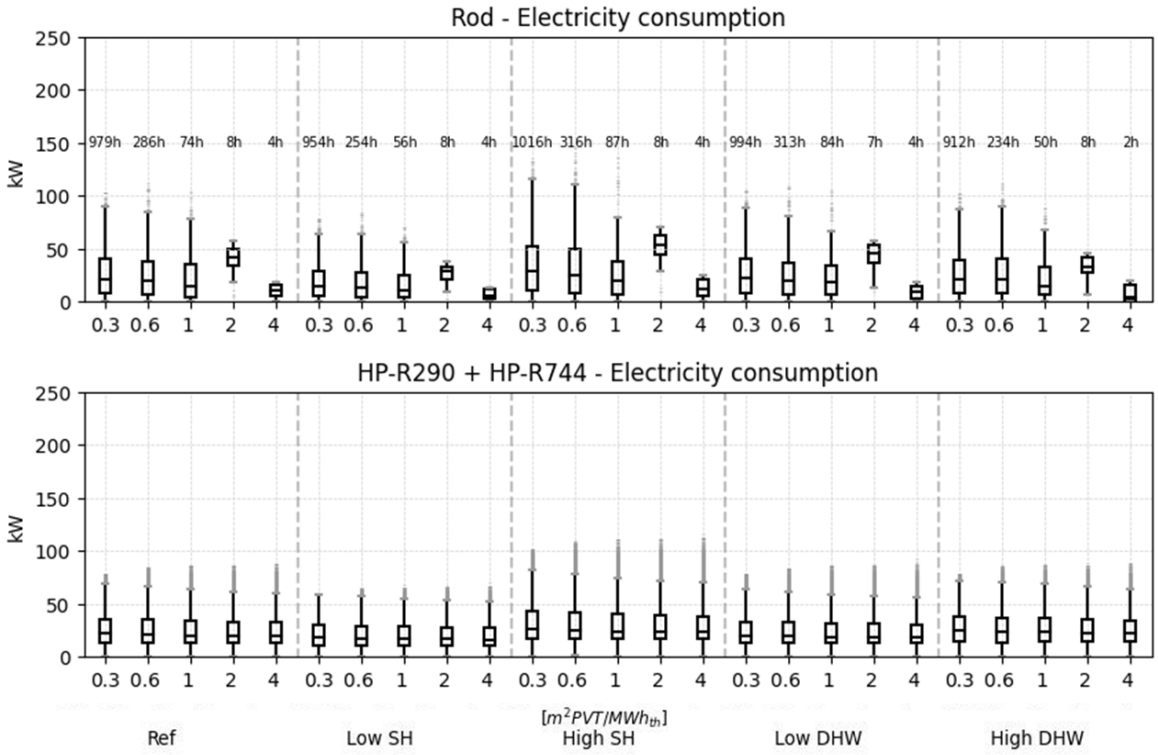

Figure 63 System 2 - Distribution of the power consumption by the rod (top) and the HPs (bottom) for different building heat demand. Power consumption calculated from 15-minute average.

In summary, energy performance improvements and CO_{2eq} savings are small for both System 1 and 2 once the PVT area exceeds 1-2 m² PVT/MWh$_{th}$ or 500-1000 m² of PVT. Additionally, within this same range, the need for the electrical backup becomes negligible (monovalent system). It is interesting to note that this falls within the range of Consolar's sizing recommendations for the PVT area. Systems with smaller PVT field have to be operated in bivalent mode.

6.5 Comparison with an air-source heat pump system

In this section, TriSolHP systems are compared to a monovalent air-source HP system (ASHP) in terms of energy performance and greenhouse gas emissions.

Energy performance and emissions of the monovalent ASHP system is taken from a sensitivity analysis conducted as part of the AirBiVal project [22]. That analysis involved the same heat demand variations (High SH, Low SH, etc.), sizing method, and emissions calculation method as used for the TriSolHP systems. Findings from that project indicate that, regardless of heat demand, the monovalent ASHP system consistently achieves a SPF_{HP} of approximately 2.86 and emissions of around 45 gCO_{2eq}/kWh_{th}. Since no backup and no local PV system were considered in that analysis, all three energy performance indicators (SPF_{HP}, $SPF_{HP\text{-}rod}$ and $SPF_{grid.sys}$) are identical.

Figure 64 shows the results of performance indicators and emissions of the TriSolHP systems as a function of the PVT collector area (in m² PVT/MWh$_{th}$), as well as the SPF and emissions of the ASHP system.

Both TriSolHP systems outperform the ASHP system when the PVT collector area exceeds about 0.5 m² PVT/MWh$_{th}$. The TriSolHP systems achieve an SPF (SPF_{HP_rod}) ranging from 2.5 to 3.5, while the ASHP system maintains a value of 2.86. Emissions for the TriSolHP systems range between 31 to 54 gCO_{2eq}/kWh_{th}, while the air-source HP stands at 45 gCO_{2eq}/kWh_{th}. Above approximately

0.5 m² PVT/MWh$_{th}$, the TriSolHP systems leads to up to 32% emissions savings compared to the ASHP system.

It is important to note that emissions and SPF$_{grid.sys}$ calculations for the TriSolHP systems include self-consumption from the local PV electricity production, while the ASHP system are based only on electricity consumption from the grid. Emissions and energy performance from the ASHP system could potentially be improved if a PV system is incorporated to cover part of the HP electricity consumption. However, in practice, it is often necessary to cascade several small ASHP units on the roof to meet the capacity requirements of existing buildings (due to structural constraints of the roof, noise emissions of larger units, …) [22]. This approach can therefore limit the available space for a PV system. Therefore, for a given building heat demand and roof area, the total PV capacity installed would likely be greater with a TriSolHP system, than with an ASHP and PV system.

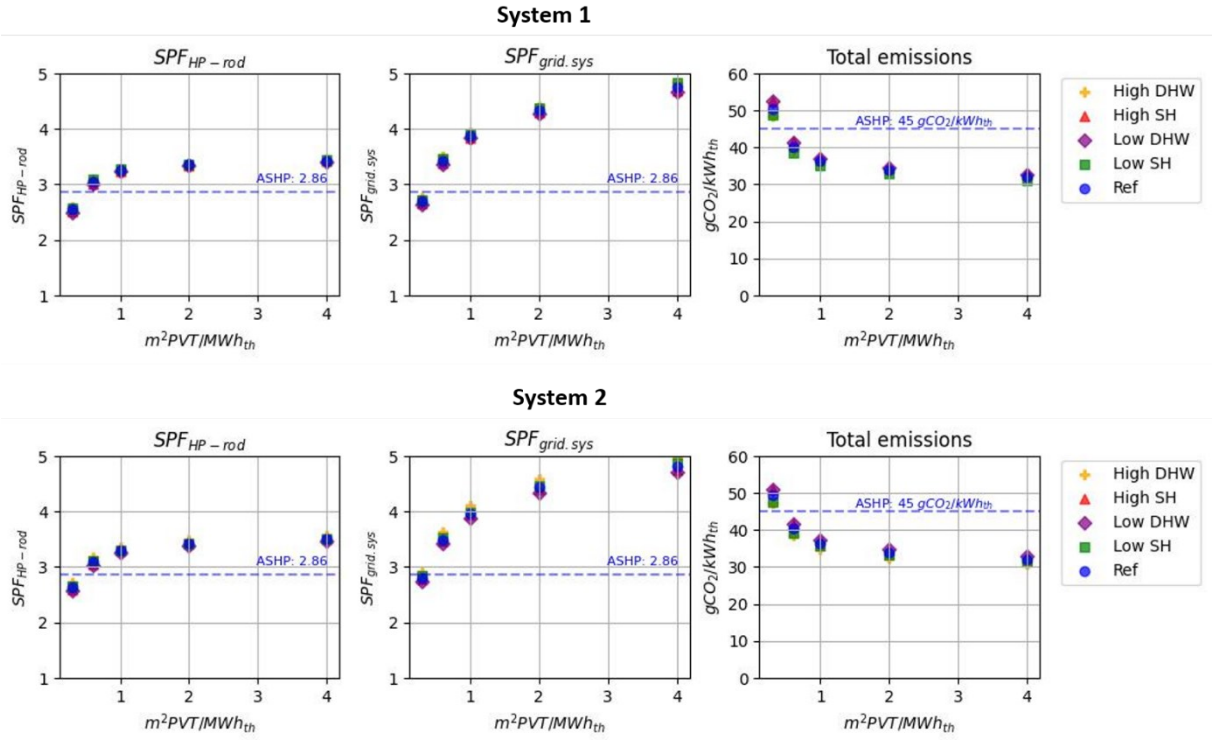

Figure 64 Energy performance and CO_2 emissions comparison between the TriSolHP systems and an ASHP system

6.6 Conclusions

Simulation results of the two TriSolHP systems, presented in this section, provide valuable insights on their energy and environmental performance for existing multifamily buildings. We conduct a sensitivity analysis to assess the impact of building typology (PVT surface area and building heat demand) on several key indicators, and we compare the TriSolHP systems to an air-source HP system.

System 1 (R290 HP for SH & DHW) and System 2 (R290 HP for SH & R744 HP for DHW), effectively meet the building's heat demand, displaying similar energy balances and performance indicators.

For a given ratio between PVT area and building heat demand (m² PVT/MWh$_{th}$), variations in heat demand minimally affect energy performance and emissions for both systems. It seems that the TriSolHP system performance is mainly limited by the PVT collector area.

The sensitivity analysis demonstrates that increasing the surface area from 0.3 to 4.0 m² PVT/MWh$_{th}$ leads to notable improvements in HP energy performance, self-consumption of the local PV electricity

production, as well as emissions savings. The seasonal performance factor of the system (SPF), considering the electricity consumption of the HP as well as a backup heating rod placed at evaporator inlet, rises from 2.58 to 3.56. Furthermore, when considering the self-consumption of PV electricity by the HP, the SPF increases from 2.74 to 4.97. Additionally, self-consumed PV electricity covers approximately 6% to 28% of the HP electricity consumption. Emissions reduce from 52 to 31 gCO_{2eq}/kWh_{th}, with the majority attributed to HP electricity consumption from the grid (78% to 93% of total emissions).

It is important to note that, the improvements of the energy performance and emissions savings are small when the PVT area exceeds 1 m² PVT/MWh_{th} or 500-1000 m² of PVT. Above this range, there is minimal need for the heating rod, and these systems may even operate without it or use it solely as an emergency backup (monovalent system). To confirm this assumption, it would be necessary to simulate these systems without the heating rod, or with a heating rod of limited capacity. In addition, it would be interesting to evaluate the impact of the setpoint temperature of the back-up heating rod (-10°C) on the minimum PVT area required to obtain a monovalent system.

For areas below 1 m² PVT/MWh_{th}, a significant amount of energy is supplied by the heating rod, and its maximum power usage (kW) is greater than or equal to the power usage of the HP. It is not cost-effective to install an electrical backup heater with the same or greater electrical capacity than required by the HP. In addition, the practice shows that on-site connection power is often limited and, in some cantons, the use of direct electric heating is subject to restrictions. For low PVT areas, it could therefore make more sense to implement a bivalent system with a gas boiler (on the condenser side of the HP), but this might increase CO_2 emissions of the system. While the use of gas boiler might increase the system CO_2 emission, it may offer more cost-efficient alternative to monovalent systems. The gas boiler may then be used until the building SH demand is reduced by retrofitting.

Both TriSolHP systems outperform a monovalent air-source HP system when the PVT collector area exceeds about 0.5 m² PVT/MWh_{th}. The TriSolHP systems achieve an SPF ranging from 2.5 to 3.5 when considering the HP and heating rod electricity consumption, while the air-source HP system maintains a value of 2.86. In addition, above 0.5 m² PVT/MWh_{th}, the TriSolHP systems leads to up to 32% emissions savings compared to the monovalent air-source HP system. This reduction of CO_2 emissions is partly due to self-consumption of PV electricity.

While both TriSolHP systems show promising energy performance and emission savings, their implementation in a building and the selection of the installed PVT area depends on economic considerations, as well as the available roof area and volume in the boiler room. In the next section (**Section 7**), we focus on the economic aspects of such systems. In addition, in **Section 8**, we evaluate the potential application of the TriSolHP systems in Geneva's multifamily building stock using geo-referenced data on building heat demand and available roof area.

7 Financial analysis of the various systems simulated

In the pursuit of sustainable and efficient energy solutions, a comprehensive economic analysis is essential to evaluate the financial viability and long-term benefits of an energy system. The economic aspect plays an important role in estimating the overall economic sustainability of a proposed energy solution.

The two energy production systems under study have been compared from the economic point of view based on a series of assumptions and models derived both from literature and from communications with experts in the field. By examining the various economic components associated with each system, including initial capital expenditures (i.e., CAPEX) and operational costs (OPEX), the economic analysis seeks to perform a cost comparison between the solutions under study to establish common grounds for comparison of their performance with benchmark solutions already widespread in the heat generation industry.

7.1 Methodology and main KPIs

The economic analysis of the two heat energy generation systems described in **Section 4** is based on a series of sources of information, spanning from literature to private communications with project partners, in particular SIG and Sol-Top Energies.

To estimate the overall cost, each of the two circuits has been first subdivided in the following subsystems:

- **A low temperature heat source**, made of a solar field of Solink PVT collectors and including the field components, like connecting conduits, decoupling tanks, valves, etc.;
- **A heat pump subsystem**, including only the HP (a unique R290 HP for System 1; an R290 HP together with an R744 HP for System 2);
- **DHW and SH distribution subsystems**, including hygienic tanks and technical storages;
- **The electrical equipment** required for the PVT panels, comprising inverters and cables.

The economic analysis has focused on deriving CAPEX and OPEX estimations for each subsystem in [37] to compute the Levelized Cost of Heat (LCOH):

$$LCOH = \frac{\sum_{t=1}^{n} \frac{C_t + O_t + V_t}{(1+d)^t}}{\sum_{t=1}^{n} \frac{E_t}{(1+d)^t}} \qquad \text{Eq. 24}$$

where t is the period ranging from year 1 to year n (i.e., the lifetime of the energy system); C_t is the capital cost in period t, O_t is the operation fixed expenditures and V_t is the variable operating expenditures, while E_t is the energy generated in period t and d is the discount rate, assumed to be 3% (see **Table 8** for a list of the main general parameters of the economic analysis).

By adopting the LCOH as a key performance indicator, the two energy generation systems can be directly compared considering their operating life, their performance and their fixed and variable costs.

Table 8 Main general parameters of the economic analysis

Parameter	Value	Unit
Energy system service time	30	years
Own capital	100	%
Discount rate	3	%
PV degradation & electricity fare	~0	%
Component renewal time (HP)	15	years
Component renewal time (MCR of PVT)	15	years

The LCOH is thus calculated for most of the scenarios assumed during the sensitivity analysis described in **Section 6**. To reduce the number of cases, the scenarios shown in **Appendix 13.9** have been reduced in number by selecting those for which the solution envisaged by the TriSolHP project makes sense, as the required roof area available for the installation of the PVT field allows the adoption of the system for buildings higher than at least 3 floors. To derive this indicator, the required PVT surface is beforehand "translated" in effective roof area by using a 70% fill-factor between the collector aperture area and the gross surface of a solar field covering a flat roof, taking into consideration the spaces left as pathways between rows and the typical distances to the roof edges. Once derived, the effective solar field footprint can be compared to the gross roof area that a building would require to host the solar field installation. In practice, the maximum number of floors that a building equipped with a solution envisaged in the TriSolHP project could have, is given by the ratio of the required roof footprint (i.e., the solar field gross area) and the 4'000 m^2 Energy Reference Area (ERA) .

Table 9 shows the scenarios for which the economic analysis has been performed, based on the fact that the roof area required by the heat source allows covering the energy needs of a building with a heated floor area of 4'000 m^2 distributed over, at least, 3 floors.

Table 9 List of cases selected for the economic analysis (for only R290 HP is used for System 1 whereas both R2909 and R744 are used for System 2).

Scenario	Case ID	PVT Area, in [m^2]	Ratio PVT/PAC, in [m^2/kW]	HP power (R290 @ B0W35), in [kW]	HP power (R744 @ B0W10-65°), in [kW]	Maximum number of building floors
DHW and SH reference demand	Dim. SOLINK	681	1.81	377	134	4
	2	315	0.84	377	134	9
	3	526	1.40	377	134	5
Low SH needs	8	428	1.50	286	134	7
	9	856	2.99	286	134	3
High SH needs	12	385	0.79	485	134	7
	13	642	1.32	485	134	4
High DHW needs	17	294	0.78	377	134	10
	18	491	1.30	377	134	6
Low DHW needs	22	347	0.92	377	134	8
	23	578	1.53	377	134	5

7.2 Cost assumptions

The investment and operating costs of the two energy production systems under study (System 1 and System 2, see description in **Section 4.1**) have been estimated by combining economic data for the following sub-systems:

- the heat source, needed to supply environmental energy to the evaporator side of the heat pump unit;
- the heat pump unit; either a single R290 heat pump for System 1, or an R290 HP for SH combined with a R744 HP for DHW preparation in the case of System 2;
- the accessories of the heat pump circuit (valves, piping, MCR, preliminary studies, etc…);
- the tanks and systems required for storing DHW or SH energy and distributing it to the user circuits.

Each subsystem has undergone a cost analysis to determine CAPEX and OPEX data.

7.2.1 The heat source

Both System 1 and System 2 involve the adoption of brine-water HP, either based on propane gas (i.e., R290), or on CO2 refrigerant (i.e., R744). In both cases, the low temperature heat source is made by a Solink PVT solar field, whose dimensions depend on the assumptions of the simulated scenario.

In order to estimate the CAPital EXpenditure (CAPEX) of the Solink PVT field, one of the project partners has communicated a typical quote for a field of about 300 m^2 together with one for about 800 m^2. From these quotations (see Appendix 13.10 for details), the following expressions have been derived to model the initial investment costs either on the solar field extension (aperture area, A_p, in [m^2]) or on the PV electrical power (peak PV power, P_{PV}, in [kW$_{el}$]):

- *Main field* (including collectors, supporting structures, expansion system, hydraulic decoupler, glycol, installation and commissioning):

$$CAPEX_{MainField} = 870 * A_p + 3933 \ [CHF] \quad \text{Eq. 25}$$

- *Transport & engineering:*

$$CAPEX_{T\&E} = 22 * A_p \ [CHF] \quad \text{Eq. 26}$$

- *Solar field piping:*

$$CAPEX_{FieldPiping} = 0.54 * 200 * A_p \ [CHF] \quad \text{Eq. 27}$$

- *Piping descending from roof:*

$$CAPEX_{FromRoofPiping} = 2 * 4 * N_f \ [CHF] \quad \text{Eq. 28}$$

- *Piping glycol content:*

$$CAPEX_{PipingGlycol} = (0.61 * A_p - 83.6) * 5.95 \ [CHF] \quad \text{Eq. 29}$$

- *PVT MCR:*

$$CAPEX_{PVT\_MCR} = 20670 \ [CHF] \ if \ Ap > 600 \ m^2$$

$$CAPEX_{PVT\_MCR} = 10140 \ [CHF] \ if \ Ap < 300 \ m^2 \quad \text{Eq. 30}$$

$$CAPEX_{PVT\_MCR} = 15405 \ [CHF] \ if \ 600 \ m^2 < Ap < 300 \ m^2$$

- *Electrical part of PVT system* (inverters, electrical material including planning and installation):

$$CAPEX_{PV} = 0.183 * 5356.1 * (P_{PV})^{-0.284} * P_{PV} \ [CHF] \quad \text{Eq. 31}$$

The relationships above should be adopted to estimate the CAPEX of solar fields made of Solink PVT collectors with an aperture area ranging from 200 to 1000 m^2.

Based on partner information and interpolation of data found in literature, the OPerational EXpenditures (OPEX) have been computed by considering OPEX related to the PV field and OPEX related to the solar thermal part of the PVT field:

$$OPEX_{PVT} = OPEX_{ST} + OPEX_{PV} \quad \text{Eq. 32}$$

and in particular:

- *Solar thermal OPEX ($OPEX_{ST}$):*

$$OPEX_{ST} = 3.45 * A_p + 714 \ [CHF/y] \quad \text{Eq. 33}$$

- *PV field OPEX ($OPEX_{PV}$):*

$$OPEX_{PV} = 23.15*100*(P_{PV})^{-0.318}\ [CHF/kWh_e/y] \quad \text{Eq. 34}$$

OPEX figures are given with reference to the produced electricity in the case of the PV part of the PVT field, and as a yearly expense for the solar thermal part. The $OPEX_{PV}$ includes maintenance and operation expenses (excluding the electricity consumption of HP), taking into account the substitution of the PV inverters during the plant service life. The solar thermal OPEX includes operation and maintenance during the field service life, but no component substitution or renewal during the plant lifetime. As a consequence, in the economic analysis it is assumed that on the 16th year, the PVT MCR part is renewed and the corresponding capital expenditure is repeated accordingly.

7.2.2 The heat pump unit and its accessories

Based on information received form project partners (see **Appendix 13.10**), heat pumps investment and operational costs can be expressed as a function on the heat pump nominal thermal power at the condenser (i.e., on the user's circuit), according to the following relationships:

- *Heat pump unit*:

$$CAPEX_{HP} = 500\ CHF/kW_{th}\ [CHF] \quad \text{Eq. 35}$$

- *HP accessories (valves, MCR, buffer tank)*:

$$CAPEX_{HPA} = 800\ CHF/kW_{th}\ [CHF] \quad \text{Eq. 36}$$

In the following economic analysis, it is assumed that the HP unit price doesn't change between an R290 HP and an R744 HP. This implies that the total HP cost is higher in System 2 than System 1. As SH and DHW preparation are decoupled in System 2, in fact, System 1, that is based on a single R290 for both SH and DHW preparation, requires a smaller HP size to cover both energy needs as the SH circuit requires higher power than the DHW system. This is valid because production in System 1 is scheduled to be in alternance between the two loads with 6 cycles per day for DHW preparation. In the case of System 2, then, the overall HP power is equal to the sum of the power of the SH HP and the DHW preparation HP, while for System 1, the unique R290 HP satisfies both power requirements. The nominal heating power for the R290 HP is based on conditions B0W35, while the R744 performance is based on B0W10-65 conditions.

According to partner's suggestion, OPEX for the HP subsystem has been considered a function of the nominal HP thermal power P_p, based on the following relationship:

$$OPEX_{HPA} = 6152 + 13.3*P_p\ [CHF] \quad \text{Eq. 37}$$

7.2.3 The balance of plant (BOP)

In the analysis, it is assumed that the SH system and the DHW preparation system have a similar specific CAPEX in the two circuits. The difference in specific price between System 1 BOP and System 2 BOP is considered negligible. The following formulation of the SH and DHW system CAPEX is a function of the total HP nominal thermal power P_p:

$$CAPEX_{SH,DHW} = 1000*P_p\ [CHF/kW_{th}] \quad \text{Eq. 38}$$

Since System 1 is equipped with a HP featuring a lower total power output, it follows that the total CAPEX of System 1 BOP is lower than that of System 2, since this latter adopts more components.

The OPEX for SH and DHW systems has been considered included in the one for the HP subsystem described at Section 7.2.2.

7.2.4 Electricity cost

The electricity consumption of both systems has been estimated by considering only the HP consumption and the energy needed by an auxiliary heating system in the cases where the PVT field extension was undersized.

The cost for electricity has been modelled on SIG electricity fare "Tarif Pro BT" double period with optimization A, and in the investment estimation, connection expenses have been included. For more details, see Appendix 13.11.

7.2.5 Incentives & subsidies

Incentives for PV investment have been included in the calculations as a “Retribution Unique”, computed as 30% of the reference costs. These latter are derived based on the formulation included in [38] or the reference installations. Furthermore, PV electricity not consumed by the HP has been assumed to be reinjected in the grid and paid by the utility according to SIG fares (**Appendix 13.11**).

Financial incentives for heat pumps, on the other hand, depend on the type of adopted technology, e.g. if it is an air/water HP or a brine/water HP. For the latter, the low temperature source has to be at least 5°C to be eligible to the incentive (Mesure M-06 dans le catalogue des subventions du canton de Geneve). As a consequence, since the PVT field is a low temperature source that can go down to -15°C (e.g. for air at -7°C and a mean difference between air and collector of 8 K), incentives foreseen for air/water HP are applied to the TriSolHP solution (Mesure M-06 dans le catalogue des subventions du canton de Geneve) . According to these latter incentives, the HP nominal power has to be evaluated in conditions A-7W35.

For a brine/water HP, these conditions translate in a nominal point evaluated at B-15W35. In fact, given air at -7°C, for a nominal Solink PVT collector flow rate of 100 l/h, a ratio between PVT area and HP power of 2.55 m^2/kW_{th} at a COP of 3.5, the mean temperature difference between air and PVT collectors is 8 K and the glycol temperature at the HP inlet is ca -15°C. According to **Figure 42**, the R290 HP heating power, when evaluated at $T_{in\text{-}C}$ = -15°C and $T_{in\text{-}H}$ = 35°C, decreases by 40%. By contrast, an air-water HP evaluated at A7W35 lowers only by 30% when evaluated in conditions A-7W35.

By referring to the HP power P_p estimated in A-7W35 conditions, the incentive corresponds to the following amount:

$$Incentive_{HP} = 13000\ CHF + 200 * P_p\ [CHF] \qquad \text{Eq. 39}$$

with

$$P_{p,A\text{-}7W35} = (1-0.4) * P_{p,B0W35}\ [CHF] \qquad \text{Eq. 40}$$

for brine/water HP, while:

$$P_{p,A\text{-}7W35} = (1-0.3) * P_{p,A7W35}\ [CHF] \qquad \text{Eq. 41}$$

for an air/water HP.

7.3 Comparison results

The LCOH has been computed over the service time of the system (i.e., 30 years) for both System 1 and System 2 and in each case of **Table 9**, listed in **Table 10** for convenience. **Table 10** shows also the consumption values for each heat demand scenario. Energy needs are covered by the combined consumption of the HP and the auxiliary energy source, modelled by an electric heating resistance on the evaporator side of the HP.

Figure 65 shows the LCOH calculation results for both Systems and for the different cases as a function of the ratio between the PVT collector field area, in [m^2], and the nominal HP power on the condenser side, in [kW]. Data labels correspond to the share of heat demands covered by the auxiliary heating (electrical rod). **Figure 65** confirms that System 2 energy is more expensive than the one produced by System 1, as the larger investment required for System 2 doesn't translate in a significantly higher efficiency (see discussion in Section 6.3). For both circuits, on the other hand, for a given HP power, the levelized energy cost is higher for larger PVT fields but the energy demand is covered with less energy from the auxiliary heating source.

Figure 66 shows the LCOH of the two circuits as a function of the seasonal performance factor $SPF_{grid,sys}$, defined in Section 6.2. For both HP systems, a higher SPF value requires a larger PVT field area for the same HP nominal power. It can also be seen that System 2 consistently features higher SPF than System 1 due to the higher efficiency for DHW preparation with R744 HP.

Figure 67 shows the LCOH components for both System 1 and 2 for the cases 9 and 22, which feature the highest (24.6 ctsCHF/kWh) and the lowest (19 ctsCHF/kWh) LCOH value, respectively. In case 22, the PVT/kW ratio is sensibly lower than in case 9 and the economic impact of the heat source for the HP on the overall energy price is limited (~16%), while the HP economic impact increases from System 1 to System 2, as the latter requires a higher total installed HP power. In case 9, with high PVT_{Area}/HP_{kW} ratio (i.e., 2.99), the PVT field has a large impact on the final cost of energy, as more than a third of it can be imputed to this subsystem. At the same time, the electricity consumption share in LCOH decreases from more than 25% in case 22 to about 18% in case 9, due to the higher electricity production from larger PVT fields.

Table 10 Cases and scenario selected for the economic analysis.

Scenario	Case ID	Total heat demand, in [kWh_{th}]	PVT Area, in [m^2]	Ratio PVT/PAC, in [m^2/kW]	HP power (R290 @ B0W35), in [kW]	HP power (R744 @ B0W10-65°), in [kW]	Maximum number of building floors
DHW and SH reference demand	Dim. SOLINK	524000	681	1.81	377	134	4
	2	524000	315	0.84	377	134	9
	3	524000	526	1.40	377	134	5
Low SH needs	8	432000	428	1.50	286	134	7
	9	432000	856	2.99	286	134	3
High SH needs	12	640000	385	0.79	485	134	7
	13	640000	642	1.32	485	134	4
High DHW needs	17	492000	294	0.78	377	134	10
	18	492000	491	1.30	377	134	6
Low DHW needs	22	580000	347	0.92	377	134	8
	23	580000	578	1.53	377	134	5

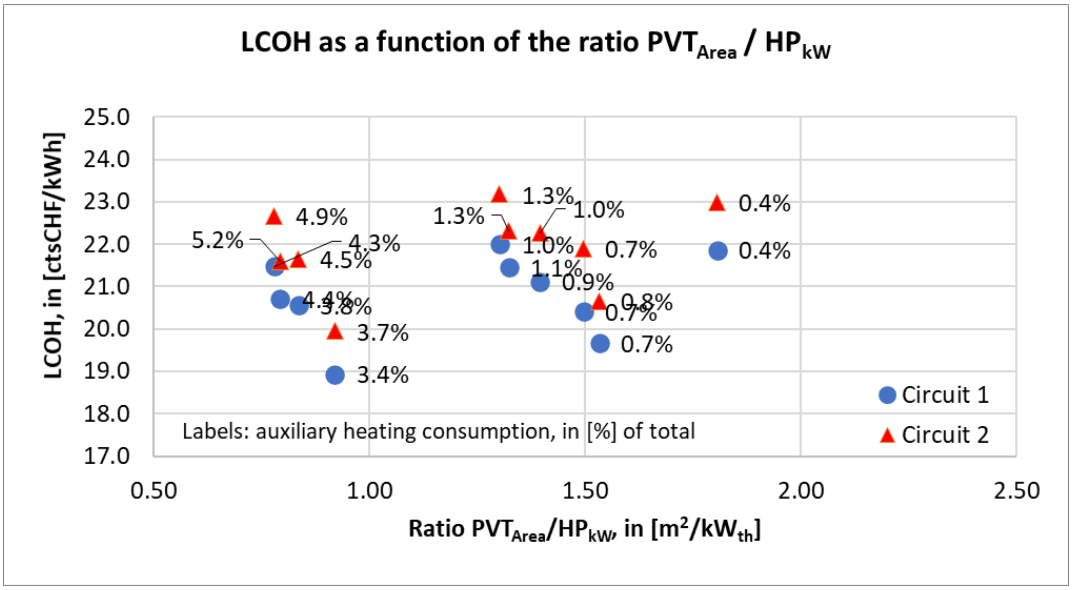

Figure 65 LCOH as a function of the ratio between PVT area, in [m^2], and HP thermal power, in [kW], in nominal conditions. Labels represents the heat demand share covered by the auxiliary heating (electrical rod) on the evaporator side of the HP.

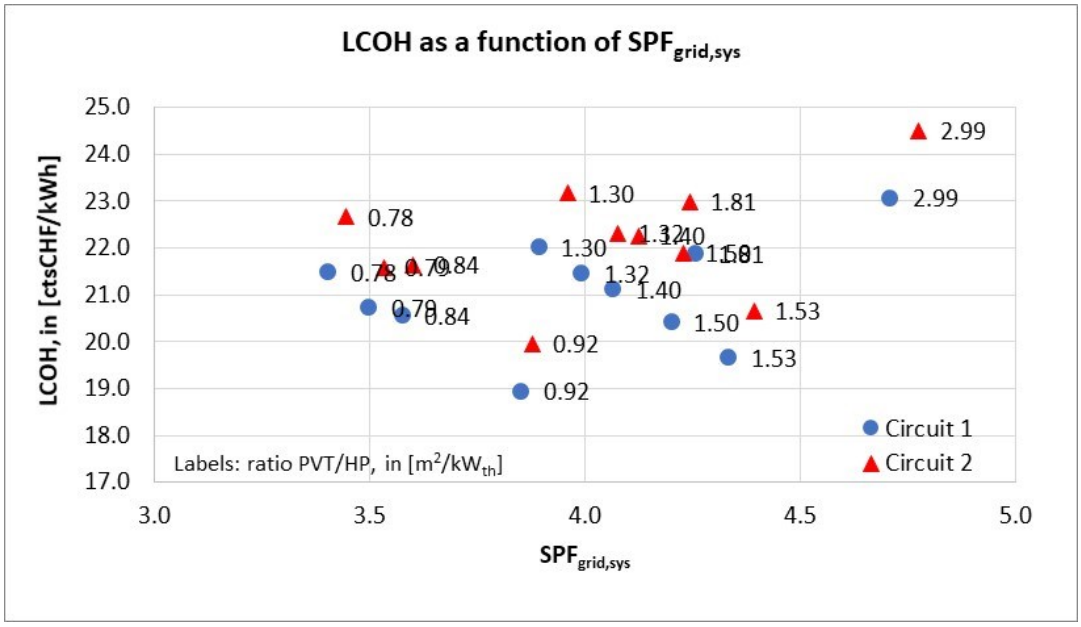

Figure 66 LCOH as a function of the $SPF_{grid,sys}$, the seasonal performance factor including the auxiliary energy consumption and the self-consumed PV production.

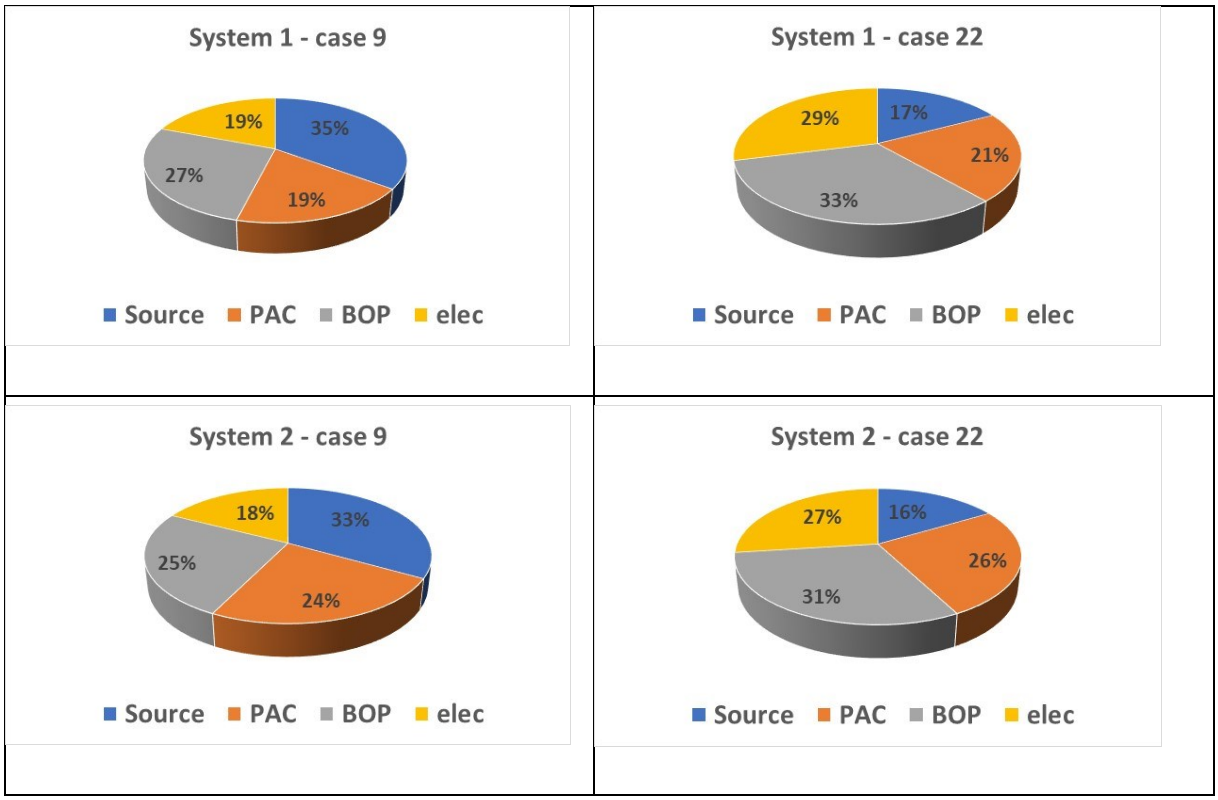

Figure 67 LCOH breakdown for System 1 and System 2 in cases 9 and 22.

Table 11 LCOH calculation results for the cases of interest. Case 9 and 22, in particular, feature the highest and lowest computed LCOH.

Energy demand scenario	case	Ratio PVT/HP in [m^2/kW]	HP P_p B0W35, in [kW]	HP P_p R744, in [kW] (Circuit 2)	Self-consumption		$SPF_{grid,sys}$		LCOH		Max N. floor
					Circuit 1	Circuit 2	Circuit 1	Circuit 2	Circuit 1	Circuit 2	
Ref.	Dim. SOLINK	1.81	377	134	26%	25%	4.3	4.2	21.9	23.0	4
	2	0.84	377	134	40%	41%	3.6	3.6	20.6	21.6	8
	3	1.40	377	134	30%	32%	4.1	4.1	21.1	22.3	5
Low SH	8	1.50	286	134	31%	33%	4.2	4.2	20.4	21.9	6
	9	2.99	286	134	20%	21%	4.7	4.8	23.1	24.5	3
High SH	12	0.79	485	134	38%	40%	3.5	3.5	20.7	21.6	6
	13	1.32	485	134	29%	31%	4.0	4.1	21.4	22.3	4
low DHW	17	0.78	377	134	39%	39%	3.4	3.4	21.5	22.7	8
	18	1.30	377	134	30%	31%	3.9	4.0	22.0	23.2	5
high DHW	22	0.92	377	134	41%	43%	3.9	3.9	18.9	19.9	7
	23	1.53	377	134	30%	32%	4.3	4.4	19.7	20.7	4

Table 11 shows the LCOH calculation results for each studied case. Case 9 and 22 are enlightened as they feature the maximum and minimum LCOH values.

7.4 Comparison to air-water heat pump

The energy production solution studied in AirBiVal project [39], was based on an air-to-water heat pump (ASHPO) solution used for multi-family building in urban setting. Sensitivity analysis performed in the framework of AirBival project included energy demand scenarios equivalent to those that have been used as a reference in the project TriSolHP.

It is interesting then to compare the LCOH computed for the reference consumption scenario in the case of System 1 and System 2, to the results coming from the AirBiVal project, at about 16.6 ctsCHF/kWh when computed over a service lifetime of 30 years. As it is shown in **Figure 68**, the air/water solution for covering the energy needs of both the SH and the DHW preparation without any PV installation is the cheapest among the depicted cases. Such LCOH difference, nevertheless, is highly dependent on the evolution of electricity cost over the system lifetime. With higher COP and a capacity to produce decentralized renewable electricity, the TriSolHP system is less sensitive to electricity cost inflation.

For the same BOP and electricity consumption, it is clear from the energy cost breakdown that the brine / water HP and PVT cold source have to reduce their investment requirements by about 35-50% in total to have the same LCOH of an equivalent system based on an air / water HP.

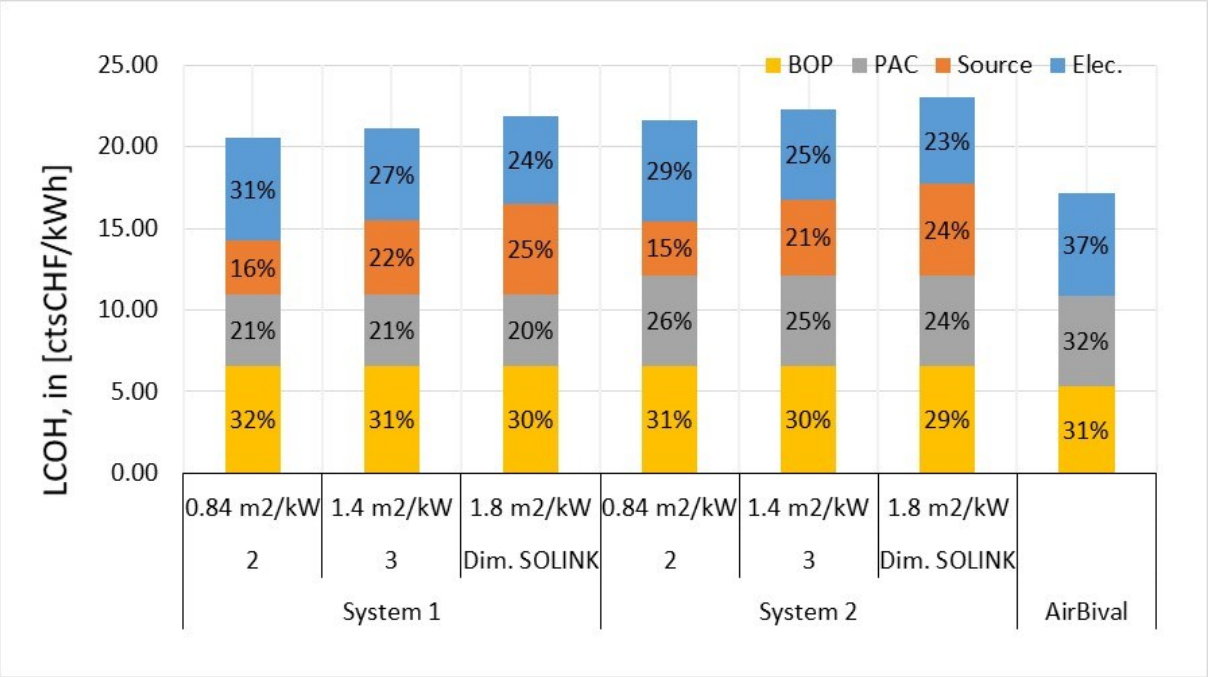

Figure 68 Comparison between the LCOH of the air-to-water heat pump system studied in [39] and the LCOH computed for the reference scenario as a function of the ratio between the PVT area and the nominal HP power.

8 TriSolHP decarbonation potential for multifamily buildings

This section examines the potential for CO_2 emissions reduction from multifamily buildings using the TriSolHP system. The analysis is based on the multifamily building stock in the canton of Geneva. It begins by presenting the proportion of multifamily buildings eligible for the TriSolHP system, then describes the current composition of the canton's building stock. Finally, the potential for reducing CO_2 emissions is estimated by presenting four scenarios for 2040, corresponding to different levels of TriSolHP system penetration.

8.1 Building eligibility for the TriSolHP system

Having set out the modelling results concerning the thermal and environmental performance of the TriSolHP system (see **Section 6)**, it is crucial to look at its application potential, in particular to assess the number of buildings that could benefit from this type of system. Indeed, results have shown that as soon as a ratio of 1.0 m^2 PVT/MWh_{th} is reached, the TriSolHP system can operate in monovalent mode, and with a ratio of minimum 0.6 m^2 PVT/MWh_{th}, it can operate in bivalent mode, as indicated in **Section 6.6,** while significantly reducing CO_2 emissions (compare to a gas boiler).

It is therefore imperative to determine the available roof area to heat demand ratio for all multifamily residential buildings (see **Appendix 13.7**). This makes it possible to determine the proportion of the multifamily building stock eligible for the TriSolHP system (see **Table 12**), disregarding the building's current and likely future energy source.

Table 12 Share of Geneva's multifamily building stock eligible for the TriSolHP system

	Mode	ratio [m^2 PVT/MWh_{th}]	Number of EGID	% of EGID	ERA [mio m^2]	% of ERA	Total heat demand [GWh]	% of total heat demand
Eligible for TriSolHP system	Monovalent	> 1.0	6'869	47%	6.4	30%	710	26%
	Bivalent	> 0.6	11'036	76%	13.6	63%	1'606	59%
Whole multifamily building stock	**-**		**14'555**	**100%**	**21.7**	**100%**	**2'739**	**100%**

Almost 65% of the total ERA and total demand of the multifamily building sector could be eligible for a TriSolHP system in bivalent mode, and around a third in monovalent mode. These results demonstrate the high penetration potential of this type of technology. However, it is important to emphasize that it competes directly with other renewable heat production technologies, notably district heating.

8.2 Geneva's multifamily building stock in 2020

For the purposes of this study, all data relating to the building category, heated floor area and heat demand of buildings in Geneva are taken from the DataRen database [25]. It is considered to be the most accurate data available and covers the entire building stock of the canton in 2020. **Appendix 13.7** provides further information on the data source of the heat demand.

In 2020, the entire Geneva canton has just over 43.4 million m^2 of energy reference area (ERA), spread over more than 56'000 buildings, with a total heat demand of 56.3 TWh. The distribution of ERA and heat demand within the various categories of the Swiss Society of Engineers and Architects (SIA) is shown in the **Figure 69**.

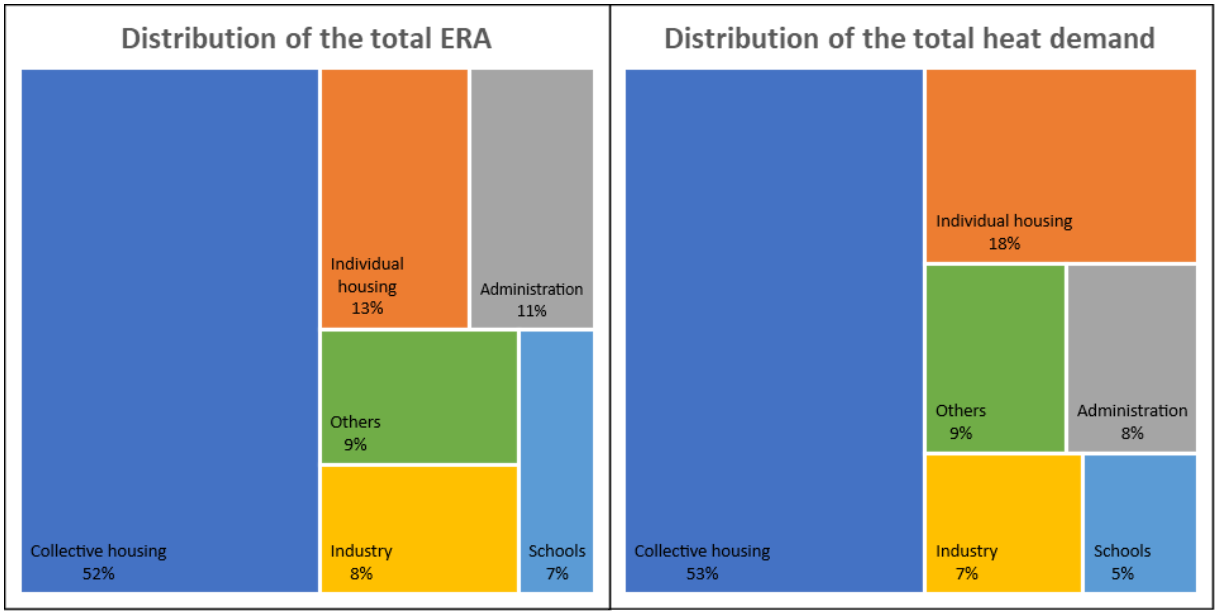

Figure 69 Distribution of cantonal energy reference area (left) and total heat demand (right) by SIA building category

Multifamily buildings account for more than half of the total heated area and total heat demand, representing 15'271 building entrances (EGID), i.e. 27% of all EGID in the canton. The distribution of the ERA of this building category, by period of construction and energy source, is detailed in the **Figure 70**.

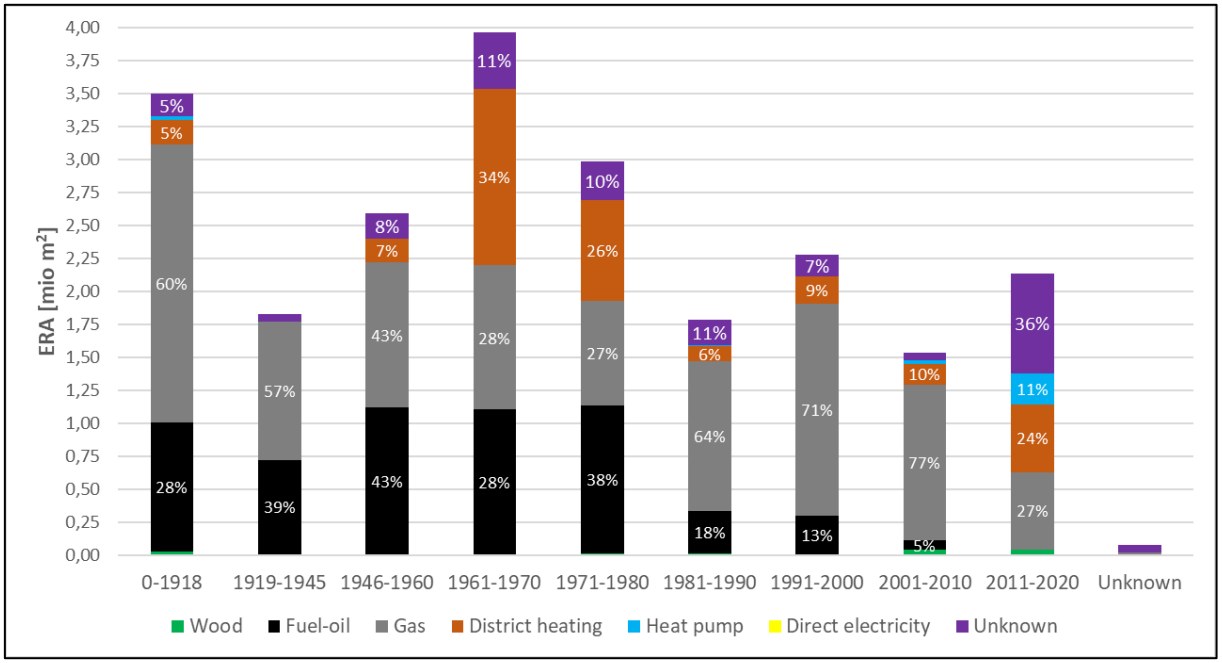

Figure 70 Distribution of energy reference area of multifamily buildings by period of construction and energy source of heating system

It has been observed that the multifamily building stock is quite old, since more than half of the heated surface area, i.e. 11.9 million m^2, is located in buildings built before the 1970s. In addition, with the exception of post-2001 buildings, the vast majority of the ERA is heated with fossil fuels. Thus, the decarbonization potential of the canton's multifamily buildings is significant, with almost 16.4 million m^2 (or 72% of the total) using natural gas or fuel-oil.

8.3 Assessment of heat demand in 2040

In order to assess the possibility of reducing CO_2 emissions, the heat demand for Geneva's multifamily building stock was projected in 2040. To do this, we used the building stock existing in 2020, which we extrapolated to 2040 by calculating the heat demand for each building using the following equation:

$$Qhww_{2040} = Qww_{2020} + Qh_{2020} * f_{cc} \qquad \text{Eq. 42}$$

With :

Qww_{2020} : heat demand for DHW

Qh_{2020} : heat demand for SH

f_{cc} : climate correction factor (based on observed HDD decrease in Geneva)

However, it is essential to note that the study assumes that the total heated floor area in 2040 remains identical as it was in 2020, thus excluding any demolition or construction. Furthermore, no renovations have been taken into account. As a result, the variation in heat demand derives solely from the climate correction factor. This one corresponds to a reduction of around 15% of the space heating demand and corresponds to the average decrease of 129 HDD/10 years observed in Geneva and extrapolated to 2040[5].

8.4 CO_2 emissions reduction potential for 2040

CO_2 emissions in 2040 from the multifamily building stock are estimated according to four scenarios. These scenarios aim to change the energy source of each building, taking into account parameters such as: (i) the expansion of the district heating (DHN) (see **Appendix 13.13**); (ii) the ratio of available PVT area to the total heat demand (see **Section 5.4)**. In addition, it has been assumed that all buildings running on fuel-oil in 2020 will switch to at least gas by 2040. The four scenarios are summarized in **Table 13** below.

Table 13 Summary of selection criteria for energy source change according to scenarios

Change of energy source	Base case	Scenario 1	Scenario 2	Scenario 3
Fuel-oil ➔ Gas	Yes	Yes	Yes	Yes
DHN if building is in future extension zone of DH	Yes No (if HP)	Yes No (if HP or TriSolHP)	Yes No (if HP)	Yes No (if HP)
TriSolHP if ratio (PVT area/heat demand [m^2/MWh]) > 0.6	No	Yes	Yes No (if DHN or HP)	Yes (if ratio > 1.0) No (if DHN or HP or ratio < 1.0)

The base case scenario reflects the normal development predicted by the canton, without any integration of the TriSolHP system. The first scenario represents the maximum potential of the TriSolHP system, where priority is given to its implementation whenever the roof surface is suitable for a

[5] *Office fédéral de météorologue et de climatologie MétéoSuisse*

monovalent or bivalent system (even if the building is currently supplied by a HP or the DHN). Scenario 2 aims to restrict TriSolHP installations (monovalent or bivalent) in favor of district heating (existing or new) and already existing heat pumps (HP). Finally, the third scenario further restricts the implementation of TriSolHP systems to monovalent systems only (available PVT area to heat demand greater than 1 m^2/MWh_{th}).

The evaluation of CO_2 emissions associated to the heat production is done for each building based on its energy source. CO_2 emissions by energy source are taken directly from LCA data for the construction industry [35], and are presented in **Table 14** below.

Table 14 Summary of considered CO_2 content of heat by of energy source (final energy)

Energy source	Emissions in 2020	Emissions in 2040
	kg CO_2 eq. / kWh	kg CO_2 eq. / kWh
Fuel-oil	0.301	-
Gas	0.228	0.228
DHN[1]	0.2015	0.134
Wood	0.027	0.027
Direct electricity	0.102	0.102
HP[2]	0.046	0.045
TriSolHP[3]	-	0.032 – 0.04
Unknown	0	0

[1] For 2020, the value corresponds to a DH mix of 80% natural gas and 20% waste heat for the incineration plant. For 2040, the value corresponds to a DH mix of 20% natural gas and 80% waste heat.
[2] The value corresponds to results from the AirBiVal study [22].
[3] Emissions vary based on the ratio of m^2 of PVT to MWh_{th} of heat demand.

The **Figure 71** illustrates the total heat demand and CO_2 emissions broken down by energy source.

Total heat demand in 2020 for the 14'555 multifamily buildings amounts to 2'739 GWh, while in 2040 (for all four scenarios) it is estimated at 2'437 GWh. This reduction of 11% in total heat demand is solely due to the foreseeable reduction in space heating demand caused by global warming.

Between 2020 and the base case scenario for 2040, a reduction in CO_2 emissions of around 53% is estimated. This is due to: (i) the reduction of the space heating demand caused by global warming; (ii) the replacement of oil-fired boilers; (iii) the expansion of the DHN; and (iv) the decarbonization of DHN heat production.

Without the TriSolHP system or other type of heat pump systems, more than 36% of the heat demand would be met by gas. The expansion of the DHN should, at best, cover about 61% of total heat demand. Despite fairly restrictive implementation criteria, the TriSolHP system is able to cover a fifth of total heat demand in the least favorable scenario (scenario 3). Conversely, it could reach a maximum heat demand coverage of around 70% (scenario 1).

In addition, compared with the base case for 2040, TriSolHP installations could reduce CO_2 emissions by around 51% in the best case (scenario 1), and around 26% in the worst case (scenario 3). Furthermore, it is interesting to note that the loss of 1'526 buildings to the TriSolHP system between scenario 2 and 3 (due to the increase in the minimum m^2 PVT/MWh_{th} ratio for the eligibility) results in an increase of over 52 kt CO_2. These buildings are located outside the expansion zone of the DHN, and will therefore be supplied by gas (scenario 3) rather than a bivalent TriSolHP system (scenario 2).

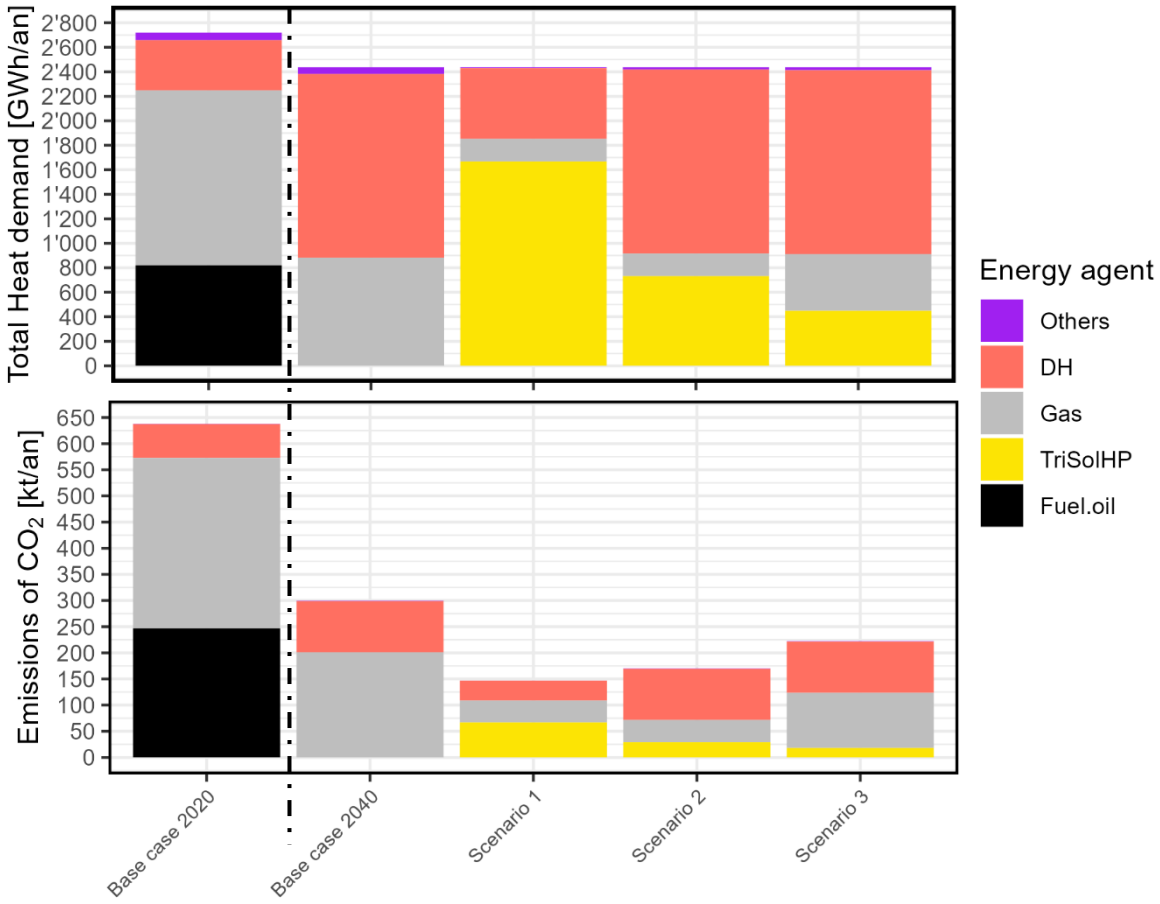

Figure 71 Comparison of energy sources and CO_2 emissions between 2020 and the different scenarios in 2040 for the heat demand of the canton of Geneva's multifamily building stock

9 Conclusions

The TriSolHP project has evaluated the energetic, environmental and financial performance of a renewable heat production system based on HP with natural refrigerant (R290 and R744) using a PVT collector field as heat source to satisfy SH and DHW demand of multi-family building in urban area. The PVT technology studied in this project has been specifically developed to be used as heat source for HP with an improved ability to capture heat from ambient air thanks to fins located on the backside of the collector. Those fins offer an exchange surface of 10 m^2 per m^2 of PV. This system could offer an attractive alternative to ASHP for the decarbonation of existing multi-family buildings.

During the first phase of the project (see **Section 2**), the PVT collector performances have been measured in a climatic chamber without irradiation. Those experimental measurements served two purposes: (1) evaluate the impact of frost formation on the PVT thermal performance and (2) compare experimental performances with simulated performances using Solar Keymark model. The measurements demonstrated that the formation of frost reduces the overall heat coefficient of the collector of maximum 20-25%. The Solar Keymark model was not able to predict accurately the heat production of the PVT collector. Indeed, wind direction is not a input parameter in the Solar Keymark model. The experimental measurements have shown that this category of PVT collector (WISC) is very sensitive to wind speed **and** direction.

In order to simulate the performance of the complete TriSolHP system, it was necessary to develop simple but realistic numerical models for HP using natural refrigerant. Those models are described in **Section 3**. The developed models can effectively assess the impact of operating conditions, particularly temperature and flow rates at both the heat source and heat sink, on the HPs performance and capture the fundamental distinctions between the two cycle types (classical and transcritical). As anticipated, the results demonstrate that a transcritical HP, compared to a conventional HP, is not adapted at all for space heating (SH) but can exhibit higher efficiency for domestic hot water (DHW) production, provided the HP's inlet temperature is minimized and proper hydraulic arrangements and control strategies are implemented.

Two different hydraulic layouts have been defined in **Section 4** with sizing and control strategy. One hydraulic layout relies only on R290 for SH and DHW production (System 1). The second layout (System 2) combines a R744 HP for DHW production with a R290 HP for SH.

The heat demand and the characteristics of the building used as reference in the TriSolHP project is described in **Section 5**. The total heated floor area was fixed at 4'000 m² divided in three entrances. This surface corresponds roughly to the average surface of multifamily building in Geneva. Concerning the heat demand, for SH and DHW demand three levels of heat demand were defined based on a statistical analysis of the Geneva multifamily building stock. Five heat demand scenarios were then generated by combining the different heat demands for both SH and DHW. The available roof area was divided by the building heat demand to define six ratios ranging from 0.3 to 4.0 m² PVT/MWh_{th}. Those ratios were used to size the PVT collector field.

The performance of different TriSolHP systems were simulated in **Section 6** with TRNSYS with a one-minute time step. The SH and DHW demands were satisfied for all scenarios studied with a minor contribution from an auxiliary heating rod, mainly for cases with a small PVT field surface over heat demand ratio.

The system SPF depends mainly on the ratio of PVT collector field to heat demand. The $SPF_{HP\text{-}Rod}$ (without PV electricity auto consumption) increases with this ratio from 2.5 and reaches a plateau above 1 m^2/MWh_{th} at 3-3.5. The HP heat source quality does not improve significantly for ratio above 1 m^2 of PVT per MWh of heat demand. The $SPF_{grid\text{-}sys}$ (taking into account PV electricity auto-consumption) keeps on increasing from 2.7 up to almost 5 even after the 1 m^2/MWh_{th} ratio because the share of PV electricity auto-consumed by the HP and the heating rod increases with the PVT surface.

An environmental analysis was carried out by taking into account only the impact related to the system energy consumption (heat pump and back-up heating rod). This analysis confirmed the capacity of the TriSolHP concept to decarbonize SH and DHW production for multifamily building with a GHG content varying from 31 to 52 gCO_{2eq}/kWh of heat (compared to 247 gCO_{2eq}/kWh for a gas boiler).

Finally, a comparison was made with ASHP system using the results from the AirBival project. The energetic and environmental efficiency of the TriSolHP concept is always better than ASHP for ratio of PVT surface to heat demand above 1 m^2/MWh_{th}. This result confirms that the TriSolHP system is an interesting alternative to ASHP system for existing multifamily buildings. The main limitation of the TriSolHP system is related to the availability of sufficient area on building roof to install the PVT field. In some cases (high heat demand with high PVT field surface to heat demand ratio), the TriSolHP can be installed in monovalent mode on buildings with maximum 3 to 4 floors. For the other cases, buildings with more than 4 floors could be equipped with the TriSolHP system

The financial viability of various TriSolHP configurations is examined in **Section 7**. The Levelized Cost of Heat (LCOH) was calculated for each variant over a 30-year lifespan assuming a 3% discount rate. Under these conditions, the LCOH ranges from 19 to 25 ctsCHF/kWh.

Investment in the PVT collector field and the HP are the primary factors influencing LCOH. For variants with a low COP and substantial electricity consumption by the auxiliary heating rod (due to high heat demand or a small PVT field), the proportion of electricity costs in the LCOH becomes significant.

The LCOH of the TriSolHP reference scenarios is contrasted with the LCOH of ASHP systems with comparable heat demands. The LCOH for ASHP is always 5 to 25% lower than the TriSolHP LCOH. The primary factor in this difference is the cost of the PVT field. Indeed, as the ratio of PVT field area to heat demand grows, the gap between TriSolHP system LCOH and ASHP LCOH widens.

Section 8 of the report assesses the potential impact of adopting the TriSolHP concept on decarbonization efforts in the canton of Geneva. Three distinct scenarios were considered to evaluate the extent of TriSolHP implementation and its associated emissions savings.

To determine the eligibility of existing multifamily buildings for TriSolHP systems, data from the Geneva's multifamily building stock database was analyzed in conjunction with the PVT field surface to heat demand ratio. This assessment revealed that about two thirds of the total heated floor area (ERA) is compatible with the TriSolHP concept. It is important to note that this figure does not account for potential conflicts with other renewable heat production technologies like ASHP (Air Source Heat Pump) and DHN (District Heating Network).

Accounting for these potential conflicts, the study estimates that TriSolHP implementation could contribute to a CO_{2eq} emissions reduction of 26% to 51% for the Geneva's multifamily building stock. This range reflects the varying degrees of conflict with alternative renewable heat production technologies.

In conclusion, the TriSolHP concept holds promise for significantly reducing GHG emissions from Geneva's multifamily building sector. Its widespread adoption, while considering potential conflicts with other renewable heat sources, could substantially contribute to the canton's decarbonization goals.

10 Outlook and next steps

Pilot Installation and Future Research Directions for TriSolHP

The TriSolHP project demonstrated through numerical simulations the potential of residential heating systems that combine a PVT field as a heat source with heat pumps to meet the heat demand of multifamily buildings. To validate these findings, a pilot installation on an existing multifamily building (similar to those studied in the AirBival project) should be implemented and its performance monitored. Such a pilot project would provide valuable insights into the advantages and disadvantages of using PVT collectors as heat sources for heat pumps. A hybrid system with a gas boiler could be considered if the available roof area is insufficient or the building's heat demand is too high.

Alternative TriSolHP Configurations

Exploring other intriguing TriSolHP configurations could also be beneficial. A façade-mounted PVT field could be an attractive alternative to a roof installation. Additionally, investigating the integration of the PVT field with other heat sources could be fruitful. For instance, the PVT field could be coupled with geothermal probes to reduce the required probe length and recharge the geothermal probe during the summer. This configuration could enhance the heat source temperature, particularly during the coldest winter days. Utilizing two heat sources allows for a smaller PVT field and shorter geothermal probes.

Another area of interest is the combination of a PVT collector with covered or uncovered solar thermal collectors to increase the heat source temperature through more efficient solar irradiation to heat conversion. Finally, coupling a PVT field with an aero cooler could potentially reduce or eliminate the need for aero cooler fan noise, particularly during the summer months, while also minimizing the required PVT field surface area.

Improving PVT Efficiency as heat source for HP

TriSolHP's efficiency could be further enhanced by improving the PVT collector's ability to capture ambient heat. New fin designs and the utilization of forced convection could be explored to achieve this goal. Additionally, research into novel methods for converting more efficiently solar irradiation into heat could be beneficial.

11 Publications

A communication was realized during CISBAT 2023 at EPFL/Lausanne on the test and modelling of the Solink collector. This communication will be published in the 2023 CISBAT proceedings

Pauletta, S., Duret, A., & Jobard, X. (2023). Performance measurements on WISC collectors under artificial environmental conditions. Proceedings of International Conference CISBAT.

Additional studies will also be carried out as part of Omar Montero D.'s doctoral thesis (October 2020 - September 2025), funded by SIG, on the integration of air-source heat pumps in the existing multifamily building stock (constraints, potentials and alternatives). In particular, this thesis is linked to the "Renowave" project, funded by Innosuisse, which aims to boost the decarbonization of the Swiss building stock, both in terms of quantity (renovation rate) and quality (efficiency), in order to help achieve the objectives of the Swiss 2050 Energy Strategy. The work carried out in the present report will be developed further in this thesis and lead to the publication of research results in scientific journals, as well as participation in conferences.

12 References

[1] E. Romano, C. Fraga, and P. Hollmuller, “CO2 emission savings of heat-pumps in the residential sector. Case study for multifamily buildings in Geneva,” in *13th IEA Heat Pump Conference*, 2020.

[2] Groupement professionnel Suisse pour les Pompes à Chaleur (GSP), “Statistiques 2020,” 2020.

[3] F. Malaguerra, “Réglementation des fluides frigorigènes en Suisse OFEV,” in *OFEV, Swiss Cooling Expo*, 2019.

[4] G. Tornare *et al.*, “Rapport technique et de communication du projet d’assainissement Minergie-P des immeubles La Cigale(GE)–Chauffage par pompes à chaleur solaires couplées à des stocks à changement de phase,” *Office fédéral de l’énergie (OFEN), Berne*, 2016.

[5] C. De Sousa Fraga, “Heat pump systems for multifamily buildings: Which resource for what demand,” *University of Geneva: Geneva, Switzerland*, 2017.

[6] N. Calame, V. Curti, E. Da Riva, and F. Rognon, “Étude et caractérisation d’une pompe à chaleur à très faible charge de réfrigérant naturel et haute efficacité avec évaporation à moyenne température et démonstrateur en laboratoire,” 2020.

[7] B. Chhugani, M. Littwin, and F. Giovannetti, “INVESTIGATION OF PHOTOVOLTAIC-THERMAL (PVT) COLLECTOR FOR DIRECT COUPLING WITH HEAT PUMPS: HARDWARE IN THE LOOP (HIL) AND TRNSYS SIMULATIONS,” 2020. Accessed: Apr. 27, 2021. [Online]. Available: https://www.researchgate.net/publication/347033349

[8] B. Chhugani, “Model Validation and Performance Assessment of Unglazed Photovoltaic-Thermal Collectors with Heat Pump Systems,” no. September, pp. 1–12, 2021, doi: 10.18086/eurosun.2020.05.13.

[9] P. Karban, F. Mach, P. Ks, D. Panek, and I. Doležel, “Numerical solution of coupled problems using code Agros2D,” *Computing*, vol. 95, pp. 381–408, 2013.

[10] M. Stegmann, E. Bertram, G. Rockendorf, and S. Janßen, “Model of an unglazed photovoltaic thermal collector based on standard test procedures,” in *Proc. of the ISES Solar World Congress*, 2011, pp. 172–180.

[11] S. Pauletta, A. Duret, and X. Jobard, “Performance measurements on WISC collectors under artificial environmental conditions,” in *Proceedings of International Conference CISBAT*, 2023.

[12] B. Chhugani, P. Pärisch, M. Kirchner, M. Littwin, F. Giovannetti, and C. Lampe, “Model Validation and Performance Assessment of Unglazed Photovoltaic-Thermal Collectors with Heat Pump Systems,” in *13th ISES International Conference on Solar Energy for Buildings and Industry, EuroSun*, 2020.

[13] M. Littwin *et al.*, “TwinPower": integrierte Gesamtenergieversorgung von Wohngebäuden mit PV-thermischen Kollektoren als bisolare Wärmepumpenquelle,” *Förderkennzeichen*, p. 0325867B, 2020.

[14] “BOCK selection program VAP 11 (v 11.12).”

[15] “Regli webpage.” Accessed: Nov. 29, 2023. [Online]. Available: https://regli.energy/en/the-novaaqua/

[16] “Enex website.” Accessed: Nov. 29, 2023. [Online]. Available: https://www.enex.it/wp-content/uploads/2022/12/2022-09-30-Brochure-ENEX-AIRHEAT-e-GEOHEAT.pdf

[17] E. Da Riva and M. Schmidt, “Transcritical CO2 heat pump: first experimental test rig results,” in *Tagungsband der 25. Tagung des Forschungsprogramms Wärmepumpen und Kälte des Bundesamts für Energie*, 2019.

[18] WPZ Wärmepumpen-Testzentrum, “Test results of brine to water heat pumps based on EN 14511 and EN 14825,” 2023. Accessed: Nov. 29, 2023. [Online]. Available:

https://www.ost.ch/fileadmin/dateiliste/3_forschung_dienstleistung/institute/ies/wpz/sole-wasser-waermepumpen/pruefresultate_sw.pdf
[19] A. Cavallini, E. Da Riva, and D. Del Col, “Performance of a large capacity propane heat pump with low charge heat exchangers,” *International Journal of Refrigeration*, vol. 33, no. 2, pp. 242–250, 2010.
[20] WPZ Wärmepumpen-Testzentrum, “Test results of air to water heat pumps based on EN 14511 and EN 14825,” 2023. Accessed: Nov. 29, 2023. [Online]. Available: https://www.ost.ch/fileadmin/dateiliste/3_forschung_dienstleistung/institute/ies/wpz/luft-wasser-waermepumpen/pruefresultate_lw_30102023.pdf
[21] K. Saito, “Latest heat pump technologies in Japan,” in *12th IEA Heat Pump Conference*, 2017, pp. 3–4.
[22] N. Calame *et al.*, “AirBiVal: Développement et optimisation de concepts hybrides de pompes à chaleur sur l’air pour des immeubles résidentiels collectifs,” 2021, [Online]. Available: https://archive-ouverte.unige.ch/unige:156969
[23] Consolar, “Collecteur Solink – Documentation technique.” Accessed: Nov. 29, 2023. [Online]. Available: https://www.consolar.de/en/solink-heat-pump-collector/
[24] J. Khoury, *Rénovation énergétique des bâtiments résidentiels collectifs: état des lieux, retours d’expérience et potentiels du parc genevois*. Citeseer, 2015.
[25] S. Schneider and G. Desthieux, “Développement du module ENERLAB (énergie thermique – bâtiment) pour compléter la base de données ATLAS éco 21,” 2020. [Online]. Available: https://archive-ouverte.unige.ch/unige:144763
[26] L. Quiquerez, “Analyse comparative des consommations de chaleur pour la production d’eau chaude sanitaire estimées à partir de relevés mensuels: Etude sur un échantillon de bâtiments résidentiels collectifs alimentés par un réseau de chaleur à Genève,” Genève, 2017.
[27] SIA, “Norme 385/2:2015 - Installations d’eau chaude sanitaire dans les bâtiments - Besoins en eau chaude, exigences globales et dimensionnement. Société suisse des ingénieurs et des architectes,” 2015. [Online]. Available: http://shop.sia.ch/collection%20des%20normes/architecte/385-2_2015_f/F/Product/
[28] SITG, “POTENTIEL SOLAIRE - TYPE DE SURFACE DE BASE (toiture, couvert, parking),” 2023. [Online]. Available: https://ge.ch/sitg/sitg_catalog/sitg_donnees?keyword=surface%20base&topic=tous&service=tous&datatype=tous&distribution=tous&sort=auto
[29] SITG, “POTENTIEL SOLAIRE - IRRADIATION BRUTE PAR SURFACE UTILE 800 kWh/m2/an (y c. couvert et parking).” 2023. [Online]. Available: https://ge.ch/sitg/sitg_catalog/sitg_donnees?keyword=&geodataid=2869&topic=tous&service=tous&datatype=tous&distribution=tous&sort=auto
[30] C. Zhang, X. Dai, Y. Zhang, F. De Oliveira, S. Schneider, and P. Hollmuller, “DataRen, a Territorial Energy Demand Modelling Tool,” *IOP Conf Ser Earth Environ Sci*, vol. 290, no. 1, p. 012093, Jun. 2019, doi: 10.1088/1755-1315/290/1/012093.
[31] SOLINK, “SOLINK heat pump collector, TECHNICAL DOCUMENTATION.” 2019. [Online]. Available: https://www.consolar.de/en/solink-heat-pump-collector/
[32] Klein S.A. et al., “TRNSYS 18: A Transient System Simulation Program.” Solar Energy Laboratory, University of Wisconsin, Madison, USA, 2010. [Online]. Available: https://sel.me.wisc.edu/trnsys/
[33] ISFH, “TRNSYS-Type 203 for uncovered PVT collectors.” 2023. [Online]. Available: https://isfh.de/software/?lang=en
[34] E. Romano, P. Hollmuller, and M. Patel, “Émissions horaires de gaz à effet de serre liées à la consommation d’électricité–une approche incrémentale pour une économie ouverte: Le cas de la Suisse,” 2018.

[35] K. 2009/1:2022, “Données écobilans dans la construction.” 2023. [Online]. Available: https://www.kbob.admin.ch/kbob/fr/home/themen-leistungen/nachhaltiges-bauen/oekobilanzdaten_baubereich.html
[36] M. Dongellini, C. Naldi, and G. Luca Morini, “Influence of the hydronic loop configuration on the energy performance of a CO2 heat pump for domestic hot water production in a multi-family building,” in Building Simulation, vol. 17. IBPSA, 2021, pp. 3228–3235. doi: 10.26868/25222708.2021.30700.
[37] J. Aldersey-Williams and T. Rubert, “Levelised cost of energy – A theoretical justification and critical assessment,” *Energy Policy*, vol. 124, pp. 169–179, Jan. 2019, doi: 10.1016/J.ENPOL.2018.10.004.
[38] SuisseEnergie, “Simulation de systèmes d’énergie avec le Tachion Simulation Framework ,” 2022.
[39] N. Calame *et al.*, “AirBiVal: Développement et Optimisation de Concepts Hybrides de Pompes à Chaleur Sur l’Air Pour des Immeubles Résidentiels Collectifs,” *University of Geneva: Geneva, Switzerland*, 2021.
[40] L. Bloch, Y. Sauter, and F. Jacqmin, “Observation des prix de marché photovoltaïque 2022,” 2023.
[41] SuisseEnergie, “Coûts d’exploitation des installations photovoltaïques,” 2022.
[42] SITG, “ZONES DE DÉVELOPPEMENT DES RÉSEAUX THERMIQUES STRUCTURANTS (RTS).” 2023. [Online]. Available: https://ge.ch/sitg/sitg_catalog/sitg_donnees?keyword=&geodataid=3611&topic=tous&service=tous&datatype=tous&distribution=tous&sort=auto

13 Appendix

13.1 R290 compressor technical reference data

EX-HG56e/1155-4 S HC
Engine: 380-420V Y/YY -3- 50Hz PW
Refrigerant: R290
Subject:

BOCK colour the world of tomorrow

Performance data

Notes
The discharge end temperature has to be at least 20K (36R) above the condensing temperature (dew point).

Application: Heat Pump

Refrigerant	R290	Heating capacity (incl. subcooling)	65.50 kW
Reference temperature	Dew point	Evaporator refrigeration capacity	50.10 kW
Power supply	50 Hz, 400 V	Power consumption	15.40 kW
Supply frequency	50 Hz	Current draw (400 V)	37.40 A
Evaporating temperature	-10.0 °C	Coefficient of performance (COP)	4.25
Evaporating pressure (abs.)	*3.45 bar*	Condensing capacity	65.50 kW
Condensing temperature	35.0 °C	Mass flow	0.182 kg/s
Condensing pressure (abs.)	*12.18 bar*	Discharge end temperature	54.8 °C [1]
Suction gas superheat	3 K		
Subcooling (outside cond.)	0 K		
Usable superheat	100%		

Preliminary capacity data.

1) The stated value of the discharge end temperature is a mere calculated value. Additional cooling and heat dissipation are not considered. Deviations (particularly in deep freezing applications) from the real measured discharge temperature during operation are possible.

Subject to change without notice

To: From: 09.11.2022
Page 1 of 11

VAP 11.12.0

Technical data

Number of cylinders / Bore / Stroke	6 / 70 mm / 50 mm
Displacement 50/60 Hz (1450/1740 ¹/min)	100,4 / 120,5 m³/h
Voltage [1]	380-420V Y/YY -3- 50Hz PW
	440-480V Y/YY -3- 60Hz PW
Winding divided into	50% / 50%
Max. working current [2]	58.3 A
Max. power consumption [2]	33.3 kW
Starting current (rotor blocked) [2]	196.0 / 335.0 A
Motor protection	INT69 EX2
Protection terminal box	IP 66
Weight	228 kg
Frequency range [3]	25 - 70 Hz
Max. permissible overpressure (g) (LP/HP) [4]	19 / 28 bar
Connection suction line SV	54 mm - 2 1/8 "
Connection discharge line DV	35 mm - 1 3/8 "
Lubrication	Oil pump
Oil type R290, R1270	BOCKlub G68
Oil charge	3,2 Ltr.
Oil sump heater	230 V - 1 - 50/60 Hz, 180 W
Dimensions Length / Width / Height	738 / 439 / 429 mm
Sound power level L_{WA} [5]	87 db(A) @ -35/+40 °C
	82 db(A) @ -10/+45 °C
	80 db(A) @ +5/+50 °C
Sound pressure level L_{pA} [5]	74 db(A) @ -35/+40 °C
	68 db(A) @ -10/+45 °C
	66 db(A) @ +5/+50 °C

1) Tolerance (± 10%) relates to the mean value of the voltage range. Other voltages and current types on request

All data are based on voltage rms values

PW = part winding, motors for part winding starting
(no start unloaders required)

EX-HG56e/1155-4 S HC

Engine: 380-420V Y/YY -3- 50Hz PW
Refrigerant: R290
Subject:

BOCK colour the world of tomorrow

Performance data table

Application: Heat Pump
Reference temperature: Dew point
Supply frequency: 50 Hz
Voltage: 400 V
Suction gas superheat: 3 K
Subcooling (outside cond.): 0 K

tc [°C]	to [°C]										
		0.0	-5.0	-10.0	-15.0	-20.0	-25.0	-30.0	-35.0	-40.0	-45.0
10.0	Q [W] P [kW] I [A]			79600 9.70 33.00	67400 10.10 33.30	56500 10.10 33.30	46700 9.80 33.10	38000 9.20 32.70	30300 8.36 32.20	23500 7.34 31.60	
15.0	Q [W] P [kW] I [A]		90100 10.60 33.60	76800 11.10 34.00	64800 11.20 34.10	54100 11.00 33.90	44500 10.40 33.50	36000 9.69 33.00	28400 8.70 32.40	21700 7.57 31.70	
20.0	Q [W] P [kW] I [A]	102000 11.50 34.30	87000 12.10 34.80	73900 12.40 34.90	62200 12.20 34.80	51700 11.70 34.50	42400 11.00 33.90	34100 10.00 33.30	26700 8.95 32.50	20200 7.72 31.80	
25.0	Q [W] P [kW] I [A]	98000 13.30 35.60	83900 13.60 35.90	71100 13.50 35.80	59700 13.10 35.50	49500 12.40 34.90	40400 11.40 34.20	32400 10.30 33.50	25200 9.12 32.70	18900 7.79 31.90	
30.0	Q [W] P [kW] I [A]	94500 14.90 37.00	80700 14.80 37.00	68300 14.50 36.60	57200 13.80 36.10	47300 12.90 35.30	38500 11.80 34.50	30700 10.50 33.60	23800 9.22 32.70	17700 7.82 31.90	
35.0	Q [W] P [kW] I [A]	90900 16.30 38.30	77500 16.00 38.00	65500 15.40 37.40	54700 14.50 36.60	45100 13.30 35.70	36600 12.10 34.70	29100 10.70 33.70	22500 9.27 32.70	16600 7.81 31.90	
40.0	Q [W] P [kW] I [A]	87200 17.70 39.50	74200 17.00 38.90	62600 16.10 38.10	52200 15.00 37.10	43000 13.70 36.00	34800 12.30 34.90	27600 10.80 33.80	21200 9.28 32.80	15600 7.78 31.90	
45.0	Q [W] P [kW] I [A]	83300 18.90 40.70	70800 18.00 39.80	59600 16.80 38.70	49600 15.50 37.50	40800 14.00 36.30	33000 12.40 35.00	26100 10.80 33.80	20000 9.28 32.80		
50.0	Q [W] P [kW] I [A]	79400 20.00 41.90	67300 18.80 40.70	56500 17.40 39.30	47000 15.90 37.90	38500 14.30 36.50	31100 12.60 35.10	24600 10.90 33.80			
55.0	Q [W] P [kW] I [A]	75200 21.00 43.00	63600 19.60 41.50	53300 18.00 39.90	44200 16.30 38.20	36200 14.50 36.70	29200 12.70 35.20	23100 10.90 33.90			
60.0	Q [W] P [kW] I [A]	70800 22.00 44.00	59800 20.30 42.20	50000 18.50 40.40	41400 16.60 38.60	33800 14.70 36.80	27200 12.80 35.30				
65.0	Q [W] P [kW] I [A]	66200 22.90 45.00	55700 21.00 42.90	46500 19.00 40.90	38400 16.90 38.90	31300 14.90 37.00	25200 12.90 35.40				
70.0	Q [W] P [kW] I [A]	61400 23.70 46.00	51500 21.60 43.60	42800 19.50 41.30	35200 17.30 39.20	28700 15.10 37.20					

Preliminary capacity data.

Subject to change without notice

To: From: 09.11.2022

13.2 R744 compressor technical reference data

HGX12/30-4 ML CO2 T
Engine: 220-240V Δ / 380-420V Y -3- 50Hz
Refrigerant: R744
Subject:

BOCK colour the world of tomorrow

Performance data

Application: Refrigeration & AC

Refrigerant	R744		Compressor refrigeration capacity	5.21 kW
Reference temperature	Dew point		Evaporator refrigeration capacity	5.21 kW
Supply frequency	50 Hz		Power consumption	3.23 kW
Power supply	50 Hz, 400 V		Current draw (400 V)	6.49 A
Evaporating temperature	-10.0 °C		Coefficient of performance (COP/EER)	1.61
Evaporating pressure (abs.)	*26.49 bar*		Gas cooler heat rejection	8.45 kW
High pressure (abs.)	90.00 bar		Mass flow	0.035 kg/s
Gas cooler outlet temperature	35.0 °C		Discharge end temperature	121.4 °C [1]
Suction gas superheat	10 K			
Subcooling (outside cond.)	-- K			
Usable superheat	100%			

1) The information about the discharge end temperature is a purely calculated value.
Among other things, the heat dissipation of the compressor is not taken into account. In reality, the deviations from the actually measured discharge end temperature can vary depending on e.g. the ambient temperature, superheat, etc.
The displayed discharge end temperature is limited to a minimum value of 60°C, which is indicated by a preceding "<" sign.

HGX12/30-4 ML CO2 T

Engine: 220-240V Δ / 380-420V Y -3- 50Hz
Refrigerant: R744
Subject:

BOCK colour the world of tomorrow

Technical data

Number of cylinders / Bore / Stroke	2 / 36 mm / 16 mm
Displacement 50/60 Hz (1450/1740 ¹/min)	2,80 / 3,40 m³/h
Voltage	220-240V Δ / 380-420V Y -3- 50Hz
	265-290V Δ / 440-480V Y -3- 60Hz
Max. working current [1)]	12.7 / 7.4 A
Max. power consumption [1)]	4.0 kW
Starting current (rotor blocked) [1)]	111.0 / 64.0 A
Motor protection	INT69 G
Protection terminal box	IP 66
Weight	95 kg
Frequency range [2)]	30 -70 Hz
Max. permissible overpressure (g) (LP/HP) [3)]	100 / 150 bar
Connection suction line SV	22 mm - 7/8 "
Connection discharge line DV	19 mm - 3/4 "
Lubrication	Oil pump
Oil type R744	BOCKlub E85
Oil charge	1,3 Ltr.
Dimensions Length / Width / Height	500 / 293 / 338 mm
Sound pressure level L_{pA}	< 70 dB(A)

1) - The stated value for the max. power consumption is valid for the adjusted power supply.

- Starting current (rotor blocked):
  - Part winding (PW) motors: Winding 1 / Winding 1+2
  - Delta/Star (Δ/Y) motors: Δ / Y

- Take account of the max. operating current / max. power consumption for designing motor contractors, feed lines, fuses and motor protection switches. Motor contractors: Consumption category AC3.

2) The maximum permissible working current of the compressor (Imax) must not be exceeded. Take account of the guidelines for use of frequency inverter (see compressor assembly instruction or selection software).

3) LP = Low pressure
HP = High pressure

HGX12/30-4 ML CO2 T

Engine: 220-240V Δ / 380-420V Y -3- 50Hz
Refrigerant: R744
Subject:

BOCK colour the world of tomorrow

Performance data table

Application: Refrigeration & AC
Supply frequency: 50 Hz
Voltage: 400 V
Suction gas superheat: 10 K
Subcooling (outside cond.): -- K

Subcritical

tc [°C]		to [°C]									
		0.0	-5.0	-10.0	-15.0	-20.0	-25.0	-30.0	-35.0	-40.0	
10.0	Q [W] P [kW] I [A]	14600 1.19 4.43	12200 1.46 4.66	10000 1.65 4.83	8160 1.78 4.95	6560 1.85 5.01	5200 1.86 5.03	4050 1.83 5.00	3080 1.75 4.93	2280 1.64 4.82	
15.0	Q [W] P [kW] I [A]	13200 1.56 4.75	11000 1.78 4.95	9020 1.93 5.10	7330 2.02 5.18	5870 2.05 5.22	4630 2.04 5.20	3580 1.97 5.13	2720 1.86 5.03	2010 1.72 4.89	
20.0	Q [W] P [kW] I [A]	11900 1.92 5.09	9790 2.10 5.26	8020 2.21 5.37	6480 2.26 5.42	5170 2.25 5.42	4050 2.20 5.36	3120 2.10 5.26	2360 1.96 5.12	1740 1.78 4.95	
25.0	Q [W] P [kW] I [A]	10300 2.28 5.45	8510 2.41 5.58	6950 2.48 5.65	5590 2.49 5.66	4430 2.44 5.62	3460 2.35 5.52	2660 2.21 5.38	2010 2.04 5.20		
30.0	Q [W] P [kW] I [A]	8240 2.64 5.82	6790 2.72 5.91	5520 2.74 5.94	4430 2.71 5.90	3500 2.62 5.80	2720 2.49 5.66	2090 2.31 5.48			

Transcritical

tga [°C]		to [°C]									
		0.0	-5.0	-10.0	-15.0	-20.0	-25.0	-30.0	-35.0	-40.0	
30	pV2 [bar] Q [W] P [kW] I [A]	75 8810 2.76 5.96	75 7250 2.83 6.03	75 5900 2.83 6.04	75 4740 2.78 5.98	75 3760 2.68 5.87	75 2930 2.53 5.71				
35	pV2 [bar] Q [W] P [kW] I [A]	90 7860 3.33 6.61	90 6440 3.31 6.58	90 5210 3.23 6.49	90 4170 3.11 6.34	90 3290 2.93 6.14					
40	pV2 [bar] Q [W] P [kW] I [A]	100 6810 3.65 7.00	105 5690 3.71 7.07	105 4590 3.56 6.88							
45	pV2 [bar] Q [W] P [kW] I [A]	110 5910 3.95 7.37	110 4830 3.83 7.22	110 3900 3.66 7.01							
50	pV2 [bar] Q [W] P [kW] I [A]	110 4510 3.95 7.37	110 3690 3.83 7.22	110 2990 3.66 7.01							

13.3 R290 water/water heat pump technical reference data

Specifications	
Heat pump type	Brine & water/water for indoor & outdoor installation
Internet connection	Integrated LTE router, Wi-Fi, Ethernet port
Operation	Internet-enabled devices (smartphones, tablets, computers)
Integration	Circulation pumps (regulated), heating controllers

Performance data	according to EN14511	COP	NovaAqua 12
Heating capacity (kW)	B0 | W55	3.1	6.1 - 12.8
Heating capacity (kW)	B0 | W52	3.3	6.5 - 13.2
Heating capacity (kW)	Q(B0/W35)	4.9	15.3
Refrigerant	R290 (GWP 3)	/	0.8kg
Refrigerant	CO_2-Äquivalenz	/	2.4kg
Sound power level	EN12102	/	46dB(A)
Dimensions	Width; Depth; Height	/	575 x 790 x 1400 mm
Dimensions	Weight	/	215kg

Specifications	
Heat pump type	Brine & water/water for indoor & outdoor installation
Internet connection	Integrated LTE router, Wi-Fi, Ethernet port
Operation	Internet-enabled devices (smartphones, tablets, computers)
Integration	Circulation pumps (regulated), heating controllers

Performance data	according to EN14511	COP	NovaAqua 16
Heating capacity (kW)	B0 | W55	3.1	7.5 - 16.4
Heating capacity (kW)	B0 | W52	3.3	7.9 - 16.8
Heating capacity (kW)	Q(B0/W35)	4.9	18.3
Refrigerant	R290 (GWP 3)	/	1.0kg
Refrigerant	CO_2-Äquivalenz	/	3.0kg
Sound power level	EN12102	/	46dB(A)
Dimensions	Width; Depth; Height	/	575 x 790 x 1400 mm
Dimensions	Weight	/	225kg

Source: https://regli.energy/en/the-novaaqua/

(accessed on 15.11.2022)

13.4 Example of commercial air/water R290 medium capacity HP

Gamme de puissances

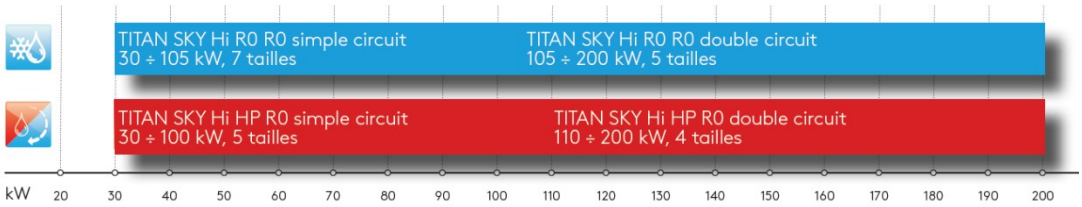

Pompe à chaleur

TITAN SKY- VERSION STANDARD (TITAN SKY Hi HP R0)

			3.1	5.1	7.1	8.1	10.1	12.2	14.2	17.2	20.2
Refroidissement											
Puissance frigorifique nominale	(1)	kW	29,4	49,7	59	74,3	87,4	99,3	117,5	147,1	174,9
Puissance total absorbée	(1)	kW	11,8	19,7	24,7	28,3	35,5	39,8	49,8	57,1	71,5
EER	(1)		2,5	2,5	2,4	2,6	2,5	2,5	2,4	2,6	2,4
Chauffage											
Puissance thermique nominale	(2)	kW	31,2	57	68,4	83,3	97,6	114,1	136,6	166,6	195,1
Puissance total absorbée	(2)	kW	9,7	17,9	21,2	26	31,2	36	42,5	52,4	62,7
COP	(2)		3,2	3,2	3,2	3,2	3,1	3,2	3,2	3,2	3,1
Compresseurs											
Compresseurs / circuits		n°	1	1	1	1	1	2	2	2	2
Étape de réduction de la capacité minimale	(7)	%	46	46	46	46	46	23	23	23	23
Charge de réfrigérant HP	(3)	Kg	2,5	4,9	5	7	7,1	9,5	9,8	14,1	14,3

(2) Température de l'air extérieur 7°C DB, 6°C WB ; température de l'eau en entrée/sortie du condenseur 40/45°C. Valeurs conformes à la norme EN 14511

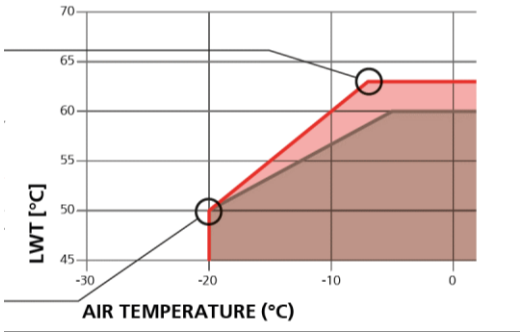

https://www.swegon.com/fr/produits/production-de-chaud-et-de-froid/refroidisseurs-et-pompes-a-chaleur-a-condensation-par-air/titan-sky-r0/

13.5 Heating curve of the system

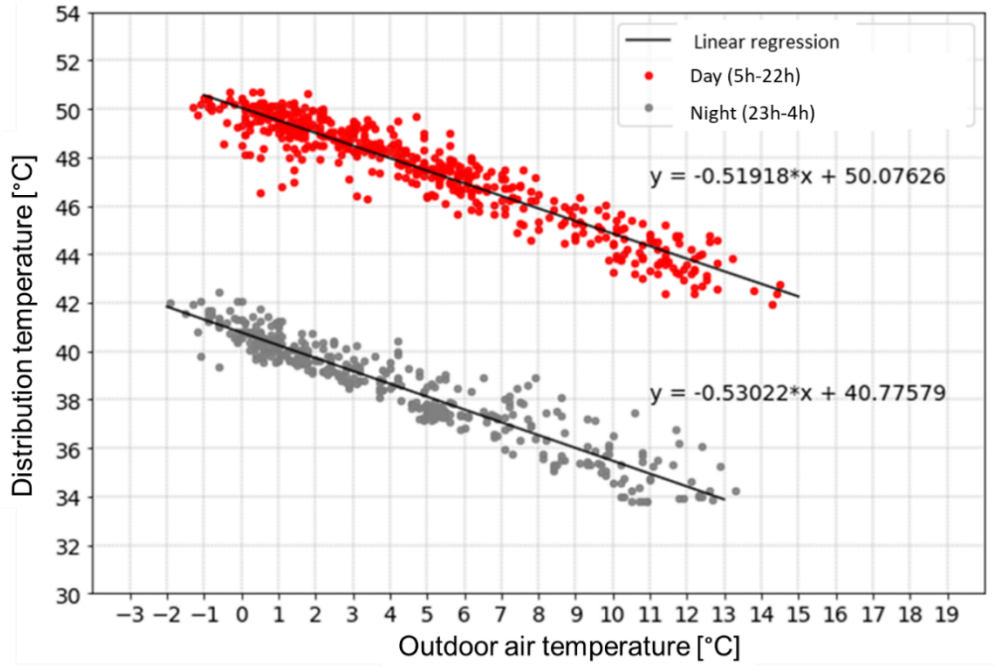

Figure 72 Daytime and nighttime heating curves from the “St-Julien” pilot project [22] used in the simulation

13.6 Statistical analysis of multifamily building SH and DHW demand in Geneva

Table 15 Statistics on energy reference area by construction period for multifamily buildings in Geneva [25]

Construction period	number of EGID	ERA [m²]					
		1st decile	1st quartile	median	mean	3rd quartile	9th decile
0-1918	2 973	271	496	1 024	1 176	1 626	2 241
1919-1945	1 336	313	705	1 366	1 367	1 856	2 415
1946-1960	1 882	376	558	1 176	1 378	1 955	2 601
1961-1970	1 989	547	966	1 842	1 990	2 689	3 327
1971-1980	1 634	522	799	1 422	1 828	2 360	3 339
1981-1990	1 103	354	706	1 354	1 614	2 056	2 724
1991-2000	1 688	423	767	1 119	1 348	1 689	2 343
2001-2010	1 257	489	741	1 045	1 217	1 481	2 001
2011-2020	1 271	569	838	1 274	1 681	2 048	2 937
Unknown	138	26	59	189	549	674	1 622
All	***15 271***	***373***	***694***	***1 226***	***1 484***	***1 960***	***2 742***

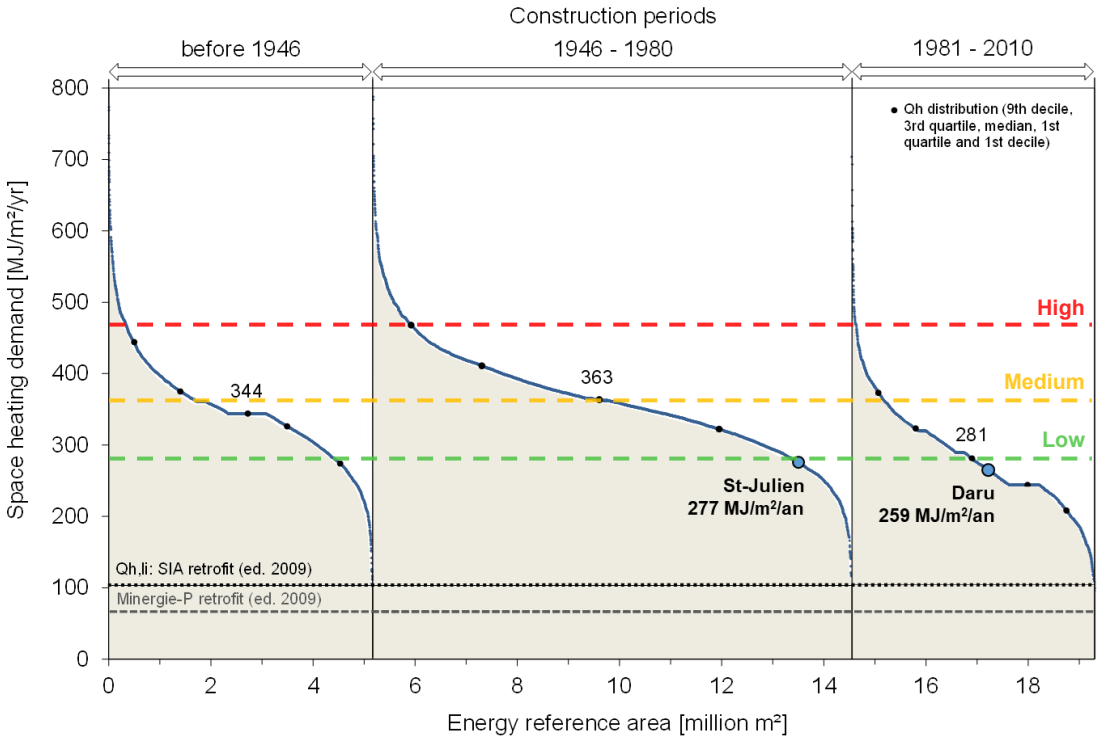

Figure 73 Space heating demand of Geneva's multifamily building stock [24] and values selected for the sensitivity analysis (horizontal lines)

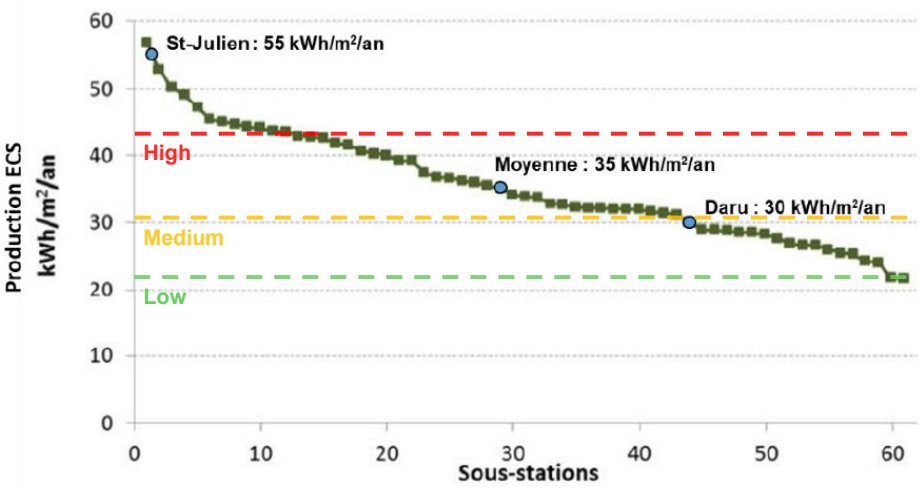

Figure 74 DHW production for 61 DH substations supplying multifamily buildings in Geneva [26] and values selected for the sensitivity analysis (horizontal lines)

13.7 Statistical analysis of the available roof area for Geneva's multi-family building stock

To assess the roof area available for the installation of PVT panels and to determine buildings eligible for the implementation of the TriSolHP system, an analysis of Geneva's multifamily building stock is done based on 3 databases:

- Solar potential – basic surface type (gross roof area) [28];
- Solar potential – gross irradiation per useable surface > 800 kWh/m²/year (useful roof area) [29];
- DataRen database (version 2020) [30].

The first two data sources provide information on roofs, i.e. slope and real roof area. The third data source provides information on collective residential buildings and their total heat demand.

The first step involves the consolidation of surface and slope data, grouped by EGID number on the basis of the usable roof area. Next, the data is merged with the DataRen database. This merge with DataRen provides information such as the building's use (SIA category) and its annual total heat demand. The combination of these two data sources is necessary to calculate a ratio of m^2 of PVT/MWh_{th}. This first step resulted in the loss of 570 of the original 15'271 buildings.

The second phase focuses, for information purposes, on the comparison between useful roof area and gross roof area. By calculating the ratio between these two areas per EGID number, it becomes possible to visualize the proportion of roofs with a solar potential in excess of > 800 kWh/m^2/year across the whole of Geneva's collective housing stock. As illustrated in the figure below, the median ratio between these two roof areas is 55%. With this median ratio, we understand that a large proportion of roofs are already unavailable for PVT panels.

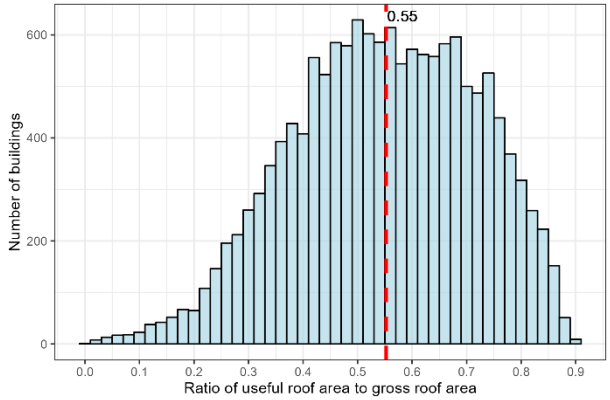

Figure 75 Histogram of the useful roof area to gross roof area ratio for multi-family buildings in Geneva (15'271 buildings).

In addition, the figure below illustrates the average roof slope of these 15'271 buildings. With a total heated floor area of 21.7 million m², the median slope is just under 20°.

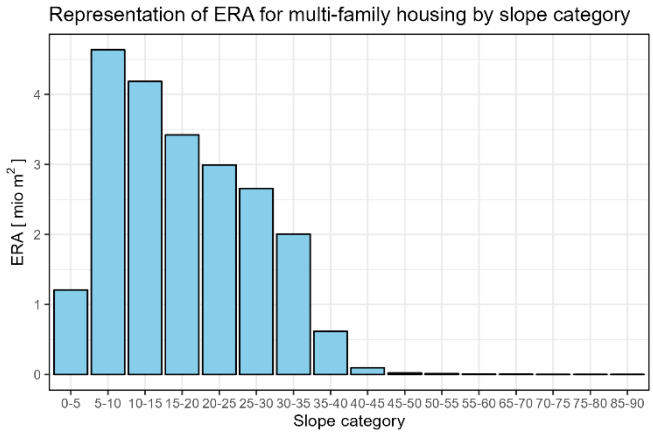

Figure 76 Representation of ERA for multifamily buildings by roof slope category.

For the purposes of this study, it was decided to restrict ourselves to buildings with an average roof slope of less than 40°. This is because it is difficult to install PVT panels on steeply sloping roofs. Following the application of this criterion, the number of buildings concerned is reduced to 14’555.

The third stage of the analysis involves the application of a roof surface reduction rate based on the average slope of the roof. The installation of PVT panels requires a margin around the edges of the roof, as well as spacing between panels to avoid shading and promote ventilation. Consequently, a 30% reduction in useful roof area was applied for flat roofs (0 to 5°), and 10% for those with an average slope of between 5 and 40°. This step makes it possible to estimate the effective surface area available for PVT panel installation (PVT collectors area).

Finally, once this area has been obtained, it is necessary to calculate the ratio between this area and the building's heat demand (see **Figure 80**). Since the heat source of the heat pump is PVT panels, this ratio has a decisive role in determining a building's eligibility to the TriSolHP system.

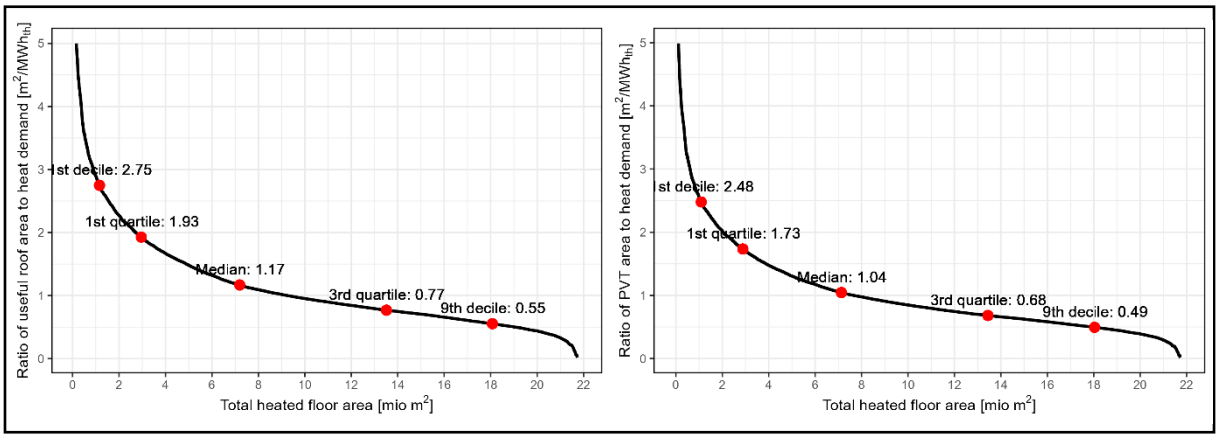

Figure 77 Comparison of ranked curves for the ratio with the useful roof area (left) and the installable PVT collectors area (right). All residential buildings in Geneva with an average slope of less than 40°: 14’555 buildings.

13.8 Daily profiles and typical days for the reference systems

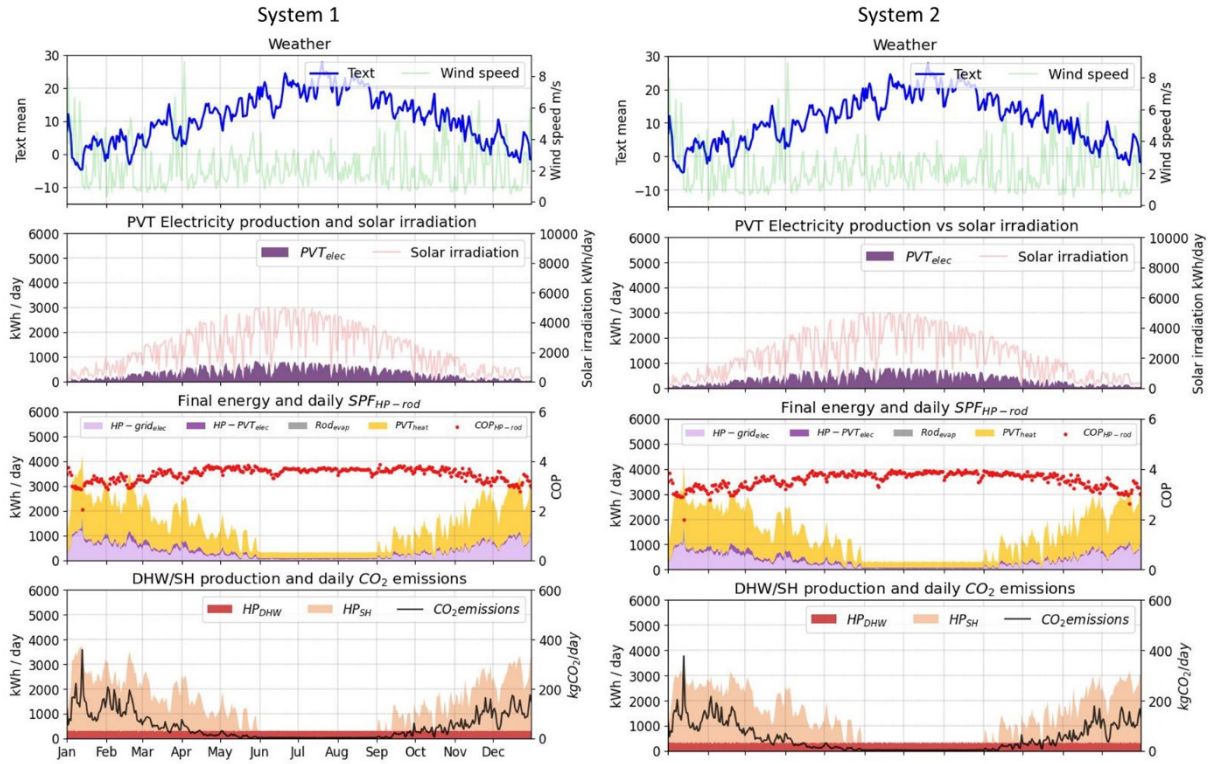

Figure 78 Daily profiles of reference systems with 3.5 m² PVT/kWth HP (i.e. 1.3 m² PVT/MWh in this case) - System 1 (left) and System 2 (right).

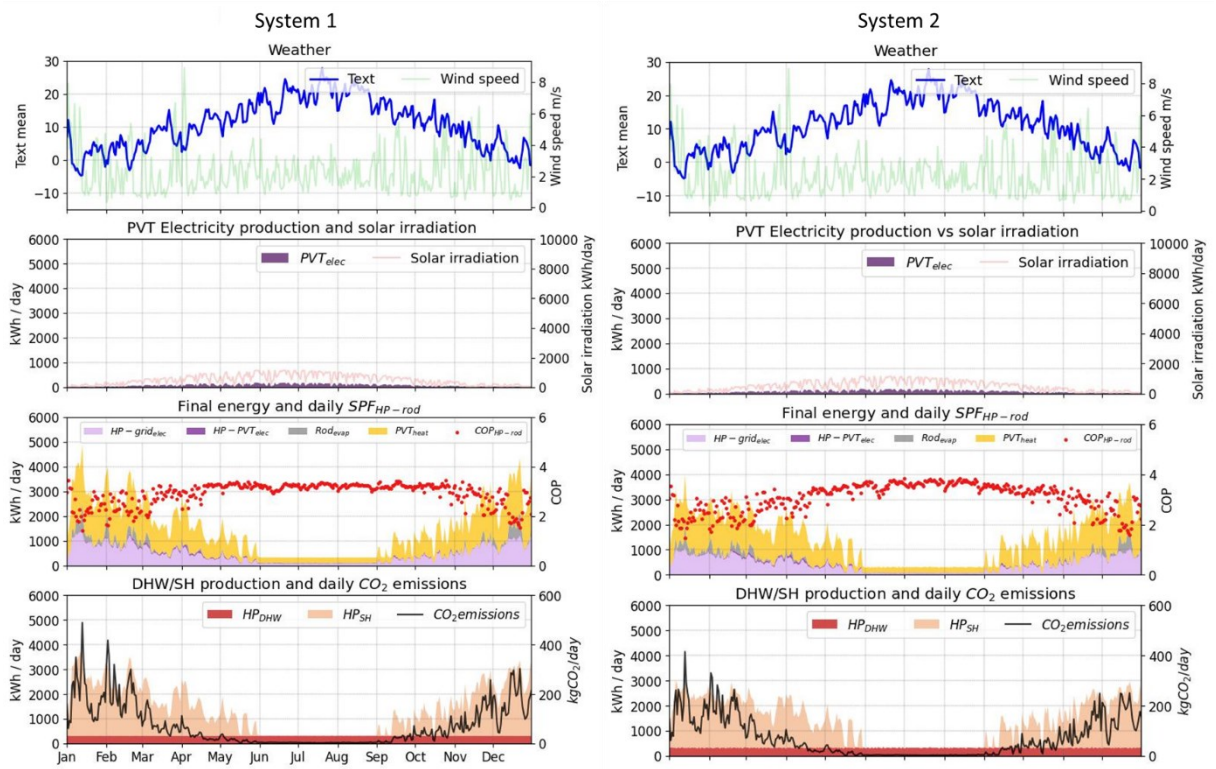

Figure 79 Daily profiles of the reference systems with a low PVT surface area (0.3 m² PVT/MWh_{th}) - System 1 (left) and System 2 (right).

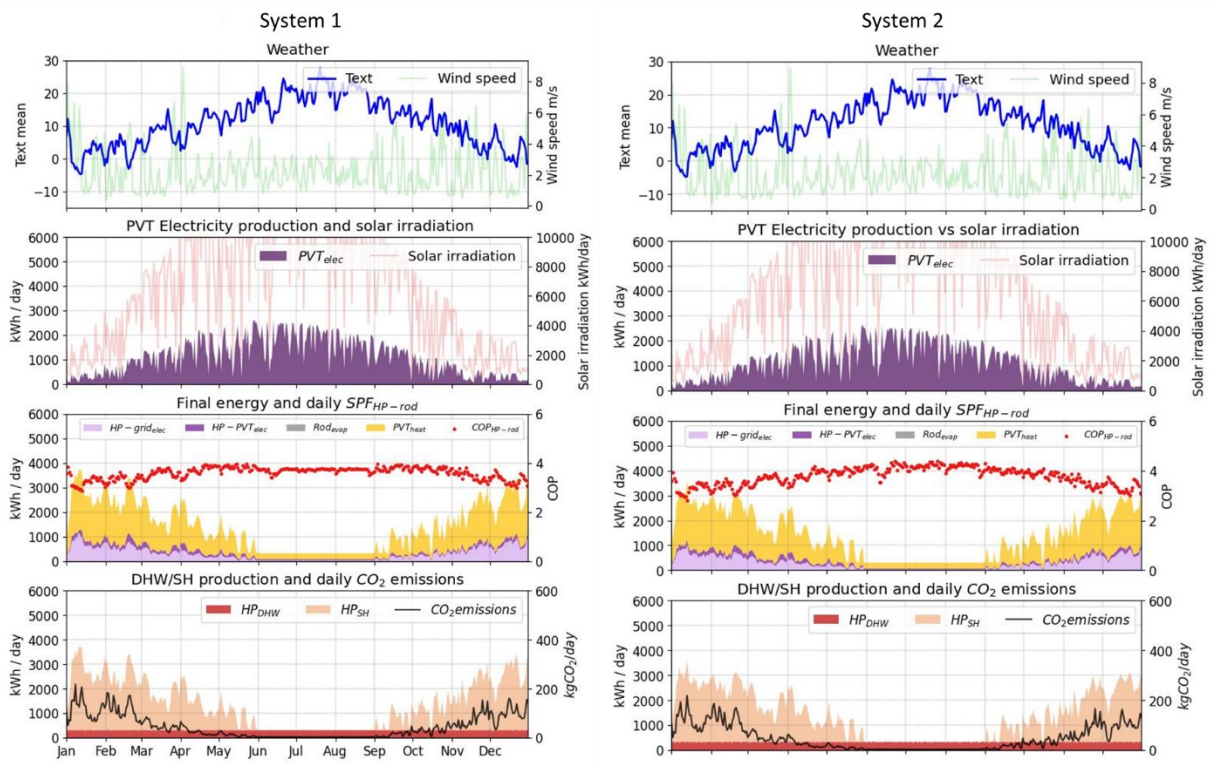

Figure 80 Daily profiles of the reference systems with a high PVT surface area (4 m² PVT/MWh$_{th}$) - System 1 (left) and System 2 (right).

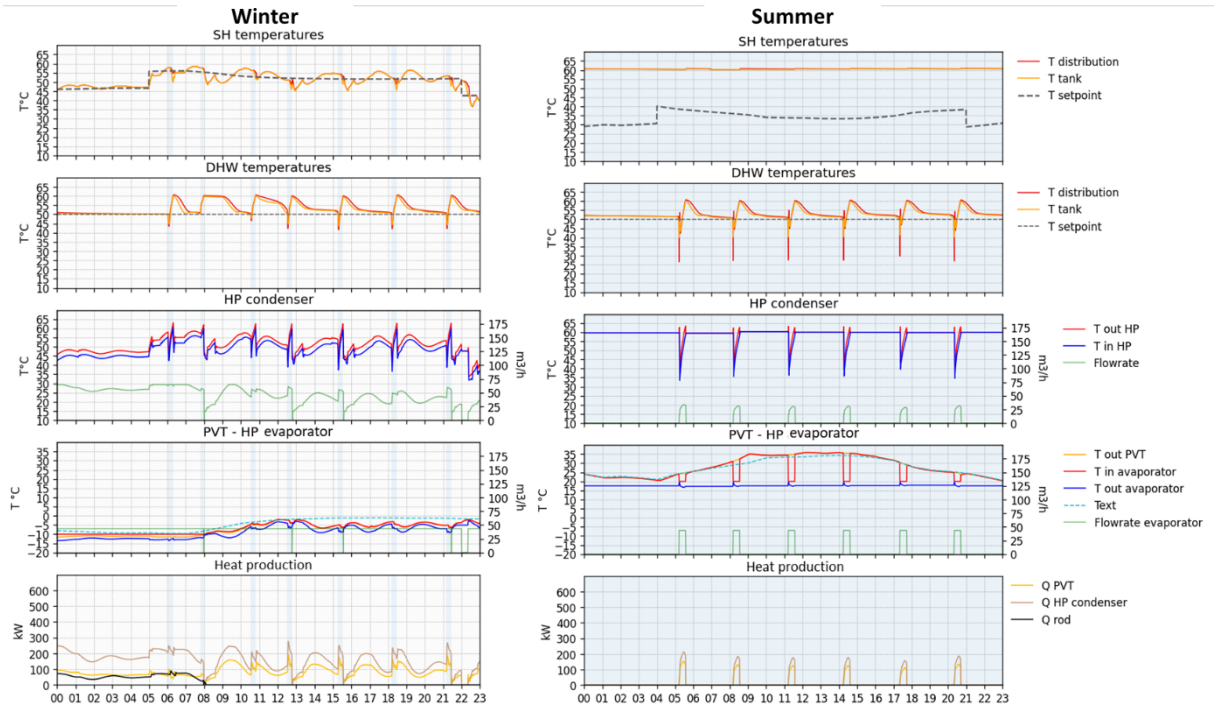

Figure 81 Typical days for the reference System 1 (1.3 m² PVT/MWh$_{th}$ = 3.5 m² PVT/kWh$_{th}$ HP): January 13th (left) and July 21st (right) with an average outdoor air temperature of respectively -4.7°C and 24.5°C.

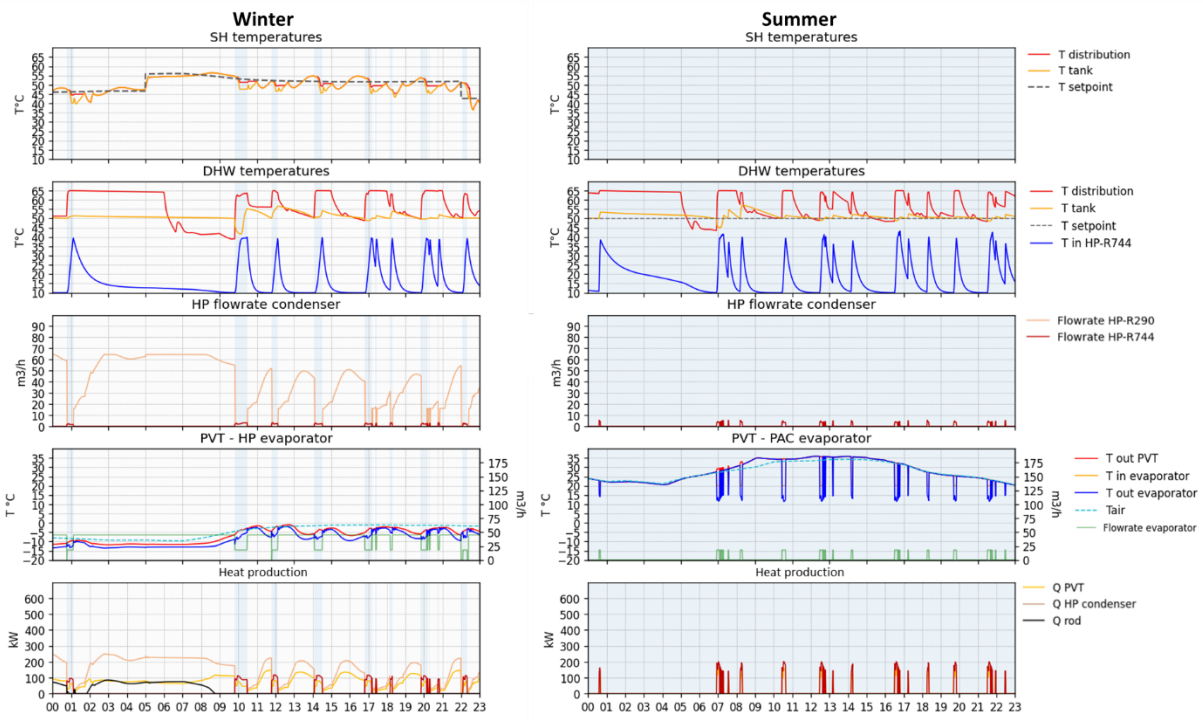

Figure 82 Typical days for the reference System 2 (1.3 m² PVT/MWh$_{th}$ = 3.5 m² PVT/kWh$_{th}$ HP): January 13th (left) and July 21st (right) with an average outdoor air temperature of respectively -4.7°C and 24.5°C.

13.9 List of simulated cases for the sensitivity analysis

Table 16 List of simulated cases and parameters of the sensitivity analysis on System 1

System 1: R290 HP for SH and DHW								
#	Scenarios	SH demand [kWh/m².yr]	DHW demand [L/pers.day]	PVT area [m²/MWh]	HP Capacity R290 (B0/W35 EN14511) [kW]	Volume of SH tank [m3]	Volume of DHW tank [m3]	PVT area [m²]
Dim. SOLINK	Reference SH and DHW demands	101	35	1.29	377	3.7	2	681
1		101	35	0.3	377	3.7	2	158
2		101	35	0.6	377	3.7	2	315
3		101	35	1	377	3.7	2	526
4		101	35	2	377	3.7	2	1051
5		101	35	4	377	3.7	2	2102
6	Low SH demand	**78**	35	0.3	**286**	**2.8**	2	**128**
7		**78**	35	0.6	**286**	**2.8**	2	**257**
8		**78**	35	1	**286**	**2.8**	2	**428**
9		**78**	35	2	**286**	**2.8**	2	**856**
10		**78**	35	4	**286**	**2.8**	2	**1712**
11	High SH demand	**130**	35	0.3	**485**	**4.8**	2	**192**
12		**130**	35	0.6	**485**	**4.8**	2	**385**
13		**130**	35	1	**485**	**4.8**	2	**642**
14		**130**	35	2	**485**	**4.8**	2	**1283**
15		**130**	35	4	**485**	**4.8**	2	**2566**
16	Low DHW demand	101	**25**	0.3	377	3.7	2	**147**
17		101	**25**	0.6	377	3.7	2	**294**
18		101	**25**	1	377	3.7	2	**491**
19		101	**25**	2	377	3.7	2	**982**
20		101	**25**	4	377	3.7	2	**1963**
21	High DHW demand	101	**50**	0.3	377	3.7	2	**173**
22		101	**50**	0.6	377	3.7	2	**347**
23		101	**50**	1	377	3.7	2	**578**
24		101	**50**	2	377	3.7	2	**1156**
25		101	**50**	4	377	3.7	2	**2312**

Table 17 List of simulated cases and parameters of the sensitivity analysis on System 2

System 1: R290 HP for SH and DHW								
#	**Scenarios**	**SH demand [kWh/m².yr]**	**DHW demand [L/pers.day]**	**PVT area [m²/MWh]**	**HP Capacity R290 (B0/W35 EN14511) [kW]**	**Volume of SH tank [m3]**	**Volume of DHW tank [m3]**	**PVT area [m²]**
Dim. SOLINK	Reference SH and DHW demands	101	35	1.29	377	3.7	2	681
1		101	35	0.3	377	3.7	2	158
2		101	35	0.6	377	3.7	2	315
3		101	35	1	377	3.7	2	526
4		101	35	2	377	3.7	2	1051
5		101	35	4	377	3.7	2	2102
6	Low SH demand	**78**	35	0.3	**286**	**2.8**	2	**128**
7		**78**	35	0.6	**286**	**2.8**	2	**257**
8		**78**	35	1	**286**	**2.8**	2	**428**
9		**78**	35	2	**286**	**2.8**	2	**856**
10		**78**	35	4	**286**	**2.8**	2	**1712**
11	High SH demand	**130**	35	0.3	**485**	**4.8**	2	**192**
12		**130**	35	0.6	**485**	**4.8**	2	**385**
13		**130**	35	1	**485**	**4.8**	2	**642**
14		**130**	35	2	**485**	**4.8**	2	**1283**
15		**130**	35	4	**485**	**4.8**	2	**2566**
16	Low DHW demand	101	**25**	0.3	377	3.7	2	**147**
17		101	**25**	0.6	377	3.7	2	**294**
18		101	**25**	1	377	3.7	2	**491**
19		101	**25**	2	377	3.7	2	**982**
20		101	**25**	4	377	3.7	2	**1963**
21	High DHW demand	101	**50**	0.3	377	3.7	2	**173**
22		101	**50**	0.6	377	3.7	2	**347**
23		101	**50**	1	377	3.7	2	**578**
24		101	**50**	2	377	3.7	2	**1156**
25		101	**50**	4	377	3.7	2	**2312**

Table 18 List of simulated cases and parameters of the sensitivity analysis on System 2

System 2: R290 HP for SH and R744 HP for DHW									
#	Scenarios	SH demand [kWh/m².yr]	DHW demand [L/pers.day]	PVT area [m²/MWh]	HP Capacity R290 (B0/W35 EN14511) [kW]	HP Capacity R744 (B0/10-65°C) [kW]	Volume of SH tank [m3]	Volume of DHW tank [m3]	PVT area [m²]
SOLINK	Reference SH and DHW demands	101	35	1.29	377	134	3.7	2	681
1		101	35	0.3	377	134	3.7	2	158
2		101	35	0.6	377	134	3.7	2	315
3		101	35	1	377	134	3.7	2	526
4		101	35	2	377	134	3.7	2	1051
5		101	35	4	377	134	3.7	2	2102
6	Low SH demand	**78**	35	0.3	**286**	**134**	2.8	2	**128**
7		**78**	35	0.6	**286**	**134**	2.8	2	**257**
8		**78**	35	1	**286**	**134**	2.8	2	**428**
9		**78**	35	2	**286**	**134**	2.8	2	**856**
10		**78**	35	4	**286**	**134**	2.8	2	**1712**
11	High SH demand	**130**	35	0.3	**485**	**134**	4.8	2	**192**
12		**130**	35	0.6	**485**	**134**	4.8	2	**385**
13		**130**	35	1	**485**	**134**	4.8	2	**642**
14		**130**	35	2	**485**	**134**	4.8	2	**1283**
15		**130**	35	4	**485**	**134**	4.8	2	**2566**
16	Low DHW demand	101	**25**	0.3	377	134	3.7	2	**147**
17		101	**25**	0.6	377	134	3.7	2	**294**
18		101	**25**	1	377	134	3.7	2	**491**
19		101	**25**	2	377	134	3.7	2	**982**
20		101	**25**	4	377	134	3.7	2	**1963**
21	High DHW demand	101	**50**	0.3	377	134	3.7	2	**173**
22		101	**50**	0.6	377	134	3.7	2	**347**
23		101	**50**	1	377	134	3.7	2	**578**
24		101	**50**	2	377	134	3.7	2	**1156**
25		101	**50**	4	377	134	3.7	2	**2312**

13.10 Cost analysis assumptions

CAPEX and OPEX data for the subsystems composing the two circuits have been derived from literature and private communications with the project partners. Collected data have been used to interpolate available costs to the cases foreseen for economic analysis.

The CAPEX for the installation of the heat source made of Solink PVT panels has been computed by linearly interpolating two quotations provided by the project partners, shown in **Table 19**. The solar block has been expressed as a step function of the following type:

$CAPEX_{MCR}$ = 20670 CHF if PVT > 600 m^2 ; 10140 CHF if PVT < 300 m^2 ; Else 15405 CHF

In order to account for the solar field piping on the roof and from the roof to the heating room it has been assumed that the building over which the solar field is installed is 4 floors and that the technical room is located underground. Hence, the economic analysis has considered 2 pipes, 4 x 5 m long to connect the solar field to the HP in the technical room. To estimate the piping length on the roof, it has been assumed that the solar field of quotation I is made by 4 subfields of PVT collectors in East-West layout, while the solar field of quotation II is made by 2 subfields. Each subfield is distanced by 80 cm from the neighbouring one and it is made by a single continuous line of collectors. Each subfield requires 3 pipes of a diameter between DN60 and DN32, with a cost of 200 CHF/m each. Furthermore, the glycol content of the piping is added to the glycol inventory of the case.

Table 19 Base data for the derivation of CAPEX formulations for the heat source.

Quotation ID	I	II
PVT aperture area, in [m^2]	856	294
Collectors, supports, glycol, expansion system, installation and commissioning, in [CHF/m^2]	856	883
Transport and technical works, in [CHF/m^2]	21.5	22.4
Solar block, in [CHF]	20670	10140
Hydraulic separator, in [CHF]	3933	3933

The CAPEX of the PV part of the PVT solar field has been derived from data concerning PV installations (see [38] and [40]). **Figure 83** shows the relationship used to derive the specific price of a PV installation. Since the collector price includes the PV module, only the fraction of the PV system consisting of inverters and electrical material needs to be considered. Based on the decomposition of the PV system price available in literature and shown in **Figure 84**, we have assumed that the CAPEX for the PVT field needs to be increased by an amount equal to 18.3% of the price of an equivalent PV system (i.e., with the same PV peak power than the PVT collector) to account for inverters and electrical material.

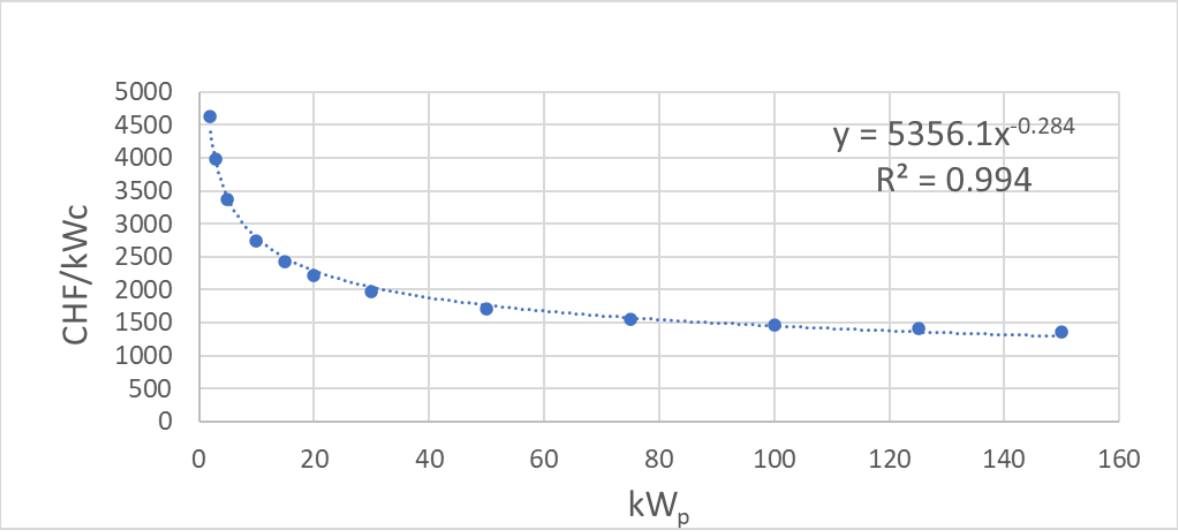

Figure 83 Spefic price of PV istallations ([40])

Table 20 PV System CAPEX

Peak power [kWc]	100 – 300	300-1000	Admis
Panels	35%	36.8%	36%
Inverter	5.5%	4.8%	5.3%
Electrical material	15%	11.6%	13%
Engineering, installation	8%	18%	13%

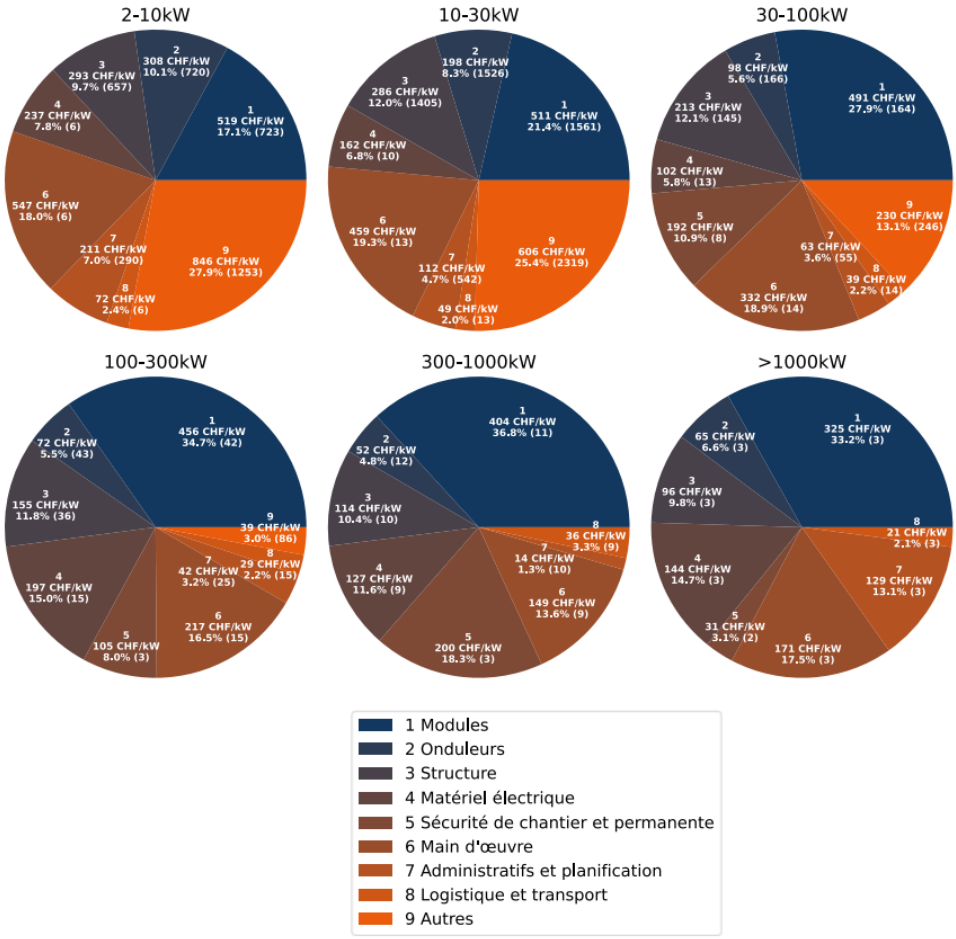

Figure 84 PV system price decomposition according to [40]

The PVT Field OPEX has been estimated by considering typical solar thermal OPEX values combined with typical PV OPEX estimations. In particular, the solar thermal OPEX has been derived from communications with the project partners and data are shown in **Figure 85** in terms of costs per year.

The PV OPEX has been derived from literature (see [41]) and it is shown in **Figure 86**. A best fit of the available data yields the following expression:

$OPEX_{PV} = 23.15 * P_{pv}^{-0.138}$ ctsCHF/kWh$_e$

Where P_{PV} is the PV system peak power.

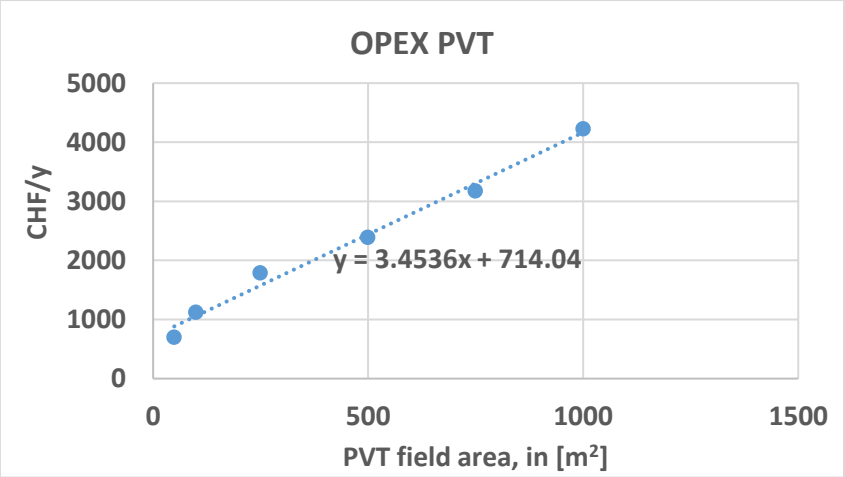

Figure 85 Costing data for the PVT OPEX.

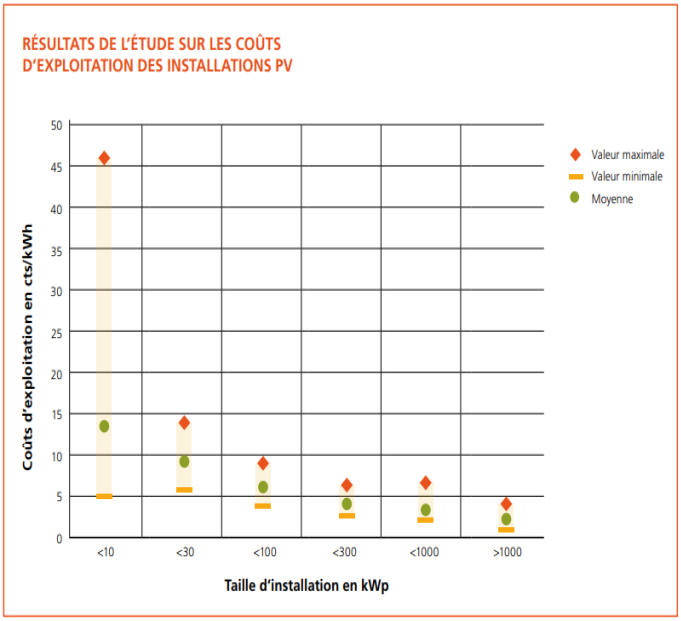

Figure 86 PV OPEX as a function of the PV plant size (see [41])

13.11 Electricity fares

During the economic analysis, it has been assumed that electricity fares follow the tarification applied by SIG in Geneva during 2023, in particular the "Tarif Pro BT" double period with optimization A, shown in **Figure 87**. The final fare applied depends on the consumption and on the enregistered peak power, according to the following relationship:

$$Price_{kWh}=(El_{HD}\,h_{HD}+El_{HP}*h_{HP})_{summer}+(El_{HD}*h_{HD}+El_{HP}*h_{HP})_{winter}+(Net_{HP,A}*+Cm_{HP,A})*El_{HP}+(Net_{HD,A}*+Cm_{HD,A})*El_{HD}+P_p*Net_{Pp,A}+Fed.Tax \quad \text{Eq. 43}$$

where El_{HD} and El_{HP} are the electrical consumption during low and high prices, respectively; h_{HD} and h_{HP} are the price coefficient from **Figure 87** for consumption happening during off-peak or on-peak hours, respectively, depending if it is in winter or summer; Net_{HP}, Net_{HD} and Net_{Pp} are the price coefficient for peak hours, off-peak hours and peak power, respectively; while P_p is the peak power effectively drawn from the grid and the *Fed.Tax* accounts for the Swiss Federal tax for the development of renewable energies and the protection of water sources.

Figure 87 shows also the fares applied for estimating connection expenditures for the simulated systems.

Table 21 shows the tariff adopted to remunerate the electricity injected into the grid and not consumed on-site.

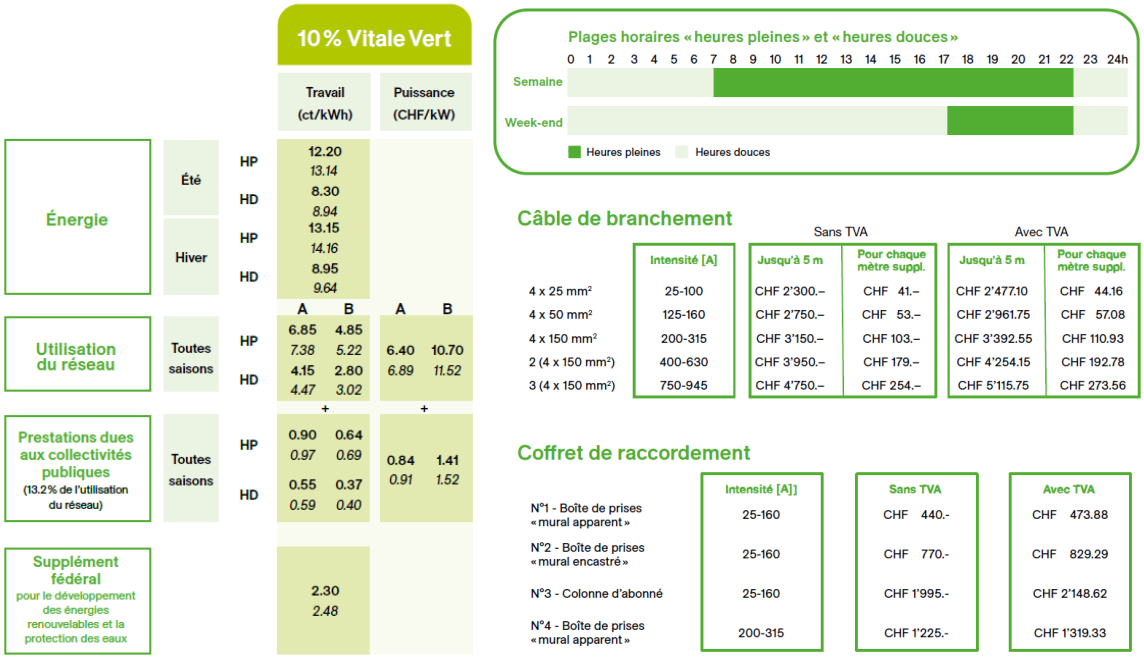

Figure 87 Electricity fares adopted for the economic analysis.

Table 21 Total financial incentive paid in 2023 by SIG for PV installations with certified production ("garantie d'origine photovoltaique").

Montants en cts/kWh	*Hors TVA*	*TVA incl.*[1]
Installations d'une puissance installée inférieure ou égale à 30 kWc	16.15	17.46
Installations d'une puissance installée supérieure à 30 kWc et inférieure ou égale à 100 kWc	15.95	17.24
Installations d'une puissance installée supérieure à 100 kWc	15.15	16.38

13.12 Data source and distribution of heat data for the entire DataRen database

The DataRen database [ref] contains heat demand, energy sources and energy reference areas (ERA) of buildings in the canton of Geneva. It includes more than 56'000 EGID, representing a total energy reference area of 43.4 million m² in 2020. As presented in the following table, it corresponds to a total heat demand of 5'372 GWh, evaluated based on different data sources.

Data source for the heat demand of Geneva's building stock in the DataRen database

Geneva's building stock						
Data source*	**Number of EGID**	**%**	**ERA [mio m²]**	**%**	**Total heat demand [GWh/yr]**	**%**
IDC	18 375	33%	32,4	75%	3 848	72%
SAP	10 051	18%	2,0	5%	331	6%
AVG1	9 505	17%	5,3	12%	563	10%
AVG2	429	1%	0,3	0%	46	1%
AVG3	17 947	32%	3,4	8%	584	11%
Total	***56 307***	***100%***	***43,4***	***100%***	***5 372***	***100%***

** Data source for the building heat demand:*
- IDC : Heat expenditure index from SITG
- SAP: SIG Gas & District Heating bills
- AVG1: Average by category and period of construction
- AVG2: Calculation extrapolated on Individual housing gas consumption
- AVG3: Average per category SIA

Multi-family buildings represent 52% of the total ERA and heat demand of the database, with a total ERA of 22.7 million m² and a total heat demand of 2'824 GWh, evaluated as follows:

Data source for the heat demand of Geneva's multi-family building stock in the DataRen database

Geneva's multi-family building stock						
Data source*	**Number of EGID**	**%**	**ERA [mio m²]**	**%**	**Total heat demand [GWh/yr]**	**%**
IDC	13 206	86%	21,1	93%	2 651	94%
AVG1	2 065	14%	1,6	7%	173	6%
Total	***15 271***	***100%***	***22,7***	***100%***	***2 824***	***100%***

** Data source for the building heat demand:*
- IDC : Heat expenditure index from SITG
- AVG1: Average by category and period of construction

13.13 Planned expansion of Geneva's main district heating network by 2050

In the canton of Geneva, a map of the expansion of the main district heating network by 2050 has been drawn up as a direct result of the Energy Master Plan 2020-2030. Existing and futures areas supplied by the DH are available in shapefiles format on SITG [42].

To locate buildings that will potentially be connected to the DH by 2040, a spatial selection was made using QGis. Thus, for the purposes of estimating CO2 emissions, all buildings in the 2030 or 2040 extension zone will have DH or HP or TriSolHP as their energy source in 2040, depending on the scenario.

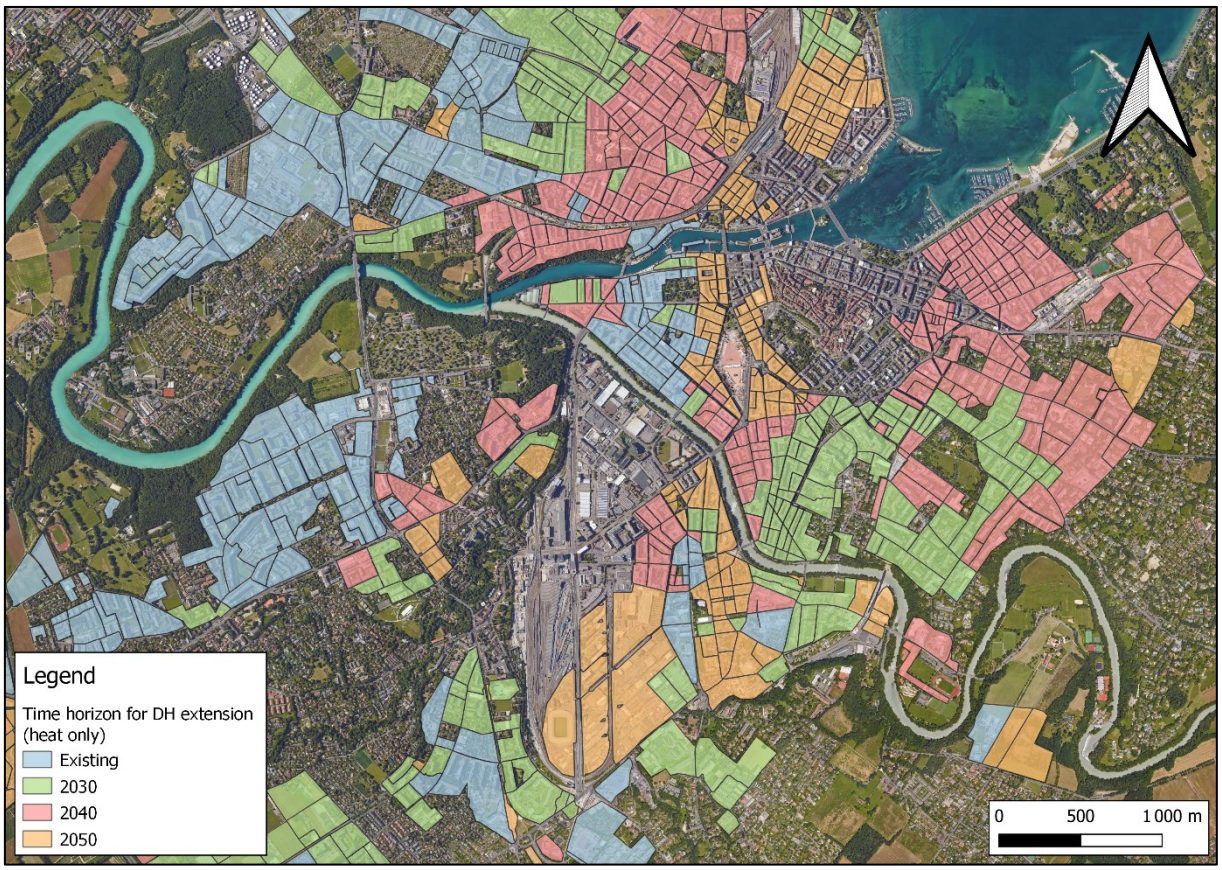

Figure 88 Map of the planned expansion of Geneva's main DH network according to different timeframes